

Parametric Transition of Stationary and Axisymmetric Bodies to Black Holes

Dissertation

zur Erlangung des akademischen Grades
doctor rerum naturalium (Dr. rer. nat.)

vorgelegt dem Rat der Physikalisch-Astronomischen
Fakultät der Friedrich-Schiller-Universität Jena

von M.Sc. Hendrick Labranche
geboren am 2. Juli 1979 in Québec, Kanada

Gutachter

1. Prof. Dr. Reinhard Meinel (Friedrich-Schiller-Universität Jena)
2. PD Dr. Claus Lämmerzahl (Universität Bremen)
3. Prof. Dr. Jutta Kunz (Carl von Ossietzky Universität Oldenburg)

Tag der Disputation: 11. Mai 2010

Contents

Zusammenfassung (auf Deutsch)	iii
Abstract (in English)	iv
1. Introduction	1
2. An Overview of Stationary and Axisymmetric Spacetimes	4
2.1. The Metric Potentials and the Einstein Equations	4
2.1.1. The Metric of Stationary and Axisymmetric Spacetimes	4
2.1.2. Uniformly Rotating Cold Perfect Fluids as Gravitational Source	5
2.1.3. The Einstein Field Equations	7
2.2. The Vacuum Domain	8
2.2.1. The Ernst Equation	9
2.2.2. The Multipole Moments	10
2.3. The Black Hole Limit of Fluid Bodies in Equilibrium	11
2.3.1. Necessary and Sufficient Conditions for a Black Hole Limit	12
2.3.2. The Extreme Kerr Black Hole Geometry	14
3. Strange Matter Stars and their Parametric Transition to a Black Hole	17
3.1. Model and Method used for Relativistic Strange Stars	17
3.1.1. Equation of State	17
3.1.2. The Ansorg-Kleinwächter-Meinell Numerical Method	20
3.2. Solutions of Strange Quark Matter	21
3.2.1. The Schwarzschild Class of Strange Quark Matter	21
3.2.2. The Ring Class of Strange Quark Matter	27
3.3. Parametric Transition to a Black Hole	28
3.3.1. Multipole Moments of Rings	28
3.3.2. Throat Geometry	35
3.3.3. Escape Energy	36

4. Ernst Potentials near the Black Hole Limit	41
4.1. Reformulation of the Conjecture	41
4.1.1. Normalized Multipoles	41
4.1.2. The Multipoles and the First Law of Thermodynamics	43
4.1.3. A Taylor Series Near the Black Hole Limit	45
4.2. Ernst Potential of the Kerr Black Hole	47
4.3. Ernst Potential of the Uniformly Rotating Disk of Dust	49
4.3.1. Ernst Potential of the Disk	50
4.3.2. Ernst Potential of the Disk in the Black Hole Limit	53
4.3.3. Derivatives of the Ernst Potential in the Black Hole Limit	54
4.4. Taylor Series of the Disk	60
4.4.1. Series of Functions of μ	61
4.4.2. Series of Functions of $(\mu, \tilde{\zeta})$	62
4.4.3. Series of the Ernst Potential of the Disk	69
5. Conclusion	75
Bibliography	77
A. Elliptic Integrals and Functions	81
B. Some Useful Functions for the Disk of Dust	84
B.1. List of Functions in the Ernst Potential of the Disk	84
B.2. Some Other Useful Relations	86
Danksagung	87
Ehrenwörtliche Erklärung	88
Lebenslauf	89

Zusammenfassung

Diese Dissertation behandelt Lösungen stationärer und axialsymmetrischer Körper und ihren parametrischen Übergang zu Schwarzen Löchern. Numerische Lösungen von Flüssigkeiten im Gleichgewicht werden unter Annahme einer “strange quark matter”-Zustandsgleichung mit sehr hoher Genauigkeit berechnet. Verschiedene Sequenzen von Konfigurationen werden für sphäroideale und toroidale Körper untersucht, um die wesentlichen Eigenschaften dieser Familie von Objekten aus “strange matter” aufzuzeigen. Konfigurationen mit maximaler Masse und maximalem Drehimpuls wurden in der Nähe von - aber nicht an - der “mass-shedding”-Grenze gefunden, im Gegensatz zu den Erwartungen.

Außerdem zeigen wir, dass “strange matter”-Ringe einen kontinuierlichen Übergang zur extremen Kerr-Lösung erlauben. Die von Geroch und Hansen definierten Multipolmomente wurden untersucht und deuten auf ein universelles Verhalten von Körpern hin, die sich parametrisch der extremen Kerr-Lösung annähern. Das Auftreten einer “throat geometry” als charakteristisches Merkmal der extremen Kerr-Raumzeit wird diskutiert. Dann zeigen wir, im Hinblick auf die Stabilität, dass ein Testteilchen, das auf der Oberfläche des Ringes liegt, niemals genug Energie besitzt, um entlang einer Geodäten ins Unendliche zu gelangen.

Ausgehend vom universellen Verhalten, welches die Multipolmomente andeuten, formulieren wir eine Vermutung bezüglich der parametrischen Annäherung gleichförmig rotierender Flüssigkeiten an die extreme Kerr-Lösung. Die Vermutung wird für ein Multipolmoment (den Drehimpuls) anhand eines “thermodynamischen Gesetzes” beschrieben, welches für alle gleichförmig rotierenden Flüssigkeiten im Gleichgewicht gilt. Die selbe Vermutung wird dann in ihrer Gesamtheit für die Staubscheibe gezeigt.

Abschließend wird das Ernst-Potential der Staubscheibe auf der Achse in eine Taylor-Reihe in der Umgebung der extremen Kerr-Lösung entwickelt. Diese Reihe scheint überall auf der Achse zu konvergieren, ausgehend vom Grenzfall des Schwarzen Lochs bis hin zur Newton’schen Grenze der Scheibenlösung, außerhalb einer kleinen Region in der Nähe der Scheibe. Die benutzte Methode erlaubt es uns sehr effizient, die Reihe in beliebig hoher Ordnung zu entwickeln.

Abstract

This thesis deals with solutions of stationary and axisymmetric relativistic bodies and their parametric transition to black holes. Highly accurate numerical solutions were produced for perfect fluids in equilibrium made of strange quark matter. Several sequences of configurations, including spheroidal bodies and rings, were produced to sketch the main features of the family of strange matter bodies. The maximal mass and maximal angular momentum configurations were found close to but not at the mass-shedding limit, contrary to what was believed.

We also show numerically that strange matter rings permit a continuous transition to the extreme Kerr black hole. The multipoles as defined by Geroch and Hansen are studied and suggest a universal behaviour for bodies approaching the extreme Kerr solution parametrically. We discuss the appearance of a “throat geometry”, a distinctive feature of the extreme Kerr spacetime. Then we verify, with regard to stability, that a particle sitting on the surface of the ring never has enough energy to escape to infinity along a geodesic.

From the universal behaviour suggested by the multipoles, we formulate a conjecture related to the parametrical approach of uniformly rotating fluids to the extreme Kerr black hole. The conjecture is explained for one multipole (the angular momentum) using a “law of thermodynamics” valid for all uniformly rotating bodies in equilibrium. The same conjecture is then proved in its entirety for the disk of dust.

Finally, the Ernst potential on the axis of the disk of dust is expanded in a Taylor series anchored at the extreme Kerr black hole limit. This series seems to converge everywhere on the axis, from the black hole limit to the Newtonian limit of the disk solution, except for a tiny region near the disk. The method used allows us to generate the series efficiently to arbitrarily high orders.

1. Introduction

Once stars exhaust their capacity to generate energy through thermonuclear reactions, it is understood that they die by a variety of dynamical processes, which combine rapid ejection of matter and contraction of the stellar core. Depending mainly on the initial mass of the star, its final remnant is expected to be either a white dwarf, a neutron star or a black hole. These remnants and the dynamical processes leading to them are all configurations where relativistic effects are important, so relevant modelling needs to be done in full accordance with general relativity. The dynamical transition to a stellar remnant is still today an arduous task and not completely understood, but interesting achievements have been published. Making use of the introduction of a local (3-D) and dynamic notion of a “horizon” such as is described in [AK04], numerical work has followed the collapse of an initial distribution of matter to a “black hole”, see e.g. [Fon03]. For sufficiently long run-times, a (4-D) event horizon can be located *a posteriori* and there exist simulations, e.g. [BHM⁺05], supporting the widely held expectation that after collapse, the configuration will settle down to a Kerr black hole. Many questions are still open however regarding the initial data, the matter model, the accuracy of the time evolution, etc.

On the other hand, the modelling of the final remnants is a much easier task and better understood, since the computation can take advantage of symmetries such as stationarity, axial and equatorial symmetries, and because of the extremely high Fermi energy expected for the degenerate fermion gas in white dwarfs and neutron stars, we can assume that their particles have zero temperature. Many discussions conclude that relativistic stellar models made of uniformly rotating cold perfect fluids are indeed reasonable simplifications of real astronomical stars such as neutron stars [Lin92, MAK⁺08].

Within the class of stationary and axisymmetric bodies, the static cases (non-rotating bodies) are the easiest to model and the best known properties are often found from (and sometimes restricted to) this category. Among these interesting properties, it was found that between static white dwarfs, neutron stars and black holes, no “smooth” (quasi-static) transition exists: such transitions imply dynamical collapses. One of these transitions assumes that the electron-degeneracy pressure in white dwarfs must fail near the so-called “Chandrasekhar limit” [Cha31] and the dwarf must suddenly collapse into

a neutron star. For the second transition, the equation of state (EOS) of neutron stars is still very speculative today, but under the assumption that the energy density in the star does not increase outwards, it can be shown that stars in hydrostatic equilibrium must satisfy the so-called “Buchdahl inequality”: they must have a radius greater than $9/8$ times the radius¹ of a black hole with the same mass [Buc59]. So a static star can become a black hole only through the process of a dynamical collapse. Contrary to the dynamics of the first transition, which is dependent on our knowledge of the EOS, the dynamical collapse in the second transition is valid for any relevant EOS.

This “Buchdahl inequality” is true only for static stars, but it would be legitimate to ask if, for the entire class of stationary and axisymmetric bodies, a smooth or “quasi-stationary” transition between a star and a black hole could exist. In [Mei04, Mei06], necessary and sufficient conditions for a quasi-stationary transition were presented and it was proved that an extreme Kerr black hole necessarily results. Using the analytic solution for the relativistic disk of dust [NM95], a transition to a black hole was found explicitly [Mei02]. Transitions have also been found numerically for rings with a variety of EOS [AKM03b, FHA05].

In this thesis, we want to investigate in detail the parametric (or quasi-stationary) transition of stationary and axisymmetric bodies to black holes. Such a transition is not plagued by all the problems of modelling dynamical collapses, but at the price of being very highly idealized. A parametric sequence of configurations can at best model a “non-dynamic” collapse. In astrophysical collapse scenarios, there may well be matter that does not fall into the centre, and the time evolution of a non-stationary spacetime will determine how gravitational radiation leaves the system and leads to changes in the angular momentum of the central region. Thus the transition to a black hole considered in this work should be seen as an instructive limit capable of shedding some light on issues regarding the path matter could take in evolving to a black hole.

The conditions for a quasi-stationary transition between a star and a black hole depends on the gravitational potential at the surface of the star, but not directly on the EOS. So many stellar models with different EOS can be candidates for a parametric transition to black holes. For this work, we wanted to focus our investigation on a stellar model with an astrophysically plausible EOS. Among the several running candidates for EOS of neutron stars, we decided to focus on a stellar model made of strange quark matter: a type of “neutron star” made of equal numbers of deconfined up, down and strange quarks.

¹radius in Schwarzschild coordinates

The work that we present here is planned as follows. We begin by summarizing in Chapter 2 the essential concepts and equations of general relativity that are needed for our work. Then, our investigation is divided in two parts.

In a first part (Chapter 3), we present solutions of a star model made of strange quark matter. The first pages are devoted to a brief description of the equation of state used here to model strange matter and the numerical method that we use to compute solutions (Sec. 3.1). Then, sequences of solutions are presented, for strange stars with spheroidal and toroidal topologies, and some extremal configurations are discussed (section 3.2). Finally, we follow the progression of multipole moments of rings as they tend to those of the extreme Kerr black hole, we discuss the appearance of a “throat region” separating an “inner” from an “outer world”, and we verify numerically that a particle resting on the ring’s surface is always gravitationally bound, a condition, which can be considered to be a minimal requirement for stability (Sec. 3.3).

In a second part (Chapter 4), we explore a property of the Ernst potential that fluid bodies in equilibrium share with black holes near the extreme Kerr black hole limit. This property, which is conjectured in chapter 3, is partially explained by a “thermodynamical law” and can take a nice form if the Ernst potential is written as a Taylor series with a suitable choice of normalized coordinates (Sec. 4.1). As an example, we write down the beginning of this Taylor series for the Ernst potential of the Kerr black hole (Sec. 4.2). We prove that this conjecture indeed holds for the uniformly rotating disk of dust (Sec. 4.3). And finally, we generate a Taylor series for the Ernst potential of the disk of dust near its black hole limit (Sec. 4.4).

Throughout this thesis, units are used in which the gravitational constant G and speed of light c are equal to one, and our sign convention of the metric signature is $(+, +, +, -)$.

2. An Overview of Stationary and Axisymmetric Spacetimes

This chapter gives a quick and concise overview of the concepts and equations of general relativity for stationary and axisymmetric spacetimes. It shows the essential information, definitions and conventions that we make use for this work. For further information on the theory of equilibrium configurations of rotating fluids, we recommend you to refer to the book *Relativistic Figures of Equilibrium* [MAK⁺08].

2.1. The Metric Potentials and the Einstein Equations

2.1.1. The Metric of Stationary and Axisymmetric Spacetimes

A spacetime with axial symmetry and stationarity requires that the metric potentials $g_{\mu\nu}$ be independent of a time coordinate t and an azimuthal angle φ . Restricting ourselves to spacetimes filled only by vacuum and a rigidly rotating perfect fluid, a decomposition of the metric into orthogonal 2-spaces becomes possible by virtue of the theorem given in [KT66].¹ The line element for such spacetimes can be written, with use of the Lewis-Papapetrou coordinates, in the form

$$ds^2 = e^{-2U} [e^{2k} (d\rho^2 + d\zeta^2) + W^2 d\varphi^2] - e^{2U} (ad\varphi + dt)^2, \quad (2.1)$$

with the functions e^{2k} , e^{2U} , W and a depending on ρ and ζ only. The equatorial plane is given by $\zeta = 0$ and the axis of rotation by $\rho = 0$. These potentials should behave in such a way that the metric becomes the Minkowski metric at spatial infinity ($\rho^2 + \zeta^2 \rightarrow \infty$) and also corresponds to Newton's theory of gravity far from the gravitational source:

$$g_{tt} = -e^{2U} = -1 + \frac{2M}{r} + \mathcal{O}\left(\frac{1}{r^2}\right), \quad (2.2a)$$

$$g_{t\varphi} = -ae^{2U} = -\frac{2J \sin^2 \theta}{r} + \mathcal{O}\left(\frac{1}{r^2}\right), \quad (2.2b)$$

¹This is the so-called ‘‘circularity condition’’, which holds for a large class of energy-momentum tensor which includes rigidly rotating perfect fluid bodies.

$$g_{\varphi\varphi} = W^2 e^{-2U} - a^2 e^{2U} = r^2 \sin^2 \theta \left[1 + \mathcal{O}\left(\frac{1}{r^2}\right) \right], \quad (2.2c)$$

$$g_{\rho\rho} = g_{\zeta\zeta} = e^{2k-2U} = 1 + \frac{2M}{r} + \mathcal{O}\left(\frac{1}{r^2}\right) \quad (2.2d)$$

where M and J are respectively the gravitational mass and the angular momentum, and where we use $r := \sqrt{\rho^2 + \zeta^2}$ and $\tan \theta := \rho/\zeta$. Since we want to deal with uniformly rotating sources, we introduce a coordinate system with a constant angular velocity Ω around the rotation axis with respect to the frame of an observer at infinity:

$$\rho' = \rho, \quad \zeta' = \zeta, \quad \varphi' = \varphi - \Omega t, \quad t' = t. \quad (2.3)$$

The metric potentials of the “rotating frame” are related to those of the “non-rotating frame” as follow:

$$e^{2U'} = e^{2U} [(1 + \Omega a)^2 - \Omega^2 W^2 e^{-4U}], \quad (2.4a)$$

$$(1 - \Omega a') e^{2U'} = (1 + \Omega a) e^{2U}, \quad (2.4b)$$

$$e^{2k'-2U'} = e^{2k-2U} \quad (2.4c)$$

and $W' = W$ is unaffected by the coordinate transformation.

2.1.2. Uniformly Rotating Cold Perfect Fluids as Gravitational Source

If we consider a perfect fluid body in thermodynamic equilibrium as the source of the gravitational field, the energy-momentum tensor becomes

$$T^{\alpha\beta} = (\epsilon + p) u^\alpha u^\beta + p g^{\alpha\beta}, \quad (2.5)$$

where u^α , ϵ and p are respectively the 4-velocity field, the energy density and the pressure of the fluid.²

The independence of the metric potentials in (2.1) on the time t and the azimuthal angle φ can be expressed using two associated Killing vectors: $\xi^\alpha = (0, 0, 0, 1)$ for stationarity and $\eta^\alpha = (0, 0, 1, 0)$ for axisymmetry; the order of the components follows $x^\alpha = (\rho, \zeta, \varphi, t)$. For solutions that are strictly stationary and axially symmetric, the source must be in thermodynamic equilibrium, which is achieved for a fluid of zero temperature and rigid rotation, and the 4-velocity must follow a time-like direction which is a linear combination of the two Killing vectors. To satisfy all these conditions,

²Greek indices run from 1 to 4.

the 4-velocity field must be

$$u^\alpha = e^{-U'}(\xi^\alpha + \Omega \eta^\alpha) = e^{-U'}(0, 0, \Omega, 1) \quad \text{or} \quad u'^\alpha = e^{-U'}(0, 0, 0, 1) \quad (2.6)$$

where u^α and u'^α are respectively in the frame of an observer at infinity and in the “co-rotating frame” (rotating with the fluid), and we see that Ω becomes the angular velocity of the source with respect to infinity. For a fluid in hydrostatic equilibrium, the constant Ω can be expressed through several different concepts [HS67]:

$$\Omega = \frac{d\varphi}{dt} = \frac{u^\varphi}{u^t} = -\frac{\partial u_t}{\partial u_\varphi} = \left. \frac{\partial M}{\partial J} \right|_{M_B=\text{constant}},$$

where the two last partial derivatives refer to nearby configurations in equilibrium, with M_B being the baryonic mass of the source.

The baryonic mass, the angular momentum J and the gravitational mass M can be obtained from the energy-momentum tensor with the following integrals over a 3-dimensional volume containing the source:

$$M_B = 2\pi \iint \epsilon_B e^{2k'-3U'} W \, d\rho \, d\zeta, \quad (2.7a)$$

$$J = -2\pi \iint (\epsilon + p) a' e^{2(k'-U')} W \, d\rho \, d\zeta, \quad (2.7b)$$

$$M = 2\Omega J + 2\pi \iint (\epsilon + 3p) e^{2(k'-U')} W \, d\rho \, d\zeta, \quad (2.7c)$$

where ϵ_B is the baryonic mass density, corresponding to the total energy density of a volume element less the internal energy density ($\epsilon_B = \epsilon - \epsilon_{\text{int}}$). The mass and angular momentum from the volume integrals are the same as those measured in the asymptotic behaviour at infinity in Eqs(2.2) [HS67], so the two methods of measurement provide an important test of consistency for numerical solutions.

To describe the surface of a fluid body, the co-rotating potential U' has a useful and intuitive meaning: the function is constant along isobaric surfaces. We rename the potential $V \equiv U'$, and the surface of the fluid body, defined to be the surface of vanishing pressure, can thus be denoted by $V = V_0$. The constant V_0 is related to the relative redshift Z_0 , the redshift of zero angular momentum photons emitted from the surface of the body and observed at infinity:

$$e^{-V_0} - 1 = Z_0. \quad (2.8)$$

For zero temperature fluid bodies, one can relate the baryonic mass density ϵ_B to ϵ and p through

$$\epsilon_B = \frac{\epsilon + p}{h(p)} , \quad (2.9)$$

where $h(p)$ is the specific enthalpy, and has the property that at any location in the source, the product $h(p) e^V$ is always constant.

Nearby configurations in equilibrium with the same equation of state are related by a law which looks like an analogue of the first law of thermodynamics at zero temperature [HS67]:

$$dM = \Omega dJ + \mu_c dM_B , \quad \mu_c = h(0) e^{V_0} . \quad (2.10)$$

For sequences of constant angular momentum J , which contain an extremum of the gravitational mass M within the sequence, it can be shown from the last equation that the configuration with extremal M marks a limit of stability, provided that there exists a dissipative mechanism which conserves J and M_B . The unstable part of the sequence near the extremum can be identified by the condition

$$\frac{d^2 M}{dM_B^2} > 0 . \quad (2.11)$$

With the arbitrary 4-velocity u^α of a test particle and the Killing vector ξ_α corresponding to stationarity, one can define the specific energy of a test particle with respect to infinity, i.e. the energy per unit mass, as $E = -u^\alpha \xi_\alpha$, which is a conserved quantity along any geodesic. For a fluid element, the specific energy is thus

$$E = -u^\alpha \xi_\alpha = e^V (1 - \Omega a') . \quad (2.12)$$

This quantity can tell us how the matter is gravitationally bound. If $E < 1$, then the test particle is bound and cannot escape to infinity on a geodesic; if $E > 1$, then the particle has enough energy to escape.

2.1.3. The Einstein Field Equations

The computation of the Einstein field equations (without cosmological constant)

$$R^{\alpha\beta} - \frac{1}{2} R g^{\alpha\beta} = 8\pi T^{\alpha\beta}$$

from the co-rotating potentials of (2.4) and the energy momentum tensor (2.5) in the co-rotating frame leads to the following system of differential equations:

$$\nabla^2 U' + \frac{\nabla W \cdot \nabla U'}{W} + \frac{e^{4U'}}{2W^2} (\nabla a')^2 = 4\pi W e^{2(k'-U')} (\epsilon + 3p) , \quad (2.13a)$$

$$\nabla^2 a' - \frac{\nabla W \cdot \nabla a'}{W} + 4\nabla U' \cdot \nabla a' = 0 , \quad (2.13b)$$

$$\nabla^2 W = 16\pi W e^{2(k'-U')} p , \quad (2.13c)$$

$$\nabla^2 k' + (\nabla U')^2 + \frac{e^{4U'}}{4W^2} (\nabla a')^2 = 8\pi e^{2(k'-U')} p , \quad (2.13d)$$

$$k'_{,\rho} W_{,\zeta} + k'_{,\zeta} W_{,\rho} - W_{,\rho\zeta} + \frac{e^{4U'}}{2W^2} a'_{,\rho} a'_{,\zeta} - 2W U'_{,\rho} U'_{,\zeta} = 0 , \quad (2.13e)$$

$$k'_{,\rho} W_{,\rho} - k'_{,\zeta} W_{,\zeta} + \frac{1}{2}(W_{,\zeta\zeta} - W_{,\rho\rho}) + \frac{e^{4U'}}{W}(a'_{,\rho}{}^2 - a'_{,\zeta}{}^2) - W(U'_{,\rho}{}^2 - U'_{,\zeta}{}^2) = 0 , \quad (2.13f)$$

where ∇^2 and ∇ are the Laplace and del operators on scalar potentials as if ρ and ζ were **Cartesian coordinates** and where a comma denotes partial derivatives.

To find solutions of these Einstein field equations, one must first solve the three first equations in (2.13) for U' , a' and W in the whole spacetime, such that the asymptotic conditions in (2.2), $a'(\rho = 0, \zeta) = 0$ and $W'(\rho = 0, \zeta) = 0$ hold.³ Then, k' can be obtained via a line integration in Eq.(2.13e) and (2.13f) such that along the rotation axis ($\rho = 0$) the condition

$$e^{k'} = \lim_{\rho \rightarrow 0} \frac{W}{\rho}$$

also holds. Eq.(2.13d) is then fulfilled automatically.

An ingredient missing for solving the Einstein FE is an equation of state (EOS), relating ϵ and p . Specifying an EOS provides the solution with an absolute scale and the solution is then specified by choosing two extra physical parameters (e.g. mass, angular momentum, central pressure, equatorial radius of the body...). The absolute scale can be “hidden” if we use normalized dimensionless coordinates, which thus gives a solution independent of scale.

2.2. The Vacuum Domain

Consider now the vacuum region exterior to the mass distribution and extending to infinity. The right hand sides of the field equations in vacuum vanish because of $\epsilon = p = 0$.

³Since we are restricting our attention to the axis, the asymptotic behaviour is the same in both non-rotating and co-rotating frames.

In this region, there exists a conformal coordinate transformation⁴ $z' = z'(z)$, where $z' := \rho' + i\zeta'$ and $z := \rho + i\zeta$ allowing one to choose $\rho'(\rho, \zeta) = W(\rho, \zeta)$, which then leads to

$$ds^2 = e^{-2U} [e^{2k'} (d\rho'^2 + d\zeta'^2) + \rho'^2 d\varphi^2] - e^{2U} (ad\varphi + dt)^2 . \quad (2.14)$$

This is the metric in canonical Weyl coordinates. The Cauchy-Riemann conditions for the transformation from (2.1) to (2.14) imply $W_{,\rho\rho} + W_{,\zeta\zeta} = 0$, which is valid only in the vacuum domain by virtue of (2.13c) and thus justifies our restricting ourselves to that region here. Now, we need to introduce two interesting formalisms which are valid in this domain of spacetime: a complex gravitational potential defined by Ernst, Kramer and Neugebauer, and the gravitational multipole moments defined by Geroch and Hansen.

2.2.1. The Ernst Equation

With the Einstein FE in the vacuum written in Weyl coordinates, Eq.(2.13b) may be regarded as the integrability condition for the existence of a function $b(\rho', \zeta')$ defined by

$$b_{,\rho'} = -\frac{e^{4U}}{\rho'} a_{,\zeta'} \quad \text{and} \quad b_{,\zeta'} = \frac{e^{4U}}{\rho'} a_{,\rho'} . \quad (2.15)$$

In other words, Eq.(2.13b) becomes $b_{,\rho'\zeta'} = b_{,\zeta'\rho'}$, and it implies that b must satisfy a new field equation

$$(\rho' e^{-4U} b_{,\rho'})_{,\rho'} + (\rho' e^{-4U} b_{,\zeta'})_{,\zeta'} = 0 , \quad (2.16)$$

which is the integrability condition $a_{,\rho'\zeta'} = a_{,\zeta'\rho'}$. By combining Eqs (2.16) and (2.13a) in the vacuum, the Einstein equations governing a and e^{2U} can be rewritten using the single, complex Ernst equation [Ern68,KN68]

$$(\Re f) \nabla^2 f = \nabla f \cdot \nabla f , \quad (2.17)$$

where f is the complex function $f := e^{2U} + ib$. Also, e^{2U} and b are obviously real, so $\Re f \equiv e^{2U}$, and ∇^2 and ∇ are respectively the Laplace and the gradient operators in a three dimensional Euclidean space, as if ρ' , ζ' and φ are **cylindrical coordinates**. To fit with Eqs(2.2), the behaviour of the potential at infinity must be

$$f = 1 - \frac{2M}{r} + \frac{2(M^2 - iJ \cos \theta)}{r^2} + \mathcal{O}\left(\frac{1}{r^3}\right) , \quad (2.18)$$

⁴The prime notation that we use now identifies the Weyl coordinates, so it has nothing to do with the prime notation which identified the “co-rotating frame” in the previous section.

where $r := \sqrt{\rho'^2 + \zeta'^2}$ and $\tan \theta := \rho'/\zeta'$.

Once a and U have been solved for, the metric function k' can be calculated via a line integral. Solutions of the Ernst equation lead to solutions of the Einstein equations and the metric potentials in the vacuum can be calculated from:

$$a_{,\rho'} = \rho' e^{-4U} b_{,\zeta'} \quad (2.19a)$$

$$a_{,\zeta'} = -\rho' e^{-4U} b_{,\rho'} \quad (2.19b)$$

$$k'_{,\rho'} = \rho' [U_{,\rho'}^2 - U_{,\zeta'}^2 + \frac{e^{-4U}}{4} (b_{,\rho'}^2 - b_{,\zeta'}^2)] \quad (2.19c)$$

$$k'_{,\zeta'} = 2\rho' [U_{,\rho'} U_{,\zeta'} + \frac{e^{-4U}}{4} b_{,\rho'} b_{,\zeta'}]. \quad (2.19d)$$

Not only the form (2.17) of the Ernst equation is valid in both the “co-rotating” and “non-rotating” frame, the Laplace and gradient operators can also be used in other 3-dimensional Euclidean coordinate systems.

The Ernst equation is a powerful tool to solve the Einstein field equations of axisymmetric and stationary spacetimes in the vacuum since once we have a solution for f , the whole metric (2.14) can then be systematically determined. On the other hand, this formalism cannot be extended inside matter, so it is not sufficient to generate global solutions.

2.2.2. The Multipole Moments

From the Ernst potential f , one can define another complex gravitational potential ξ :

$$\xi = \frac{1-f}{1+f} \quad \Leftrightarrow \quad f = \frac{1-\xi}{1+\xi}. \quad (2.20)$$

Taking the potential ξ on the positive part of the axis of rotation ($\rho' = 0$, $\zeta' > 0$), we can make a series expansion of it at infinity:

$$\xi(\rho' = 0, \zeta') = \sum_{n=0}^{\infty} \frac{m_n}{\zeta'^{m+1}}. \quad (2.21)$$

By assuming reflectional symmetry about the equatorial plane, which is expected for stationary fluid figures in equilibrium, it follows that m_n is real for even n and imaginary for odd n [Kor95, MN95].

The multipole moments P_n defined by Geroch [Ger70] and Hansen [Han73] are algebraic combinations of the coefficients m_n and characterize the Ernst potential uniquely.

An algorithm is presented in [FHP89] which generates the infinite set of P_n as a function of the m_n . In this work, we will extract the first multipoles of fluid solutions, so we write down here the 7 first multipole moments that will be calculated later:

$$P_j = m_j \quad \text{for } j = 0, 1, 2, 3 \quad (2.22a)$$

$$P_4 = m_4 - \frac{1}{7}M_{20}m_0 \quad (2.22b)$$

$$P_5 = m_5 - \frac{1}{3}M_{30}m_0 + \frac{1}{21}M_{20}m_1 \quad (2.22c)$$

$$P_6 = m_6 - \frac{1}{33}M_{20}m_0^3 - \frac{5}{231}M_{20}m_2 \\ + \frac{4}{33}M_{30}m_1 - \frac{8}{33}M_{31}m_0 - \frac{6}{11}M_{40}m_0, \quad (2.22d)$$

where $M_{jk} \equiv m_j m_k - m_{j-1} m_{k+1}$. These multipoles can then be normalized as follows:

$$y_n = i(-2i\Omega)^{n+1} P_n. \quad (2.23)$$

For the Kerr black hole, the multipole moments are simply

$$P_n^{(\text{Kerr})} = M(iJ/M)^n, \quad (2.24)$$

where M and J are respectively the mass and the angular momentum of the black hole. Let Ω_H be the angular velocity of the horizon. This quantity is the analogue of the constant angular velocity Ω of rotating matter. Using the relation

$$J = \frac{2M^2(2\Omega_H M)}{1 + (2\Omega_H M)^2}. \quad (2.25)$$

we then find

$$y_n^{(\text{Kerr})}(y_0) = y_0 \left(\frac{2y_0^2}{1 + y_0^2} \right)^n. \quad (2.26)$$

Through this normalization, all multipoles y_n vary at a different rate from zero for the Schwarzschild BH to one for the extreme Kerr BH, as can be seen by taking respectively $y_0 = 2\Omega_H M = 0$ or 1.

2.3. The Black Hole Limit of Fluid Bodies in Equilibrium

It is usually shown in the first or second lecture of general relativity, that a spherically symmetric relativistic model star of uniform density with mass M and radius R cannot

be compressed beyond the limit $R/R_S = 9/8$ (R_S is the Schwarzschild radius) without dynamically collapsing, since the pressure in the centre of the body becomes infinite. The same logic can be extended to a larger class of equations of state for which the energy density decreases monotonically from the centre of the star to its surface: static stars can only be in equilibrium for $R/R_S > 9/8$. There is no continuous sequence of static fluid bodies in equilibrium leading to a black hole.

However, we could ask if a continuous sequence of fluid bodies in equilibrium can exist for the more general class of stationary and axisymmetric spacetimes. For the static case, the Tolman-Oppenheimer-Volkoff equation is used to relate the radius of a star to its pressure in the centre. With such an approach in the rotating case, we would probably be restricted to searching for a black hole limit through numerical methods for different rotating star configurations near the infinite pressure limit. Instead, we should begin by asking what conditions need to be satisfied for a fluid body in equilibrium to realize in the limit a black hole.

2.3.1. Necessary and Sufficient Conditions for a Black Hole Limit

The horizon of a black hole can be intuitively described as a hypersurface boundary, where it becomes impossible for events “inside the boundary” to have time-like or null-like curves that can reach and influence the future of the domain “outside the boundary”. The usual mathematical approach to define a horizon is to identify it as a null hypersurface, i.e. a hypersurface whose normal at every point is a null vector ($n^\alpha n_\alpha = 0$). In the case of the Kerr BH, the horizon corresponds to the condition $e^{2V} = 0$ and a normal vector can be obtained by the gradient

$$e^{2V}{}_{,\alpha} = -2\kappa(\xi_\alpha + \Omega_H \eta_\alpha) ,$$

where κ and Ω_H are respectively the surface gravity and the angular velocity of the horizon, related to the mass M and angular momentum J of the black hole by

$$\kappa = \frac{\sqrt{M^2 - (J/M)^2}}{2M \left[M + \sqrt{M^2 - (J/M)^2} \right]} , \quad \Omega_H = \frac{J}{2M^2 \left[M + \sqrt{M^2 - (J/M)^2} \right]} . \quad (2.27)$$

Thus, the only linear combination of Killing vectors which does not become space-like on the horizon of a black hole is a null one:

$$(\xi^\alpha + \Omega_H \eta^\alpha)(\xi_\alpha + \Omega_H \eta_\alpha) = 0 . \quad (2.28)$$

On the other hand, the surface of a fluid body, characterized by the 4-velocity field of Eq.(2.6) and the constant potential $U' \equiv V = V_0$, has the surface condition

$$(\xi^\alpha + \Omega \eta^\alpha)(\xi_\alpha + \Omega \eta_\alpha) = -e^{2V_0} , \quad (2.29)$$

because the norm of 4-velocities is always $u^\alpha u_\alpha = -1$. If a continuous sequence of fluid figures in equilibrium can reach a black hole limit, it must be a sequence of bodies with time-like rotating velocity. Then, the surface of the body can only approach the limit of a BH horizon for $\Omega = \Omega_H$, the only non-space-like Killing vector combination on a horizon. Comparing Eqs (2.29) and (2.28), we see that a sequence of fluid surfaces requires $V_0 \rightarrow -\infty$ to approach, in the limit, a horizon surface. We will see now that this condition puts a constraint on the mass and angular velocity of a fluid body.

From Eqs(2.7), the mass and angular momentum of a rotating fluid are related through

$$M = 2\Omega J + \int \frac{\epsilon + 3p}{\epsilon_B} e^V dM_B ,$$

where we use the short form $dM_B \equiv \epsilon_B e^{2k' - 3V} W d\rho d\zeta d\varphi$. Substituting the baryonic mass with Eq.(2.9) and using the property $h(p)e^V = h(0)e^{V_0}$, we get

$$M = 2\Omega J + e^{V_0} h(0) \int \frac{\epsilon + 3p}{\epsilon + p} dM_B .$$

We can easily see that the integral can range only from M_B to $3M_B$. If we assume that $h(0)M_B$ is always finite, the limit $V_0 \rightarrow -\infty$ gives the constraint

$$M = 2\Omega J .$$

The Kerr BH that has a mass and angular momentum such that $M = 2\Omega_H J$ is the extreme Kerr BH, where $\Omega_H = \pm 1/(2M)$ and $J = \pm M^2$. Since we stated above that the black hole limit can only be reached for $\Omega = \Omega_H$, the conclusion from [Mei04] is that the only possible candidate for a black hole limit of fluid bodies in equilibrium is the extreme Kerr BH, characterized by $J = \pm M^2$.

A question that arises now: does a fluid body with $V_0 \rightarrow -\infty$ necessarily have an event horizon? If we consider the specific energy of Eq.(2.12) for particles of fluid resting on the surface of the source, with the 4-velocity of Eq.(2.6), it reads

$$-e^{V_0} E = (\xi^\alpha + \Omega \eta^\alpha) \xi_\alpha .$$

Assuming that particles on the surface are at least marginally bound ($E \leq 1$), the last equation implies in the limit $V_0 \rightarrow -\infty$ that

$$(\xi^\alpha + \Omega \eta^\alpha)\xi_\alpha \rightarrow 0, \quad \text{and thus} \quad (\xi^\alpha + \Omega \eta^\alpha)\eta_\alpha \rightarrow 0.$$

Thus, the Killing vector $(\xi^\alpha + \Omega \eta^\alpha)$ becomes orthogonal to ξ_α and η_α on the surface of the fluid, and because the Killing vectors ξ^α and η^α are always orthogonal to surfaces of constant (φ, t) , it can be seen that the vector $(\xi^\alpha + \Omega \eta^\alpha)$ becomes orthogonal to three linearly independent tangent vectors at each point of the fluid hypersurface. Then, $(\xi^\alpha + \Omega \eta^\alpha)$ is a normal vector at every point of that hypersurface, and because of Eq.(2.29) and $e^{2V_0} = 0$, this normal vector is a null vector. The surface of the fluid corresponds to a null hypersurface and then satisfies the conditions for a horizon. Therefore, the metric of an extreme Kerr BH results outside the horizon, whenever a sequence of fluid bodies admits the limit $V_0 \rightarrow -\infty$ [Mei06].

2.3.2. The Extreme Kerr Black Hole Geometry

Because the extreme Kerr solution results in the black hole limit of fluid bodies, some basic information should be given about it. Some properties of the spacetime are particular and unique compared to the Kerr solution in general. The extreme Kerr BH is uniquely characterized by a single physical parameter; it is usual to choose either M , J or Ω , which are related through:

$$J = M^2, \quad M = 2\Omega J \quad \text{or} \quad 2\Omega M = 1. \quad (2.30)$$

With the spherical-like version of Weyl coordinates $r = \sqrt{\rho'^2 + \zeta'^2}$ and $\tan \theta = \rho'/\zeta'$, the Ernst potential of the extreme Kerr BH reads

$$f = \frac{r/M - 1 - i \cos \theta}{r/M + 1 - i \cos \theta}. \quad (2.31)$$

The metric can be rewritten using Eqs(2.19), and it takes the form

$$ds^2 = e^{-2U} [e^{2k} (dr^2 + r^2 d\theta^2) + r^2 \sin^2 \theta d\varphi^2] - e^{2U} (ad\varphi + dt)^2,$$

with the following metric potentials:

$$e^{2U} = \frac{r^2 - M^2 \sin^2 \theta}{(r + M)^2 + M^2 \cos^2 \theta},$$

$$a = \frac{2M^2(r+M)\sin^2\theta}{r^2 - M^2\sin^2\theta},$$

$$e^{2k} = \frac{r^2 - M^2\sin^2\theta}{r^2}.$$

The transformation of the metric into the better known Boyer-Lindquist coordinates can be achieved using the substitution $r = r_{BL} - M$, with r_{BL} being Boyer-Lindquist's radial coordinate. Note that this last substitution holds only for the extreme Kerr BH; more complicated transformation relations are needed to link the Weyl-Lewis-Papapetrou coordinates with Boyer-Lindquist coordinates for the whole class of the Kerr solution.

The most particular property of the extreme Kerr BH is certainly its degenerated horizon. The event horizon of the black hole is the surface where g_{rr} goes to infinity, which occurs here at $r = 0$, i.e. in a single point at the origin of the coordinate system. The Weyl coordinates do not show it very well, but the horizon still has a finite area $A = 8\pi M^2$ and the point $r = 0$ contains an infinite 3-dimensional volume, as we can see by measuring a proper radial distance from the centre

$$\delta(R) = \int_0^R \sqrt{g_{rr}} \, dr = \int_0^R \sqrt{\left(1 + \frac{M}{r}\right)^2 + \frac{M^2 \cos^2 \theta}{r^2}} \, dr = \infty \quad (2.32)$$

for any radial coordinate R outside the origin ($R > 0$). The geometry at the origin can be better described by transforming the Weyl coordinates into a new set of coordinates proposed by Bardeen and Horowitz [BH99]:

$$r = \lambda r', \quad \theta = \theta', \quad \varphi = \varphi' + \frac{t'}{2M\lambda}, \quad t = \frac{t'}{\lambda}.$$

In the limit $\lambda \rightarrow 0$, a new line element reveals a infinitely long “throat geometry” for the corresponding origin in Weyl coordinates:

$$ds^2 = \frac{1 + \cos^2 \theta'}{2} \left[\frac{2M^2}{r'^2} dr'^2 + 2M^2 d\theta'^2 - \frac{r'^2}{2M^2} dt'^2 \right] + \frac{4M^2 \sin^2 \theta'}{1 + \cos^2 \theta'} \left[d\varphi' + \frac{r'}{2M^2} dt' \right]^2.$$

This metric is no longer asymptotically flat at spatial infinity. In the case of fluid bodies reaching the black hole limit, the throat geometry realizes a separation between two infinitely distant worlds. At one extremity of the throat, an outside world has the expected extreme Kerr BH solution, with the throat located near the horizon. At the other extremity, an inner world contains the source around its centre and has the throat

geometry at its spatial infinity. It should be noted that the horizon is a feature of the throat geometry, so the surface of the fluid does not become a horizon. When we required in 2.3.1 that the body's surface needs to satisfy the conditions on the horizon, it was from a typical point of view of the outside world, where it becomes impossible to distinguish the throat from the source: they are both located at the origin of the Weyl coordinate system.

Thus, it is possible to fit different solutions with matter in the inner world without affecting the gravitational field of the outside world, as long as the parameters in (2.30) are kept constant. It has been found that the inner world can contain matter such as rings of perfect fluid or a rigidly rotating disk of dust. Moreover, continuous sequences of stationary and axisymmetric solutions exist for these bodies, from the Newtonian limit to the extreme Kerr-BH limit. These given examples will be the central topics of the next two chapters.

3. Strange Matter Stars and their Parametric Transition to a Black Hole

Today, astronomical observations have identified more than a thousand compact objects thought to be neutron stars, most of them being pulsars. Although there is little doubt as to their existence, there is still much debate as to the properties of the extremely high density matter that comprises them. One of the competing models to describe neutron stars includes strange quark matter: matter that contains a mixture of strange quarks along with the usual up and down quarks. It is even suggested that strange quark matter could be more stable than nuclear matter, in which case “neutron stars” could in fact be mainly composed of a pure quark matter core surrounded by a thin nuclear matter crust [Web05].

In this chapter, we will consider a stellar model made entirely of strange quark matter. Solutions are produced by numerical methods. We first produce a class of solutions with spheroidal topology, then we will look in detail at the parametric transition of strange matter rings to a black hole. The approach we use to study this transition differs from those in other papers [NM95, Mei02, AKM03b, FHA05], since we here concentrate on the behaviour of multipole moments and on the appearance of a region of spacetime typical of metrics close to the extreme Kerr limit. The properties of axially symmetric and stationary strange matter have already been studied for spheroidal configurations [GHL⁺99], but they have not yet been considered for ring topologies and their parametric transition to a black hole. Moreover, we include a comparison with the corresponding transitions of rings governed by other equations of state.

The main results of this chapter were published in [LPA07].

3.1. Model and Method used for Relativistic Strange Stars

3.1.1. Equation of State

Our equation of state is based on the MIT bag model [CJJ⁺74, CJJT74, FJ84, AFO86]. Under extremely high pressure, the nuclear boundaries of “neutron star” matter may dissolve to create a phase of a deconfined Fermi gas of quarks, i.e. quarks do not

form hadrons anymore. Up (u) and down (d) quarks could convert to other flavours with the weak interactions in order to reach a state of lower Fermi energy. But if we consider the mass of each flavour of quarks, only the strange (s) quark ($m_s \approx 0.1$ GeV) would be added to the quark population since the others have much larger masses ($m_c, m_b, m_t > 1$ GeV) than the chemical potentials involved (~ 0.3 GeV). Electrons can also be present in order to keep the star electrically neutral. Chemical equilibrium between the different fermions is maintained via weak interactions:

$$d \leftrightarrow u + e^- + \bar{\nu}_e, \quad s \leftrightarrow u + e^- + \bar{\nu}_e, \quad s + u \leftrightarrow d + u. \quad (3.1)$$

The two first reactions involve neutrino escape which cools down the star to near zero temperature in comparison to the Fermi energy of the quarks. One obtains from the weak interactions of Eq.(3.1) the following chemical potential relations:

$$\mu_u + \mu_e = \mu_d = \mu_s \equiv \mu.$$

In its simplest form, the bag model ignores the strong interaction and assumes the mass of the three light quark flavours to be zero. The equilibrium configuration of massless quarks has equal numbers of each flavour. Thus, the quark population becomes electrically neutral and the electron population vanishes. With all these considerations, the thermodynamic Landau potential of each flavour reads

$$\Omega_q = -\frac{\mu_q^4}{4\pi^2} \quad \text{for } q = u, d, s.$$

The QCD confinement of the quarks is established by a constant energy density B , the ‘‘bag constant’’, which describes the energy difference between the QCD vacuum and the true vacuum. When summed, the pressures p_q and energy densities ϵ_q of each quark flavour are related to the total pressure p and total energy density ϵ in the star according to

$$\begin{aligned} \epsilon - B &= \sum_q \epsilon_q = \sum_q \left(\Omega_q - \mu_q \frac{\partial \Omega_q}{\partial \mu_q} \right) = \frac{9\mu^4}{4\pi^2}, \\ p + B &= \sum_q p_q = \sum_q -\Omega_q = \frac{3\mu^4}{4\pi^2}. \end{aligned}$$

These two last equations lead to a simple equation of state (EOS):

$$\epsilon - 3p = 4B . \quad (3.2)$$

One can see that for any pressure, the bag constant maintains the quark gas at finite density. The limits of the bag correspond in our case to the surface of the star, such that the star is entirely composed of strange matter. Thus, like the homogeneous EOS, but unlike polytropic models, the density of strange matter is discontinuous at the surface. Sometimes, we will compare results of strange quark stars with homogeneous fluids which has the EOS $\epsilon = \text{constant}$.

The bag constant B constitutes a natural unit to normalize most physical quantities into dimensionless values. A typical estimate of this constant is $B = 60 \text{ MeV fm}^{-3} = 9.6 \times 10^{33} \text{ J/m}^3$ [GHL⁺99]. Using the solar mass as a second natural unit (with $G = c = 1$), this estimate translates to $B^{-1/2} = 76.0 M_{\odot}$ (e.g. a star with $M = 2 \times 10^{-2} B^{-1/2}$ would mean $M = 1.52 M_{\odot}$). For the baryonic mass, dimensionless values should be given by taking into account the specific enthalpy from Eq.(2.9). The enthalpy of our model is given by

$$h(0) = \frac{E_0^{(\text{uds})}}{E_0^{(\text{ud})}}$$

which is the ratio between the energy per unit baryon number of strange quark versus normal matter at zero pressure. A typical estimate for this ratio is $h(0) = 0.899$, which leads to $(h(0)\sqrt{B})^{-1} = 84.5 M_{\odot}$ with the values given here. It is interesting to note that $E_0^{(\text{uds})} < E_0^{(\text{ud})}$ suggests that strange quark matter would be the true ground state of matter at zero pressure.

In the Newtonian limit, the pressure p is low and negligible in comparison to B , so the EOS takes the form $\epsilon = \text{constant}$. Therefore, all the known Newtonian solutions for homogeneous bodies will be found in the Newtonian limit of the MIT bag model. If unstable at low pressure, a quark model of matter is not relevant in the Newtonian limit, but it is taken as a limiting case of our EOS. In the most relativistic equilibrium configurations, the star can reach either infinite central pressure or infinite redshift on its surface. This first relativistic limit concerns stars with spheroidal topology, while the latter corresponds to the extreme Kerr BH limit for a class of stars with ring topology.

3.1.2. The Ansorg-Kleinwächter-Meinel Numerical Method

To generate relativistic solutions of stationary and axially symmetric fluid configurations, we used a numerical method described in [AKM03a]. In the AKM-method, the entire spacetime is compactified and divided in several domains. Because of stationarity, axial and equatorial symmetries, only one quadrant of the $\rho - \zeta$ half-plane needs to be represented in the compactification. For a given solution, the metric potentials from Eq.(2.1) are written, using the proper coordinate mapping of each domain, as a spectral expansion in the form of Chebyshev polynomials of the first kind. The Chebyshev polynomial must reproduce a numerically accurate solution of Einstein field Eqs(2.13) on a finite set of discrete grid-points covering the domain and the inter-domain boundaries. To avoid a ‘‘Gibbs phenomenon’’ on the fluid surface discontinuity, one of the domain boundaries is chosen to coincide with the surface.

By giving an initial solution, the AKM-method calls iteratively the Newton-Raphson method in order to simultaneously find the metric potentials of a targeted nearby fluid configuration which must be a solution of Einstein’s FE on the given grid-points. Through each iteration, the search is constrained by inter-domain boundary conditions and regularity conditions on the rotation axis and at spatial infinity. However, the search has to determine the shape of the fluid surface where the metric potentials and their first derivatives inside and outside the matter must behave continuously through the boundary. By fixing two independent physical parameters and by choosing a scaling parameter for the coordinates, it should lead to a unique neighbouring solution. The solution is finally given in a numerical list of Chebyshev coefficients from which one can compute the metric potentials.

In our search of new configurations, we use some physical parameters not yet mentioned, such as the ratio r_p/r_e of polar to equatorial coordinate radius and a mass-shed parameter β defined as:

$$\beta = -\frac{r_e^2}{r_p^2} \frac{d(\zeta_s^2)}{d(\rho^2)} \Big|_{\rho=r_e} = -\frac{r_e}{r_p^2} \lim_{\rho \rightarrow r_e} \zeta_s \frac{d\zeta_s}{d\rho}$$

where $\zeta_s = \zeta_s(\rho)$ is the ζ -axis position of the surface as a function of ρ . The mass-shedding limit (also called Keplerian limit in other texts) is characterized by $\beta = 0$, while the case where $\beta = 1$ holds for static solutions and Maclaurin spheroids. Fig. 3.1 shows an example of a strange star configuration in equilibrium, here at the mass-shedding limit with a cusp appearing on the surface equator.

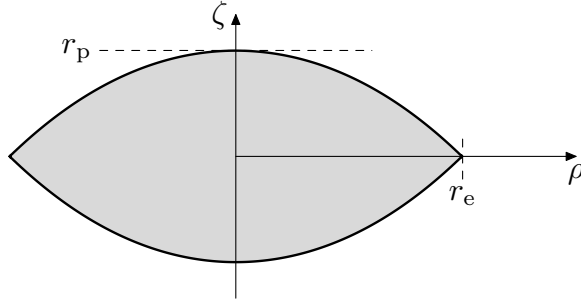


Figure 3.1: Example of a meridional cross-section of a strange matter star. The star in this example is at the mass-shedding limit, near the maximal gravitational mass configuration of the “Schwarzschild” class, with $\sqrt{B} M = 3.72 \times 10^{-2}$.

3.2. Solutions of Strange Quark Matter

3.2.1. The Schwarzschild Class of Strange Quark Matter

For homogeneous stars, it was shown that not all relativistic configurations in equilibrium are connected continuously to each other [SA03, AFK⁺04]. Starting with a static star ($\Omega = 0$) with an arbitrary central pressure p_c , one can then change the parameters to find continuous sequences of nearby equilibrium configurations that are bound by

- static solutions ($\Omega = J = 0$ or $\beta = r_p/r_e = 1$) with $p_c \in [0, \infty]$,
- stars at infinite central pressure $p_c = \infty$ with $\beta \in [0, 1]$,
- stars at the mass-shedding limit $\beta = 0$ with $p_c \in [0, \infty]$,
- Newtonian (non-Maclaurin) flat stars at $p_c = 0$ with $\beta \in [0, 1]$,
- Newtonian Maclaurin spheroids ($p_c = 0$ and $\beta = 1$) with $r_p/r_e \in [0.17126\dots, 1]$.

We call it the Schwarzschild class, although it obviously does not contain only static bodies. It is the class of bodies which contains the most relevant configurations for astrophysics.

In the case of strange quark matter, we can confirm that a Schwarzschild class exists with the same five boundaries as for homogeneous stars. Since the Newtonian limit of strange matter has the same EOS as homogeneous fluids, the two Newtonian limit sequences (Maclaurin and non-Maclaurin) have in all aspects the same physical characteristics as those of homogeneous fluids with the same constant energy density. But

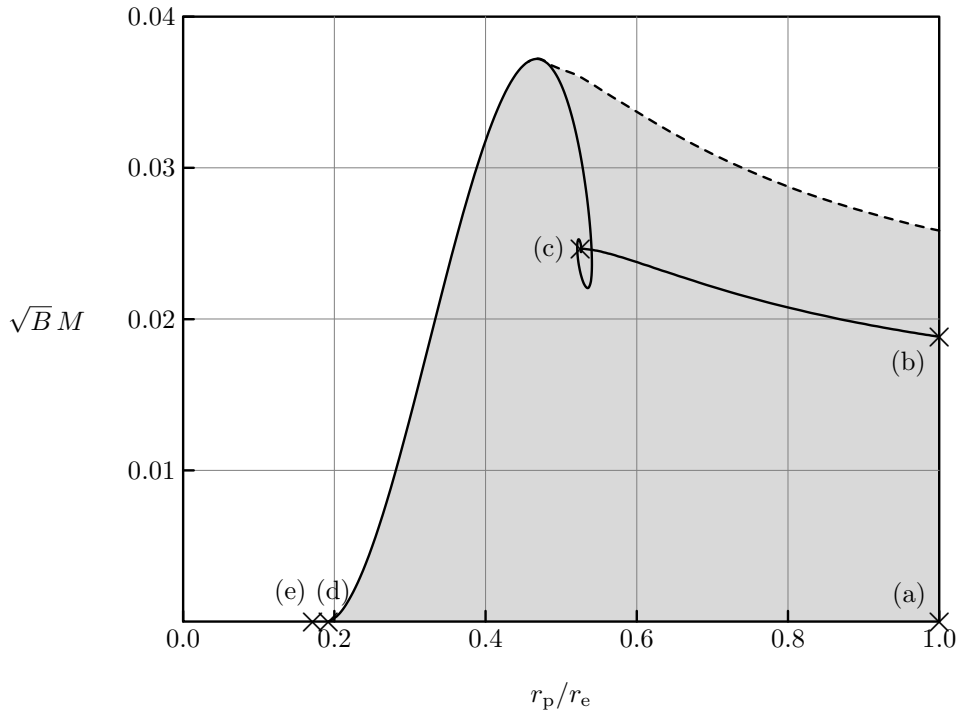


Figure 3.2: Gravitational mass of the Schwarzschild class for strange matter stars as a function of the flatness (r_p/r_e -ratio). Equilibrium configurations (grey zone) are bounded by sequences of static (a-b), infinite central pressure (b-c), mass-shedding (c-d), non-Maclaurin Newtonian flat stars (d-e) and Maclaurin spheroids (e-a) configurations. The class is folded on the upper right and the dashed line marks the maximal extension of the mass within the class.

as the configurations become more relativistic, the behaviour of strange stars differs significantly.

An important property of strange matter stars is well illustrated by comparing our Fig. 3.2 with the analogous Fig. 3 in [SA03] for homogeneous density. The Schwarzschild class of strange matter is such that for typical sequences running from zero pressure to infinite central pressure, the configuration with maximal mass is one with finite pressure. In the case of homogeneous stars on the other hand, the mass increases monotonically as the central pressure increases.

For strange matter, such a sequence of maximal mass dividing the class suggests that a region of this class might be unstable. Indeed, a test of stability using Eq.(2.11) shows us that configurations with higher central pressures are unstable. In articles concerning strange matter stars, the stability with respect to axisymmetric perturbations is usually illustrated by showing the mass-radius relationship [KWWG95]. This is done here in

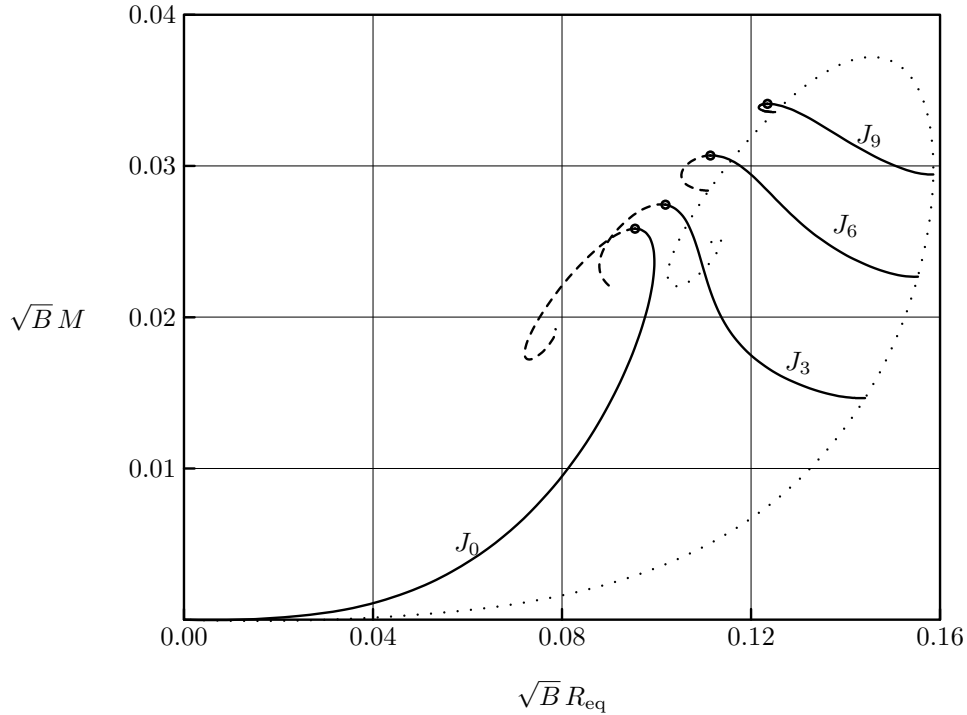


Figure 3.3: Relation between the circumferential radius R_{eq} on the equator and the gravitational mass M . Curves of constant angular momentum J_0, J_3, J_6, J_9 are respectively for $BJ = 0, 3 \times 10^{-4}, 6 \times 10^{-4}, 9 \times 10^{-4}$. The dots mark maximal masses, the dashed lines are the unstable part of the constant J sequences. The dotted line represents the sequence of configurations at mass-shedding limit and the Newtonian configurations are at origin.

Fig. 3.3, where we plot different sequences of constant angular momentum J . Each sequence with non-zero angular momentum begins with a relatively low mass along the mass-shedding limit, then the mass increases until it reaches maximum before decreasing again. The maximal mass of each sequence marks the limit of stability. On the unstable side of the sequences, J_0 (static) and J_3 evolve until the central pressure becomes infinite, while J_6 and J_9 are examples of sequences which end again on a mass-shedding limit.

Considering again that a configuration with extremal mass marks a limit of stability along sequences of constant angular momentum, we can notice in Fig. 3.3 that minima seem to exist along the mass-shedding limit. By looking more carefully, it appears that a tiny “valley” of minimal mass exists very near of this limit. Although our numerical solutions show with confidence these tiny minima inside the class, the resolution was insufficient to conclude which side of the “valley” should be unstable.

The Schwarzschild class can be summarized in Fig. 3.4 where the entire domain of equilibrium configurations fits into a rectangle parameterized by the mass-shedding parameter and a normalized central pressure. One can recognize the static solutions on the right side, the infinite central pressure boundary on the top, the mass-shedding limit on the left and Newtonian boundary at the bottom, with the entire Maclaurin sequence degenerated in the lower right corner (white dot). Different sequences of constant angular momentum (J -sequences) and constant baryonic mass (N -sequences) are shown as examples.

The constant N -sequences always start at a mass-shedding limit and they either stop on the static sequence or join again to the mass-shedding limit. These sequences interested Gourgoulhon et al. [GHL⁺99] since they represent evolutionary sequences of stars which slowly loose energy and angular momentum via electromagnetic or gravitational radiation. It turns out that a category of stars with baryonic masses higher than the value along the N_{crit} -sequence, $h(0)M_B = 3.106 \times 10^{-2} B^{-1/2}$, exist only if they rotate.

The constant J -sequences also start at mass-shedding limit and finish either at another mass-shedding limit or with infinite central pressure. Along them, configurations with maximal and minimal masses were found and are represented here by the full line. One configuration has the maximal angular momentum (black dot), with $J = 1.226 \times 10^{-4} B^{-1}$, which is very near but not exactly on the mass-shedding limit. It joins the sequences of maximal and minimal masses. The maximal mass sequence has a sharp turn near the mass-shedding limit and parallels this limit without joining it. Because of poorer numerical resolution near the limit, it was not clear which side contains the unstable configurations, like for the minimal mass sequence. As can be seen in Fig. 3.3, the minimal mass is always less than 0.1% smaller than the mass of the mass-shed configuration with same J . So physically speaking, it might be irrelevant to declare one side of the minimal mass sequence to contain unstable configurations since there is little expectation that real strange stars would be so accurately bound to this ideal model that we use. The grey shading in the figure represents the domain of axisymmetric stability including the inconclusive area near the mass shedding limit.

Some extreme configurations for the whole Schwarzschild class are presented in table 3.2 while table 3.1 is restricted to static configurations. The maximal red shift configurations, considering either static or rotating stars, are unstable with regard to axisymmetric perturbations. Instability also occurs for the configuration with maximal angular momentum. When data can be compared with [GHL⁺99], no difference is observed for static configurations, while differences are small for rotating bodies, but larger

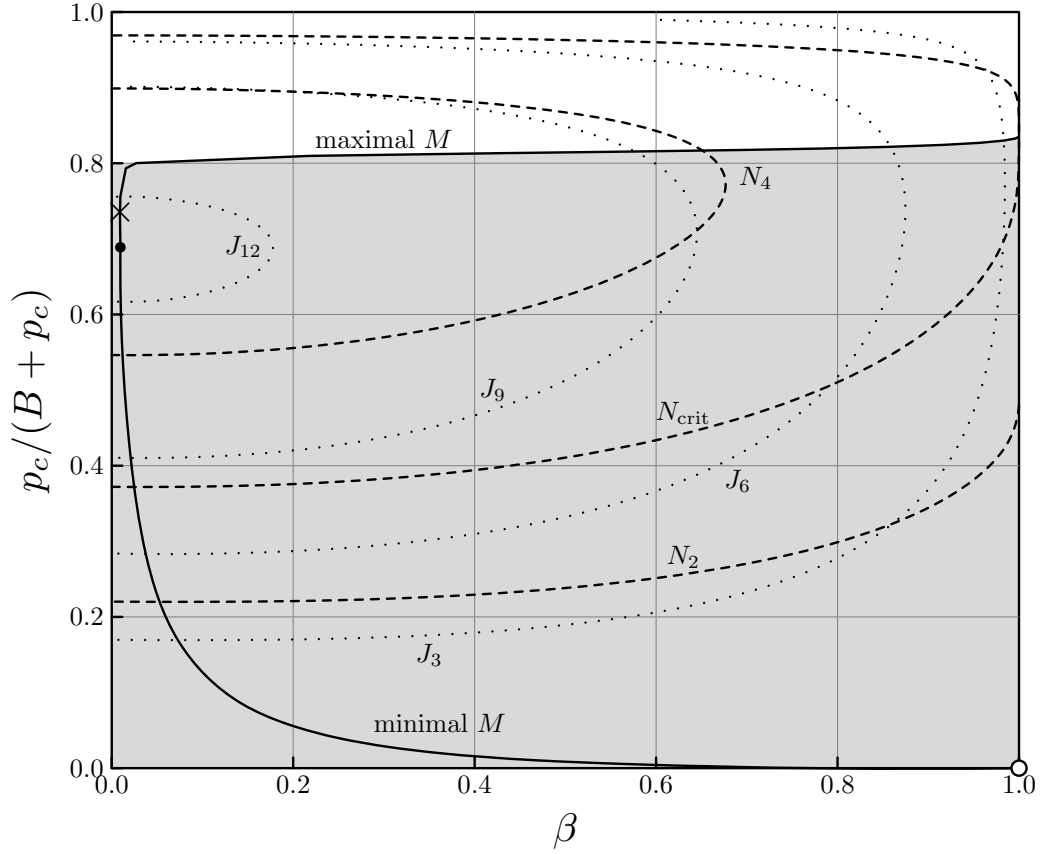


Figure 3.4: The Schwarzschild class as function of the mass-shedding parameter β and a normalized central pressure parameter. The white circle, black dot and cross mark respectively the Maclaurin sequence, the maximal angular momentum and the maximal gravitational mass configurations. The full line represent the maximal and minimal masses along sequences of constant angular momentum (separated by the black dot). Dotted lines are examples of sequences with constant angular momentum with $BJ = 3 \times 10^{-4}$, 6×10^{-4} , 9×10^{-4} , 12×10^{-4} while dashed lines N have constant number of quarks with $h(0)\sqrt{B}M_B = 2 \times 10^{-2}$, 3.106×10^{-2} , 4×10^{-2} .

Configuration	ϵ_c^*	M^*	M_B^*	R_{circ}^*	Z_0
max. circ. rad.	10.260	2.3653	2.7960	9.9545	0.38041
max. mass	19.251	2.5842	3.1061	9.5453	0.47678
max. red shift	42.241	2.4340	2.8802	8.6750	0.50953

Table 3.1: Configurations of static (no rotation) strange stars with maximal circumferential radius, mass and red shift. The physical quantities are as follows: central energy density $\epsilon_c = B \epsilon_c^*$, gravitational mass $M = 0.01B^{-1/2} M^*$, baryonic mass $M_B = 0.01h(0)^{-1} B^{-1/2} M_B^*$, circumferential radius $R_{\text{circ}} = 0.01B^{-1/2} R_{\text{circ}}^*$ and red shift Z_0 .

Configuration	r_p/r_e	β	ϵ_c^*	M^*	M_B^*	J^*	Ω^*	Z_0
max. flatness	0.1713	1.00	0.000	0.000	0.000	0.000	2.094	0.0000
max. ang. moment.	0.4567	0.01	10.64	3.701	4.394	12.26	3.500	0.7775
max. mass	0.4687	0.01	12.37	3.721	4.437	12.13	3.614	0.8177
max. pol. red shift	0.5065	0.01	25.27	3.477	4.145	9.841	4.084	0.8895
max. ang. velocity	0.5452	0.04	197.6	2.432	2.706	4.202	4.719	0.6882

Table 3.2: Configurations of the entire Schwarzschild class with maximal flatness, angular momentum, mass, polar red shift and angular velocity. Some parameters are the same as in table 3.1 and the others are: polar to equator radius ratio r_p/r_e , mass shedding parameter β , angular momentum $J = 10^{-4}B^{-1}J^*$, angular velocity $\Omega = \sqrt{B}\Omega^*$ and polar red shift Z_0 .

than expected considering their accuracy; e.g. our maximal mass is $M = 2.828M_\odot$ and Gourgoulhon et al. give $M = 2.831M_\odot$ (using $B^{-1/2} = 76.0 M_\odot$). Although this is a 0.1% difference for the mass, this configuration from the same authors has a central density $\epsilon_c = 1.261 \times 10^{18} \text{ kg m}^3$ while our computation gives $\epsilon_c = 1.323 \times 10^{18} \text{ kg m}^3$, a 5% difference.

A quark matter model that takes into account the mass of quarks, such as Kettner et al. [KWWG95], suggests that heavier charm (c) quarks would begin to populate the matter at energy densities $\epsilon > 9 \times 10^{36} \text{ J/m}^3$, where the constant $B = 57.5 \text{ MeV fm}^{-3} = 9.22 \times 10^{33} \text{ J/m}^3$ is used. Based on our EOS in Eq.(3.2), such density needs a pressure beyond $B^{-1}p > 324$. With the help of Fig. 3.4, one can identify the stable configuration with the highest central pressure, which is the most massive static configuration. The pressure reaches $B^{-1}p = 5.0835$, which means that our simple model excludes the existence of stable stars with heavier quarks than the strange quarks.

The configuration with maximal flatness (table 3.2) lies at a bifurcation point between Maclaurin spheroids and non-Maclaurin Newtonian stars. This special configuration connects the Schwarzschild class to a new class of configurations: the ring class. It is

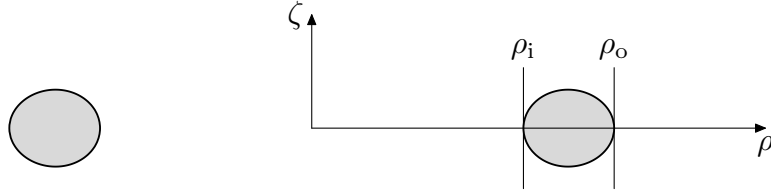


Figure 3.5: Example of a meridional cross-section of a strange matter ring. The ring in this example has the parameters $\rho_i/\rho_o = 0.7$ and $e^{2V_0} = 0.1$.

the only configuration that allows sequences of strange matter and homogeneous stars in equilibrium to exit the Schwarzschild class [AFK⁺04]. No configuration of this first class has an infinite red shift (the maximum reaches $Z_0 = 0.8895$) and so no star in equilibrium approaches the black hole limit: only a dynamical collapse can bridge a strange star to a black hole. On the other hand, the ring class contains figures of equilibrium that reach the black hole limit, so this class will interest us in the remaining part of this chapter.

3.2.2. The Ring Class of Strange Quark Matter

The ring class includes strange stars that have either spheroidal or toroidal topologies. The cross-section of a ring is given in Fig. 3.5 as an example. The ratio between the inner and outer radius ρ_i/ρ_o is a parameter of choice to characterize ring configurations. To represent rings and spheroids consistently, we introduce here a parameter A which takes the negative value $A = -\rho_i/\rho_o$ when it is a ring and the positive value $A = r_p/r_e$ for spheroids.

Sequences of strange matter bodies are again bound in the same way as for homogeneous bodies (see [AFK⁺04] for details):

- Newtonian “Dyson ring” sequence ($V_0 = 0$) with $A \in [0.17126\dots, -1]$,
- a ring singularity ($A = -1$) with two possible potentials ($V_0 = 0$ or $-\infty$),
- extreme Kerr black holes ($V_0 = -\infty$) containing rings with $A \in [-1, -0.58428\dots]$,
- bodies at the mass-shedding limit ($\beta = 0$) with $V_0 \in [-\infty, 0]$,
- Newtonian (non-Maclaurin) flat spheroids at $V_0 = 0$ with $\beta \in [0, 1]$,
- Newtonian Maclaurin spheroids with $r_p/r_e \in [0.11160\dots, 0.17126\dots]$.

The Newtonian limit of strange matter is always identical to that of homogeneous bodies. The ring singularity, an infinitely thin ring, is a limiting case where the surface potential

V_0 jumps to infinity if the ring is given a non-zero mass. The density of the ring would jump also to infinity and so, the physical interpretation of such a body is problematic. The ring singularity should be seen as a limiting case of the ring class and not as a physically relevant object.

A further comparison of rings of various EOS can be found in Fig. 3.6. Sequences of rings rotating at the mass-shedding limit, are plotted in a two-dimensional parameter space with $1 - e^{V_0}$ on the y -axis and ρ_i/ρ_o on the x -axis. The mass-shedding limit is reached when the path followed by a particle rotating at the outer edge of the ring becomes a geodesic. For a given EOS, other ring configurations (i.e. not rotating at the mass-shedding limit) lie to the left of the corresponding curve. One can see that a transition to the extreme Kerr black hole is a generic feature of all rings considered here. The transition to spheroidal bodies exists for strange matter rings, but not for all EOS. What is particularly striking is how close together the curves for strange and homogeneous rings remain right up to the black hole limit. This figure is a modified version of Fig. 1 of [FHA05]. A discussion of the polytropic and Chandrasekhar EOS can also be found in that paper.

3.3. Parametric Transition to a Black Hole

We explained in section 2.3 that the extreme Kerr solution is the only black hole limit of rotating perfect fluid bodies in equilibrium. The extreme Kerr black hole is characterized by the relation

$$J = \pm M^2,$$

where M is the mass and J the angular momentum. To study quasi-stationary transitions (sequences of bodies in equilibrium) that lead to black holes, we use bodies with a ring topology, since spheroidal bodies do not seem to have stationary sequences that lead to black holes [AFK⁺04]. For spheroidal bodies, a finite upper bound is observed for Z_0 , defined in Eq.(2.8). In contrast, the transition to a black hole occurs if and only if $Z_0 \rightarrow \infty$ (see 2.3.1). We will explore now such transitions with the concept of multipole moments.

3.3.1. Multipole Moments of Rings

The multipole moments that we use were defined in section 2.2.2. As V_0 tends to $-\infty$, we expect the multipole moments to become closer and closer to those of an extreme Kerr black hole. We tested this numerically by making use of a (slightly modified version

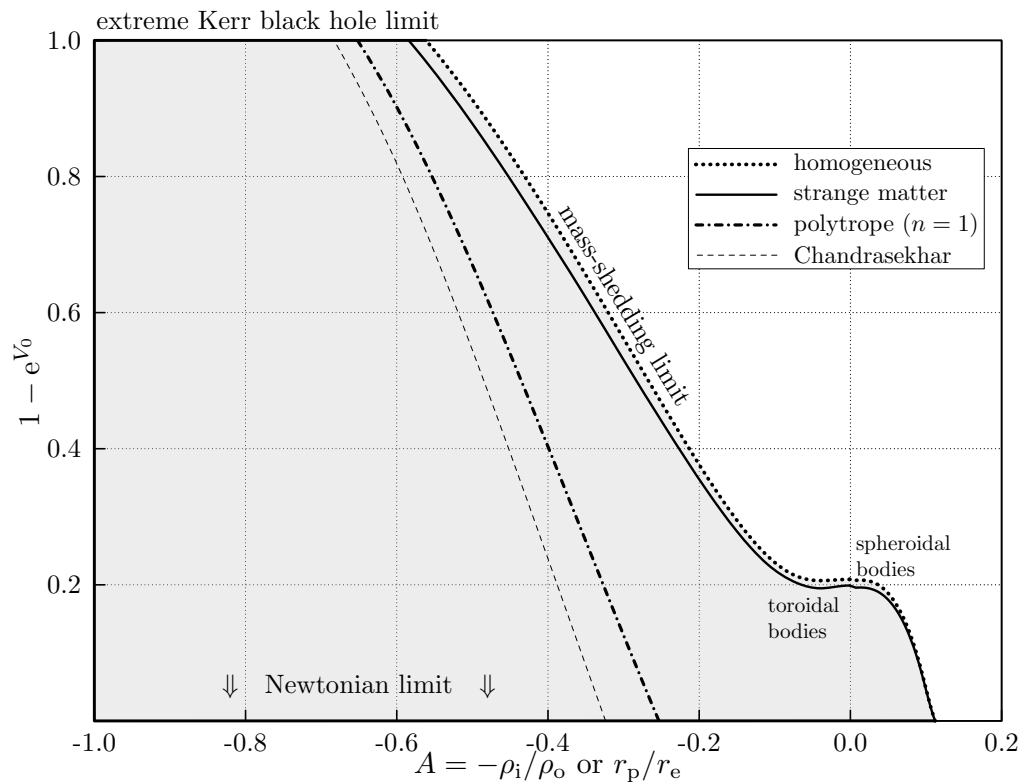


Figure 3.6: The parameter space for the ring class with a variety of EOS is considered in the $A - (1 - e^{V_0})$ plane. Each EOS is bounded on the right by the corresponding mass-shedding curve.

of a) highly accurate computer program as described in [AKM03a]. This program was used for all the results presented in this chapter.

The numerical solutions given by the AKM-method are the four potentials corresponding to the metric of Eq.(2.1) inside the body and in the vacuum domain. Since the multipoles must be read from the Ernst potential, the three potentials $U(\zeta)$, $a(\zeta)$, $W(\zeta)$ on the ζ -axis in the vacuum must be expressed as two potentials $U(\zeta')$, $a(\zeta')$ in the Weyl coordinate ζ' of Eq.(2.14). First, we write the three potentials on the axis as series of ζ in the form:

$$\lim_{\rho \rightarrow 0} e^{2U} = 1 + \sum_{j=1}^{\infty} \frac{u_j}{\zeta^j} \quad (3.3a)$$

$$\lim_{\rho \rightarrow 0} \frac{a}{W^2} = \sum_{j=3}^{\infty} \frac{q_j}{\zeta^j} \quad (3.3b)$$

$$\lim_{\rho \rightarrow 0} \frac{W}{\rho} = 1 + \sum_{j=1}^{\infty} \frac{c_{2j}}{\zeta^{2j}}. \quad (3.3c)$$

By integrating the last equation, one can express ζ on the axis as a function of the Weyl coordinate ζ' :

$$\zeta' = \int \frac{W}{\rho} d\zeta = \zeta + \sum_{j=1}^{\infty} \frac{c_{2j}}{(1-2j)\zeta^{2j-1}} \implies \zeta = \zeta' + \sum_{j=1}^{\infty} \frac{c'_{2j-1}}{\zeta'^{2j-1}}.$$

The Weyl coordinate can be directly introduced into Eq.(3.3a) to find $U(\zeta')$. Then, the potential $b(\zeta')$ can be calculated using all three series from Eqs(3.3), with the help of an integral from Eq.(2.15) and the property on the axis where $a \propto \rho^2$ implies $a_{,\rho'} \propto 2\rho'$:

$$b(\zeta') = \lim_{\rho' \rightarrow 0} \int \frac{e^{4U}}{\rho'} \frac{\partial a}{\partial \rho'} d\zeta' = \lim_{\rho' \rightarrow 0} 2 \int e^{4U} \frac{a}{W^2} d\zeta'.$$

The multipole moments can then be extracted from the Ernst potential $f(\zeta') = e^{2U}(\zeta') + ib(\zeta')$.

Figures 3.7 and 3.8 show the first seven multipole moments for homogeneous and strange matter rings where the ratio between the inner coordinate radius ρ_i and the outer radius ρ_o is held constant at a value of $\rho_i/\rho_o = 0.7$. The left side of the plots corresponds to the Newtonian limit and the right side tends to the black hole limit. As $V_0 \rightarrow -\infty$, the normalized multipoles all tend to one, demonstrating that this sequence indeed approaches the extreme Kerr solution.

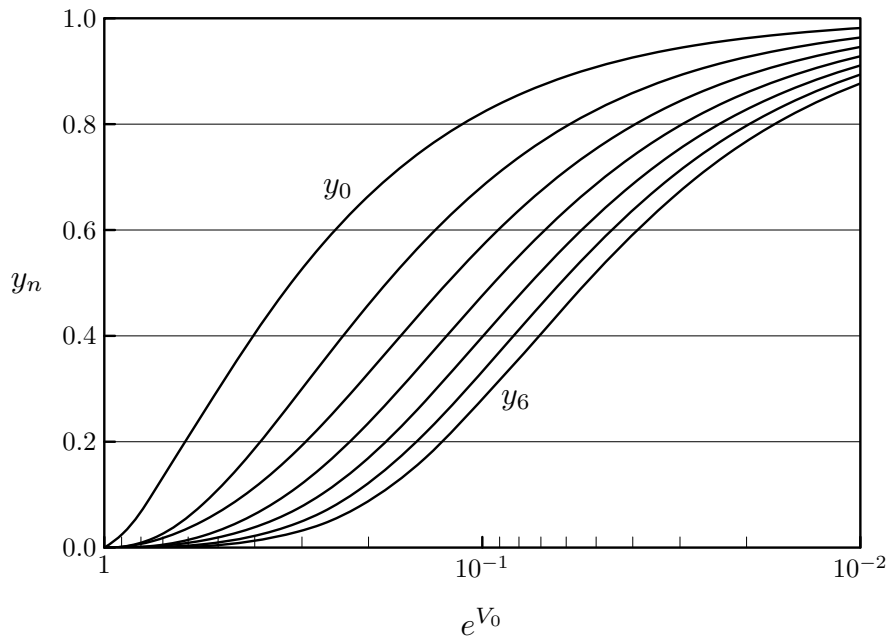


Figure 3.7: The normalized multipoles y_n versus e^{V_0} for homogeneous rings with $\rho_i/\rho_o = 0.7$.

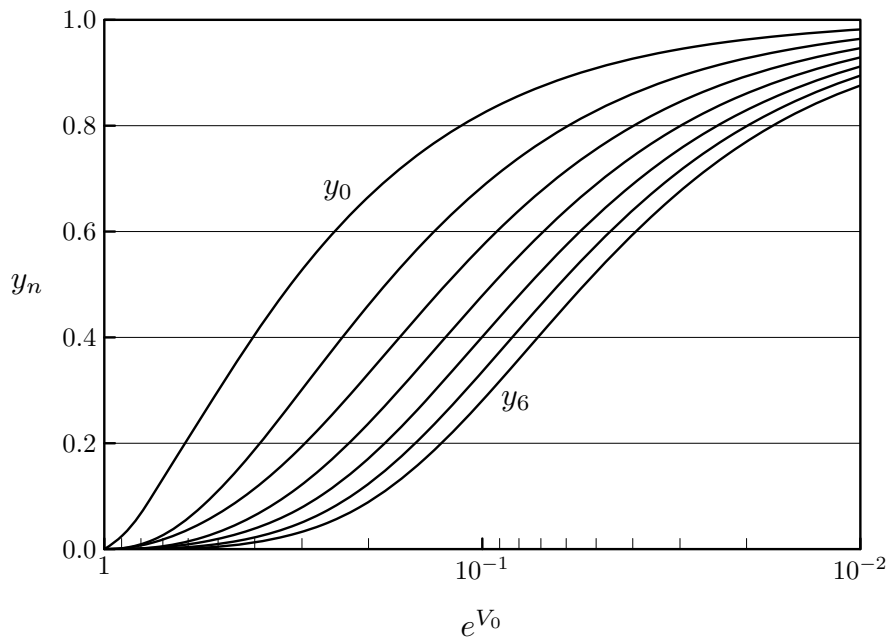


Figure 3.8: The normalized multipoles y_n versus e^{V_0} for strange matter rings with $\rho_i/\rho_o = 0.7$.

It is interesting to note, with respect to e^{V_0} (or Z_0), how slowly the exterior spacetime approaches that of a Kerr black hole. Consider, for example, the configuration from Fig. 3.8 with $e^{V_0} = 10^{-2}$. Whereas the value $J/M^2 = 1.00014$ is very close to the limiting value of one reached in the extreme Kerr limit, the product $2\Omega M = 0.9813$ deviates rather significantly from it. This makes itself felt particularly for the higher multipole moments where powers of Ω are in play. The moment y_4 , for example, has reached only a value of $y_4 \approx 0.91$ for this configuration.

To understand better the nature of the transition to the black hole, we compare the multipole moments of the above strange matter ring sequence with those of the Kerr solution. In Fig. 3.9 the y_n for $n = 1 \dots 6$ are plotted against $y_0 = 2\Omega M$ for the strange matter ring sequence from above. A corresponding picture for the sequence of Kerr solutions (see (2.26)) is displayed in Fig. 3.10. The clear similarity between these plots is emphasized in Fig. 3.11 where each y_n for the ring (solid line) and the Kerr solution (dotted line) is compared in a small figure over its whole range. The region very close to the extreme Kerr limit is then shown for y_1 – y_5 in detail. The graphs strongly suggest that the slopes

$$\frac{dy_n}{dy_0}(y_0 = 1) \quad (3.4)$$

are the same for the Kerr family and for the strange matter ring sequence discussed here. In fact, we found these slopes to be independent of the specific EOS being used.¹ For the Kerr solutions, it follows from (2.26) that

$$\frac{dy_n}{dy_0}(y_0 = 1) = n + 1, \quad (3.5)$$

which leads us to the conjecture that (3.5) holds true for all sequences of rotating bodies that admit the transition to an extreme Kerr black hole. This conjecture provides a universal growth rate with which the y_n approach unity.

In Table 3.3, a comparison of the values of the first five moments y_n for a variety of configurations all with $e^{V_0} = 10^{-2}$ is provided. The set of configurations chosen includes rings with various different EOS and various radius ratios and also includes the uniformly rotating disk of dust. A discussion of the multipoles of this last configuration as well as plots analogous to Fig. 3.8 can be found in [KMN95]. Since all multipole moments tend to one in the limit $V_0 \rightarrow -\infty$, these multipoles will provide almost no way of

¹We checked this for ring sequences governed by homogeneous, polytropic and Chandrasekhar EOS as well as for the rigidly rotating dust family (this will be shown for the disk in section 4.3.3). The Chandrasekhar EOS describes a completely degenerate, zero temperature, relativistic Fermi gas.

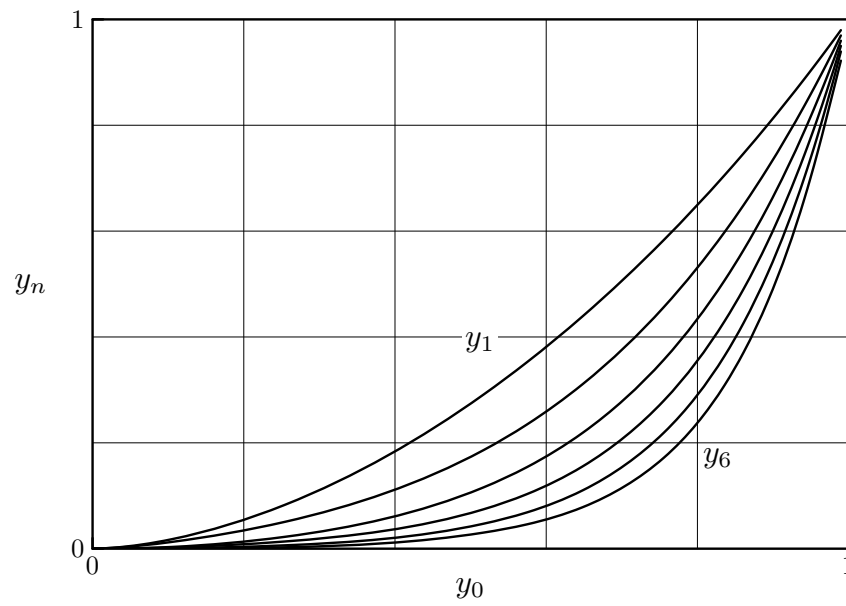


Figure 3.9: The multipole moments y_n , $n = 1 \dots 6$ versus y_0 for strange matter rings with $\rho_i/\rho_o = 0.7$.

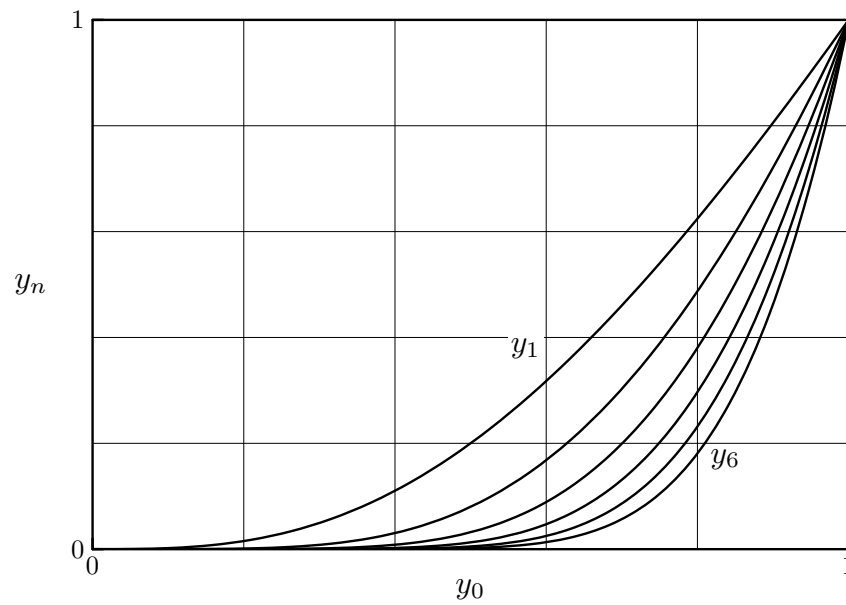


Figure 3.10: The multipole moments y_n , $n = 1 \dots 6$ versus y_0 for the sequence of Kerr solutions.

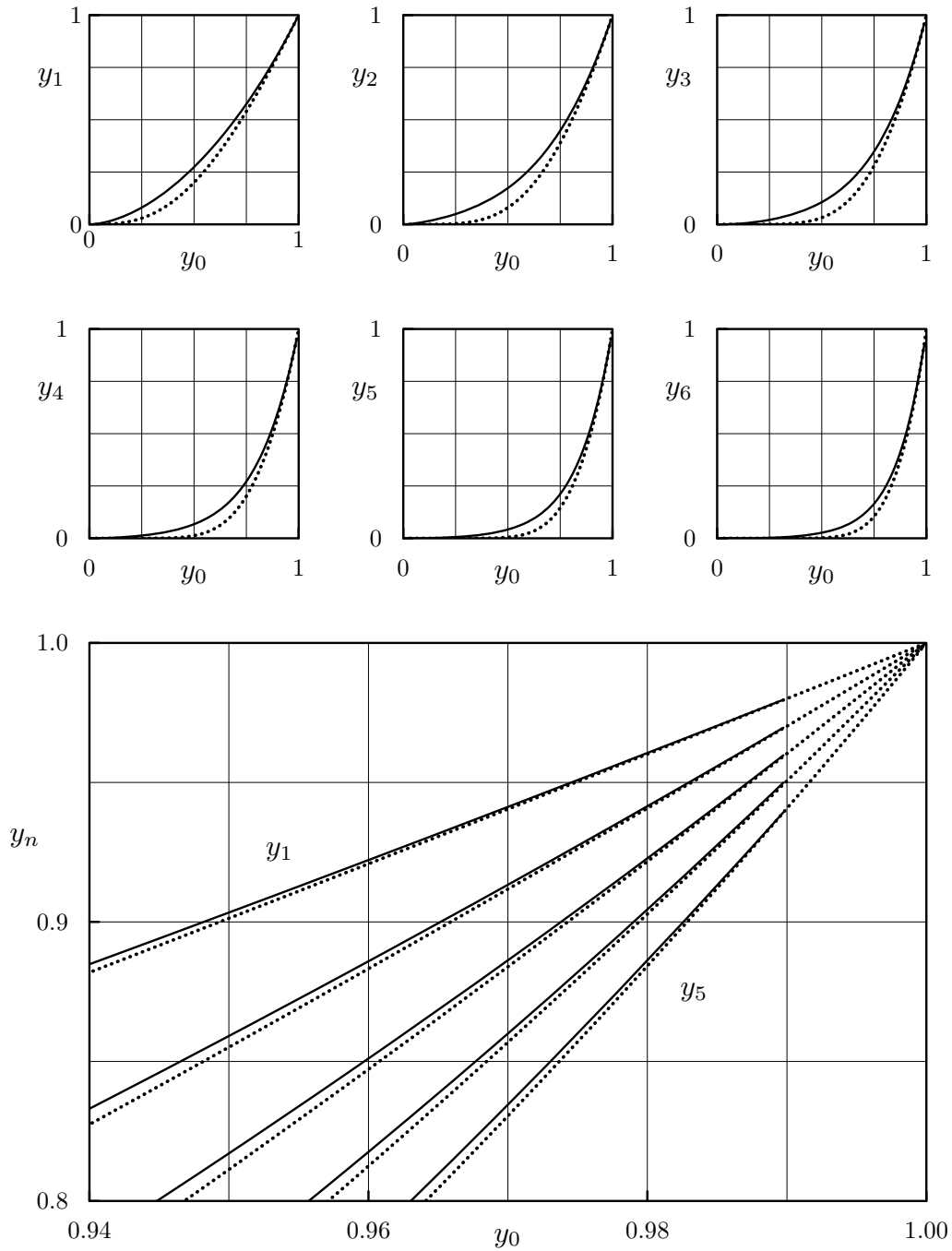


Figure 3.11: Various multipole moments y_n are plotted versus y_0 for strange matter rings with $\rho_i/\rho_o = 0.7$ (solid lines) and the sequence of Kerr solutions (dotted lines). In the detailed plot, the curve for y_6 was omitted because of slight numerical inaccuracies for higher multipole moments.

Table 3.3: The multipole moments y_n for various configurations of rings and the rigidly rotating disk of dust, all with $e^{V_0} = 10^{-2}$. The polytropic ring has a polytropic index $n = 1$ (see [MAK⁺08] for explanation of polytropic EOS).

	y_0	y_1	y_2	y_3	y_4
strange matter ($r_i/r_o = 0.6$)	0.982	0.964	0.947	0.930	0.913
strange matter ($r_i/r_o = 0.7$)	0.981	0.963	0.945	0.928	0.910
strange matter ($r_i/r_o = 0.8$)	0.981	0.962	0.943	0.925	0.907
homogeneous ($r_i/r_o = 0.7$)	0.981	0.963	0.945	0.927	0.910
polytropic $n = 1$ ($r_i/r_o = 0.7$)	0.982	0.965	0.948	0.931	0.914
relativistic disk of dust	0.984	0.969	0.953	0.938	0.924

Table 3.4: The multipole moments y_n for various configurations, all with $e^{-V_0} = 1.1 \Leftrightarrow Z_0 = 0.1$.

	y_0 ($\times 10^{-2}$)	y_1 ($\times 10^{-3}$)	y_2 ($\times 10^{-3}$)	y_3 ($\times 10^{-5}$)	y_4 ($\times 10^{-5}$)
strange matter ($r_i/r_o = 0.6$)	2.22	1.21	1.04	8.92	7.44
strange matter ($r_i/r_o = 0.7$)	2.09	1.16	1.02	8.69	7.43
strange matter ($r_i/r_o = 0.8$)	1.92	1.09	0.978	8.49	7.46
homogeneous ($r_i/r_o = 0.7$)	2.09	1.16	1.01	8.68	7.42
polytropic $n = 1$ ($r_i/r_o = 0.7$)	2.14	1.27	1.11	10.1	8.75
relativistic disk of dust	2.36	1.73	1.56	12.5	21.7

distinguishing between various configurations close to this limit.

In contrast, we present the multipole moments for configurations near the Newtonian limit ($e^{-V_0} = 1.1$) in Table 3.4. Here one can see that there is far more variation amongst the rings and that the disk of dust differs significantly from any of the rings. The values in the table also reflect the fact that strange matter has the same Newtonian limit as homogeneous matter.

3.3.2. Throat Geometry

One of the most interesting features of bodies near the extreme Kerr black hole limit is the appearance of a throat geometry [BH99, Mei02]. In the limit, the throat separates the ‘inner world’, containing the ring, from the ‘outer world’. The outer world is the asymptotically flat extreme Kerr spacetime, which is described by a single parameter and in which the horizon is located at the end of the infinitely long throat. On the other hand, the inner world is not asymptotically flat and is related to the outer world through its asymptotic behaviour, which contains information about the one free parameter that

uniquely describes the outer world. Any point in the outside world is infinitely far away from any point in the inner world. For example, in the equatorial plane, one finds that the radial proper distance δ from the point $\rho = 0$ to the point ρ is

$$\delta = \int_0^\rho \sqrt{g_{\rho\rho}}|_{\zeta=0} d\tilde{\rho}.$$

For the extreme Kerr black hole δ tends logarithmically to infinity as $\rho \rightarrow 0$ as shown by Eq.(2.32) (the horizon in the coordinates used here is located at $\rho = 0$).

One way to represent the throat is to plot $\sqrt{g_{\varphi\varphi}}/M$ in the equatorial plane as a function of δ/M . Then, the throat appears as a plateau, i.e. a region appears in which the circumference of a circle of constant radius $\rho = \rho_c$, tends toward a constant, independent of the radius ρ_c . As the extreme Kerr black hole is approached, this region becomes infinitely long. Figure 3.12 shows the appearance of the throat for a sequence of strange matter rings with $\rho_i/\rho_o = 0.7$ as the parameter e^{V_0} tends to zero. Even in the first of these pictures ($e^{2V_0} = 10^{-1}$), the highly relativistic nature of the ring is demonstrated by the fact that a small portion of the curve has a negative slope. That is, there exists a region of spacetime in which circles lying in the equatorial plane and centred about the origin have decreasing circumference with increasing radius. The last of these pictures is similar to Fig. 13 in [BW71] in which the ‘inner world’ is separated from the extreme Kerr solution by the infinite throat region. The proper distance between a point in what becomes the inner world (e.g. the outer edge of the ring $\rho = \rho_o$) and a point in what becomes the outer world (e.g. $\rho = M$) tends to infinity as $e^{2V_0} \rightarrow 0$. In a sense, we can say that the ‘throat region’ near the black hole limit ‘swallows’ the information as to what kind of configuration is sitting at the centre, as can be seen in Table 3.3.

The numerical ‘inner world’ solution was produced with a program that prescribes the asymptotic behaviour of the throat region (see [BH99]). Since the ‘asymptotically flat computer program’ is capable of rendering rings with a relative redshift Z_0 well in excess of 100, the metric behaviour provided by this program can be used as initial input for the Newton-Raphson method of the ‘inner world program’ [AKM03a].

3.3.3. Escape Energy

With u^i referring to the four-velocity of a particle resting on the ring’s surface, $E-1$ could be called the “escape energy”. If it is negative, then a sufficiently small perturbation will not suffice to induce the particle’s escape to infinity on a geodesic, and it is referred to

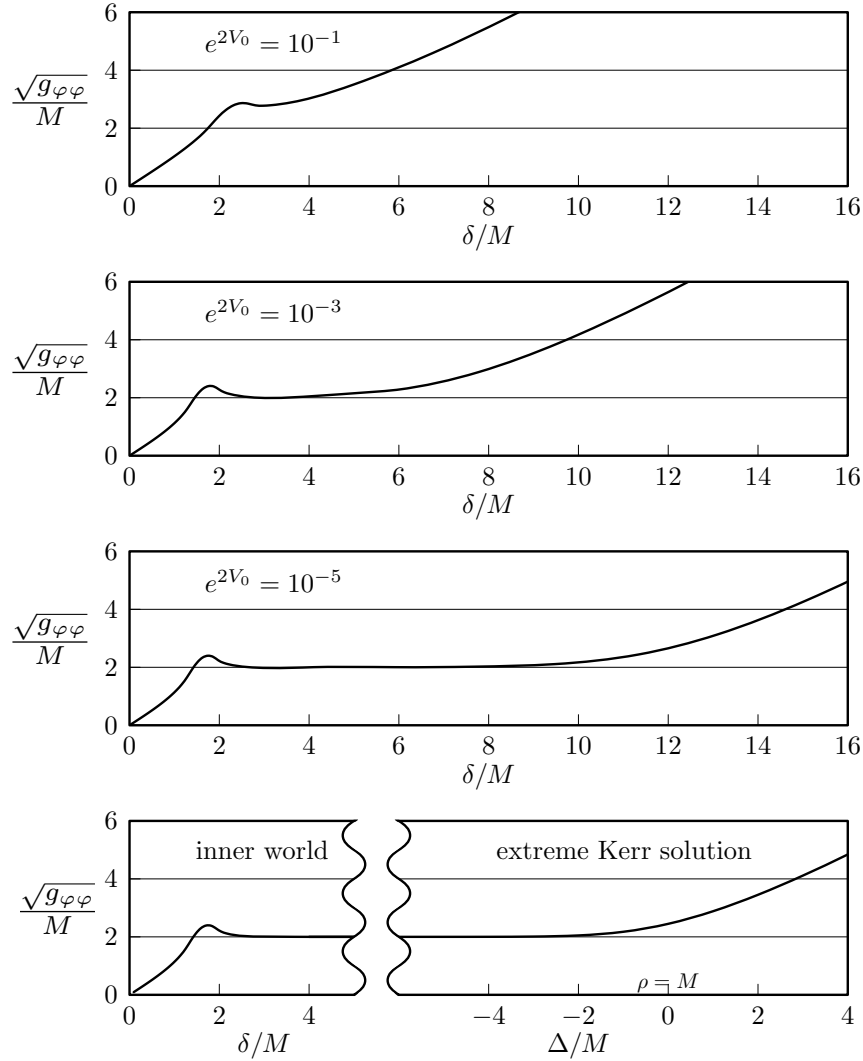


Figure 3.12: The function $\sqrt{g_{\varphi\varphi}}$ in the equatorial plane is plotted versus proper distance, both normalized with respect to the mass M . In the throat region, $\sqrt{g_{\varphi\varphi}}/M$ tends to the constant value 2. All four plots were made for a strange matter ring with a radius ratio $\rho_i/\rho_o = 0.7$ and with a value for e^{2V_0} as indicated. In the last plot, Δ gives the proper distance in the Kerr metric to the reference point $\rho = M$. Note that the proper distance between any point in the ‘inner world’ region and any point in the ‘extreme Kerr’ region tends to infinity as $e^{2V_0} \rightarrow 0$.

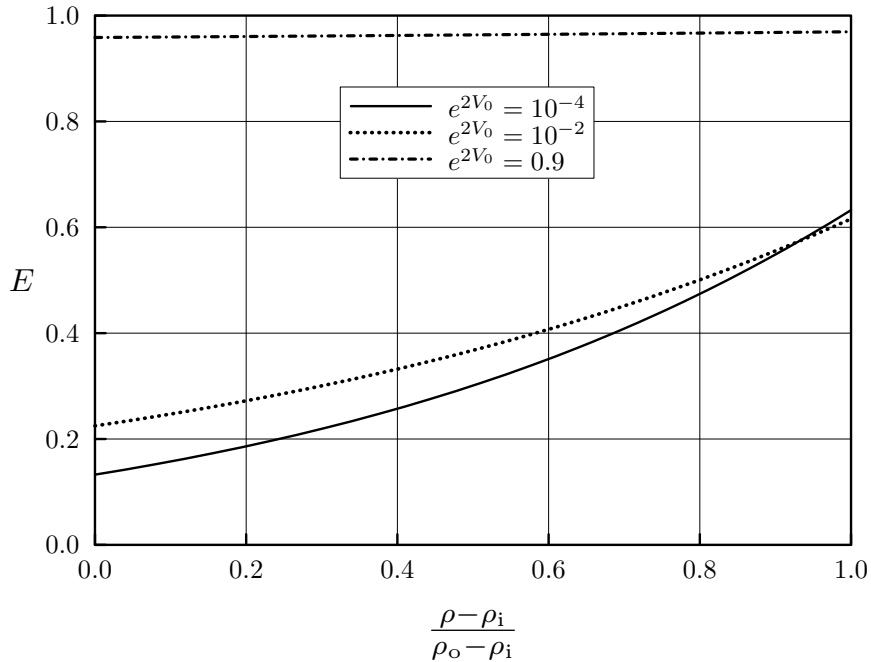


Figure 3.13: The specific energy E versus $(\rho - \rho_i)/(\rho_o - \rho_i)$ on the surface of a variety of strange matter rings with $\rho_i/\rho_o = 0.7$.

as gravitationally bound. In proving that $V_0 \rightarrow -\infty$ is a sufficient condition for reaching the black hole limit [Mei06], use was made of the reasonable assumption that particles on the fluid's surface are gravitationally bound. One expects that this minimal requirement for stability will always be satisfied. We now proceed to verify this assumption for a large class of rings.

Figures 3.13 and 3.14 show the value of E along the surface of a variety of strange matter rings as it depends on radius. The radial parameter $(\rho - \rho_i)/(\rho_o - \rho_i)$ is chosen since it runs from 0 to 1 for every ring. In Fig. 3.13 curves are plotted for a constant value $\rho_i/\rho_o = 0.7$ and for varying V_0 . We see that E tends to 1 in the Newtonian limit, which follows directly from Eq. (2.12). Figure 3.14 shows the behaviour of E for various values of ρ_i/ρ_o and constant V_0 . Since configurations with small ρ_i/ρ_o do not exist when V_0 becomes too negative (see Fig. 3.6), we chose V_0 to be in the Newtonian regime in order to be able to consider a wide range of values for the radius ratio. For every example considered in Figs 3.13 and 3.14, a maximal value at the outside edge of the ring in the equatorial plane is reached, just as one would expect. It is interesting to compare these results with the relativistic disk of dust for which $E = 1$ holds at the outer edge independent of the value of Z_0 [MK95].

Focussing our attention now on the outer edge of the ring in the equatorial plane,

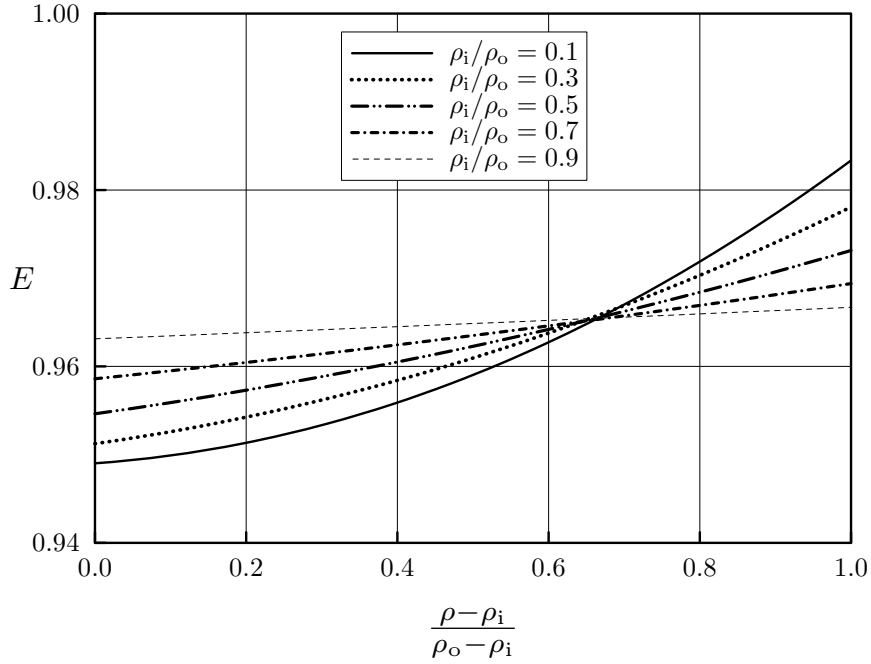


Figure 3.14: The specific energy E versus $(\rho - \rho_i)/(\rho_o - \rho_i)$ on the surface of a variety of strange matter rings near the Newtonian limit ($e^{2V_0} = 0.9$).

we see in Fig. 3.15 how E depends on V_0 for a sequence of strange matter rings with $\rho_i/\rho_o = 0.7$. It is apparent that a maximum is reached in the Newtonian limit. For rings rotating at the mass-shedding limit, the value of E is also significantly smaller than one for small e^{V_0} . The results for homogeneous rings are very similar and we can verify that $E \leq 1$ holds (i.e. the escape energy is negative) for a large class of rings.

This ends our investigation about strange matter rings and their parametric transition to the black hole. Since the behaviour given by Eq.(3.5) seems to be independent of the equation of state of our rings, we want to investigate this conjecture more in depth in the next chapter.

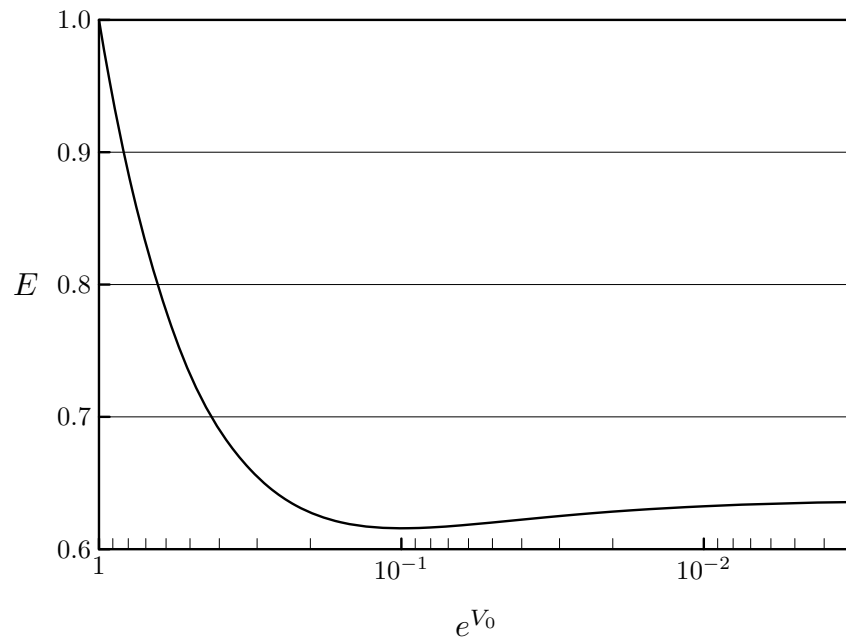


Figure 3.15: The specific energy E versus e^{V_0} at the outer edge in the equatorial plane for strange matter rings with $\rho_i/\rho_o = 0.7$.

4. Ernst Potentials near the Black Hole Limit

Among stationary and axisymmetric solutions containing a black hole or a fluid in equilibrium as the source, three categories of continuous sequences of solutions are known to reach the extreme Kerr BH: various rings of fluids [AKM03b, FHA05], the rigidly rotating disk of dust [BW71, NM93], and obviously, the Kerr BH sequence. Sequences of rings made of strange quark matter were studied in the previous chapter, and similar sequences of rings with other equation of states were also produced in the literature mentioned just above. For the rigidly rotating disk of dust and the Kerr BH, exact analytical solutions are known.

In the previous chapter, we observed that the multipole moments on the rotation axis of the rings and the Kerr black hole have a common behaviour near the extreme Kerr black hole limit, a behaviour characterized by Eq.(3.5). In this chapter, we make use of (3.5) to write down the beginning of a Taylor series of the Ernst potential of fluids in equilibrium near the black hole limit, with suitable coordinates. Then, we apply this Taylor series to the analytical solutions of the Meinel/Neugebauer disk of dust and the Kerr BH.

4.1. Reformulation of the Conjecture

4.1.1. Normalized Multipoles

Staying in the vacuum domain where we can use of the Weyl coordinates¹ and the Ernst potential, let us first introduce two new pairs of dimensionless Weyl coordinates, one normalized with the angular velocity Ω of the source, and a second one normalized with the mass M of the same source:

$$\tilde{\rho} := 2\Omega\rho, \quad \tilde{\zeta} := 2\Omega\zeta, \quad \text{and} \quad (4.1a)$$

$$\hat{\rho} := \frac{\rho}{M}, \quad \hat{\zeta} := \frac{\zeta}{M}. \quad (4.1b)$$

¹We drop here the prime notation from section (2.2.1).

From the potential ξ in Eq.(2.20), one can calculate the same series (2.21) with the dimensionless coordinates and get the same general form:

$$\xi = \sum_{n=0}^{\infty} \frac{m_n}{\zeta^{n+1}} = \sum_{n=0}^{\infty} \frac{\tilde{m}_n}{\tilde{\zeta}^{n+1}} = \sum_{n=0}^{\infty} \frac{\hat{m}_n}{\hat{\zeta}^{n+1}}. \quad (4.2)$$

The new dimensionless coefficients have the following relations, deduced from (4.2):

$$\tilde{m}_n = (2\Omega)^{n+1} m_n, \quad \hat{m}_n = \frac{m_n}{M^{n+1}} \quad \text{and} \quad \tilde{m}_n = (2\Omega M)^{n+1} \hat{m}_n. \quad (4.3)$$

Since the zeroth multipole moment is the gravitational mass of the source, $P_0 = m_0 = M$, it follows that $\tilde{M} = 2\Omega M$ and we can then also say $\tilde{m}_n = (\tilde{M})^{n+1} \hat{m}_n$. It follows also that $\hat{m}_0 = 1$ is an identity.

To avoid becoming lost with the “tilde” and “hat” notation, keep in mind that a “tilde” is added to a variable when this variable is multiplied by a power of 2Ω such that it becomes dimensionless, and the same is done with a “hat” when it involves powers of M to make it dimensionless. The multipole moments can also be transformed into normalized and dimensionless moments in a similar fashion as the m_n coefficients:

$$\tilde{P}_n = (2\Omega)^{n+1} P_n \quad \text{and} \quad \hat{P}_n = \frac{P_n}{M^{n+1}} \quad (4.4)$$

These relations seem naively copied from Eq.(4.3) when in fact the P_n for $n > 3$ are indeed long algebraic combinations of m_n , but a dimensional analysis shows that they agree.

Because of equatorial symmetry, as stated in section 2.2.2, coefficients and multipoles with even index are real and the odd ones are purely imaginary. The absolute values of \tilde{m}_n and \tilde{P}_n have a domain going from 0 to 1 for fluid bodies² and black holes. With \hat{m}_n and \hat{P}_n , their absolute values vary from 0 to ∞ for fluid bodies, except for the fixed number $\hat{P}_0 = \hat{m}_0 = 1$, while black holes are again restricted to $[0,1]$. When $\tilde{P}_n = 0$ for all n , or when $\hat{P}_n = 0$ for $n > 0$, we obtain the Schwarzschild geometry outside the source, and the scenario where $\tilde{P}_n = i^n$ or $\hat{P}_n = i^n$ for all n corresponds to the extreme Kerr geometry. More generally, the Kerr black hole has $\tilde{P}_n = i^n \tilde{M}^{n-1} \tilde{J}^n$ or $\hat{P}_n = i^n \hat{J}^n$, and it was also found empirically in [FK09] that for a rigidly rotating perfect fluid in

²But only rings and the rigid disk of dust are known to reach 1

equilibrium, surrounded by vacuum,

$$\left| \widehat{P}_n \right| \geq \left| \widehat{J}^n \right| ,$$

where the right hand side is equivalent to the $\left| \widehat{P}_n \right|$ of a Kerr black hole with the same mass and angular momentum as the fluid body. Also, the equality in this relation is only reached for the extreme Kerr black hole limit $\left| \widehat{P}_n \right| = 1$.

The normalized multipoles y_n defined in Eq.(2.23), which always gives real positive values for black holes and rings, are related here in this new notation by $\widetilde{P}_n = i^n y_n$. \widetilde{P}_n has the same absolute value as y_n , but it is not systematically real positive. This leads to $\widetilde{P}_n = \widetilde{m}_n = i^n$ in the extreme Kerr black hole limit, and Eq.(3.5), which we believe to hold for any sequences of rotating bodies in equilibrium that admit a transition to a black hole, becomes

$$\frac{d\widetilde{P}_n}{d\widetilde{M}}(\widetilde{M} = 1) = \frac{d\widetilde{m}_n}{d\widetilde{M}}(\widetilde{M} = 1) = (n + 1) i^n . \quad (4.5)$$

Note here that the algebraic structure that links \widetilde{P}_n and \widetilde{m}_n is such that choosing \widetilde{P}_n or \widetilde{m}_n in the derivative of (4.5) is equivalent for $\widetilde{M} = 1$; at least, this is verified for the 11 first multipoles shown in [FHP89], and we are confident that it holds for $n > 10$.

If we substitute \widetilde{P}_n by \widehat{P}_n in the derivative, we get

$$\frac{d\widehat{P}_n}{d\widetilde{M}} = \frac{d(\widetilde{M}^{n+1} \widehat{P}_n)}{d\widetilde{M}} = (n + 1) \widetilde{M}^n \widehat{P}_n + \widetilde{M}^{n+1} \frac{d\widehat{P}_n}{d\widetilde{M}} .$$

Putting this last result into Eq.(4.5) with $\widehat{P}_n(\widetilde{M} = 1) = i^n$, it turns out that the conjecture takes a nicer form:

$$\frac{d\widehat{P}_n}{d\widetilde{M}}(\widetilde{M} = 1) = \frac{d\widehat{m}_n}{d\widetilde{M}}(\widetilde{M} = 1) = 0 . \quad (4.6)$$

4.1.2. The Multipoles and the First Law of Thermodynamics

It can be shown that a part of our conjecture is indeed explained by the analogous form of the “first law of thermodynamics” for rotating bodies. In “classical” thermodynamics, the first law states that for an infinitesimal change in a system of N particles with a temperature T , an entropy S , a volume V , a pressure p and a chemical potential μ_c , the

internal energy U is changed by

$$dU = TdS - pdV + \mu_c dN .$$

When we refer to astrophysical bodies, their physical properties can be also related to analogous “thermodynamic laws” (or mechanics laws). Nearby configurations between black holes or between bodies of fluid in equilibrium are governed respectively by the following “first laws”:

$$\begin{aligned} dM &= \frac{1}{8\pi} \kappa dA + \Omega dJ + \emptyset , \\ dM &= \emptyset + \Omega dJ + \mu_c dM_B . \end{aligned}$$

Here, κ is the surface gravity of the black hole, given by Eq.(2.27), and is the black hole analogue of the temperature. The surface area of the horizon A is analogous to the entropy. The second equation is from Eq.(2.10). The empty sets (\emptyset) emphasize that black holes have no “chemical potential-particle” term, while our equation for fluid bodies shows no “temperature-entropy” term since we consider that our bodies in equilibrium have zero temperature.

We can see that these laws govern a relation between the two first multipole moments (M and J). As was explained in section 2.3.1, the parameters κ for black holes and μ_c for fluid bodies vanish as they approach the extreme Kerr BH limit. The result is that the “first law” of both black hole and fluid body configurations become identical in the limit:

$$dM = \Omega dJ \tag{4.7}$$

This show that in the extreme Kerr BH limit, not only the mass and angular momentum is fixed at $J = M^2$, but but the trend of M and J for configurations near this limit is the same for black holes and fluid bodies.

If we translate the normalized multipoles \widetilde{M} , \widetilde{P}_1 and \widehat{P}_1 in terms of M and J and Ω , we get for infinitesimal changes

$$\begin{aligned} d\widetilde{M} &= d(2\Omega M) = 2(\Omega dM + M d\Omega) , \\ d\widetilde{P}_1 &= d(4i\Omega^2 J) = 4i(\Omega^2 dJ + 2\Omega J d\Omega) , \\ d\widehat{P}_1 &= d(iM^{-2}J) = iM^{-2}(dJ - 2JM^{-1}dM) . \end{aligned}$$

In the extreme Kerr BH limit, we can substitute Ω , J and dJ in terms of M and dM

thanks to Eqs (2.30) and (4.7). Then we find

$$\begin{aligned}\frac{d\widetilde{P}_1}{d\widetilde{M}}(\widetilde{M} = 1) &= \frac{4i(\Omega dM + M d\Omega)}{2(\Omega dM + M d\Omega)} = 2i, \\ \frac{d\widehat{P}_1}{d\widetilde{M}}(\widetilde{M} = 1) &= \frac{0}{2(\Omega dM + M d\Omega)} = 0.\end{aligned}$$

These results are exactly what is expected in Eqs(4.5) and (4.6) for $n = 1$. This proves that what we conjectured for $n = 1$ is simply a consequence of the first thermodynamic law for fluid bodies, where its law becomes identical to the black hole thermodynamic law in the limit of the extreme Kerr BH ($2\Omega M \rightarrow 1$). No analogous “first law of thermodynamics” that implies the further multipole moments ($n > 1$) exists, so we cannot extend this proof to the entire conjecture.

4.1.3. A Taylor Series Near the Black Hole Limit

Suppose now that we have a list of coefficients \widetilde{m}_n that can be parameterized as functions of \widetilde{M} . We can thus write the normalized multipoles as a Taylor series at $\widetilde{M} \equiv 2\Omega M \rightarrow 1$ and then use the extreme Kerr black hole result $\widetilde{m}_n(\widetilde{M} = 1) = i^n$ and the conjecture in Eq.(4.5) for the two first terms:

$$\begin{aligned}\widetilde{m}_n(\widetilde{M}) &= \widetilde{m}_n(1) + \frac{d\widetilde{m}_n}{d\widetilde{M}}(1)(\widetilde{M} - 1) + \frac{1}{2} \frac{d^2\widetilde{m}_n}{d\widetilde{M}^2}(1)(\widetilde{M} - 1)^2 + \dots \\ &= i^n \left[1 + (n+1)(\widetilde{M} - 1) + \mathcal{O}[(\widetilde{M} - 1)^2] \right]\end{aligned}$$

It will be more suitable from now on to use the parameter $\varepsilon := 1 - 2\Omega M$, which becomes $\varepsilon = 0$ in the extreme Kerr black hole limit, and is small and positive near the limit. If we introduce the last result for the multipoles into Eq.(4.2), we get two sums that can be substituted into short rational functions:

$$\begin{aligned}\xi(\varepsilon; \widetilde{\zeta}) &= \frac{1}{\widetilde{\zeta}} \sum_{n=0}^{\infty} \left(\frac{i}{\widetilde{\zeta}} \right)^n [1 - (n+1)\varepsilon + \mathcal{O}(\varepsilon^2)] \\ &= \frac{1}{\widetilde{\zeta}} \sum_{n=0}^{\infty} \left(\frac{i}{\widetilde{\zeta}} \right)^n - \frac{1}{\widetilde{\zeta}} \sum_{n=0}^{\infty} \left(\frac{i}{\widetilde{\zeta}} \right)^n (n+1)\varepsilon + \frac{1}{\widetilde{\zeta}} \sum_{n=0}^{\infty} \left(\frac{i}{\widetilde{\zeta}} \right)^n \mathcal{O}(\varepsilon^2) \\ &= \frac{1}{\widetilde{\zeta} - i} - \frac{\widetilde{\zeta}}{(\widetilde{\zeta} - i)^2} \varepsilon + \mathcal{O}(\varepsilon^2).\end{aligned}$$

We can reconstitute from this result the original form of the Ernst potential f using Eq.(2.20), which yields as a series of ε

$$f(\varepsilon; \tilde{\zeta}) = \frac{\tilde{\zeta} - 1 - i}{\tilde{\zeta} + 1 - i} + \frac{2\tilde{\zeta}}{(\tilde{\zeta} + 1 - i)^2} \varepsilon + \mathcal{O}(\varepsilon^2). \quad (4.8)$$

The first part of the series can be easily recognized as the Ernst potential of the extreme Kerr BH on the ζ -axis. The second part, coming from the conjecture in Eq.(3.5), is the leading term describing the behaviour of the Ernst potential for a parameterized transition of a fluid body in equilibrium to the extreme Kerr BH solution. In other words, the Ernst potential of a black hole and any fluid body in equilibrium with the same mass M and angular velocity³ Ω , near the limit $2\Omega M = 1$, have the same Ernst potential in normalized coordinates on the rotation axis up to $\mathcal{O}(\varepsilon^2)$.

Similar series can be written using the mass as normalization. The Ernst potential is produced in the same manner as above, and it yields

$$\begin{aligned} \xi(\varepsilon; \hat{\zeta}) &= \frac{1}{\hat{\zeta} - i} + \emptyset + \mathcal{O}(\varepsilon^2), \\ f(\varepsilon; \hat{\zeta}) &= \frac{\hat{\zeta} - 1 - i}{\hat{\zeta} + 1 - i} + \emptyset + \mathcal{O}(\varepsilon^2). \end{aligned} \quad (4.9)$$

Again, the extreme Kerr solution occupies the first part of the series, but the next order correction, corresponding to the conjecture, vanishes (\emptyset). So the Ernst potential on the axis of a fluid in equilibrium would have sequences of solutions near the extreme Kerr solution with a first correcting term in $\mathcal{O}(\varepsilon^2)$. The conjecture from Eq.(3.5) or (4.6) is then equivalent, in normalized Weyl coordinates $(\hat{\rho}, \hat{\zeta})$, saying

$$\frac{df}{d\tilde{M}}(\tilde{M} = 1) = 0. \quad (4.10)$$

Moreover, the ‘‘extreme Kerr term’’ in (4.9) already gives the exact mass term $2Mr^{-1}$ in the series expansion at infinity of Eq.(2.18), so the remainder terms $\mathcal{O}(\varepsilon^2)$ of this series are not expected to contribute in r^{-1} :

$$\frac{\hat{\zeta} - 1 - i}{\hat{\zeta} + 1 - i} = 1 - \frac{2}{\hat{\zeta}} + \mathcal{O}\left(\frac{1}{\hat{\zeta}^2}\right) = 1 - \frac{2M}{\zeta} + \mathcal{O}\left(\frac{1}{\zeta^2}\right). \quad (4.11)$$

This is not expected to hold in the former normalization, since the ‘‘extreme Kerr term’’

³The angular velocity of the horizon in the case of a black hole.

in Eq.(4.8) represents a black hole with the same angular momentum as the source of f , not the same mass.

Using the extreme Kerr black hole as the “anchor” term of a parametric Taylor series of the Ernst potential near the black hole limit is certainly a relevant choice, since it was demonstrated in section 2.3 that the extreme Kerr BH is the only candidate for a BH limit of a stationary and axisymmetric rotating body in equilibrium [Mei06], and such limits exist for rings and disks of dust. We will turn our work now to two analytically solved Ernst potentials, the Kerr BH and the the rigidly rotating thin disk of dust, investigating the property that was conjectured from the rings, and deriving the Taylor series for these solutions.

4.2. Ernst Potential of the Kerr Black Hole

It is not difficult to make the Taylor series of the Kerr metric, since this metric is not only already exact, but also, it can be written in a very concise form. Much has been said about this metric in comparison to other stationary and axisymmetric solutions. The metric was first found by Kerr [Ker63], then Boyer and Lindquist provided a suitable coordinate transformation which shed light on the “black hole nature” of the metric [BL67]. More physical processes concerning rotating black holes were studied, especially by Bardeen, Press and Teukolsky in [BPT72]; of particular interest in this last article is the description of the extreme Kerr BH ($J = \pm M^2$), with its special infinitely long “throat geometry”.

Thus, it is not our goal to write down a series expansion for the purpose of investigating the Kerr solution itself, but instead, it can be used for comparison with other series of the same kind, and in particular, with the disk of dust in the next section. The Ernst potential of a Kerr BH of mass M and angular momentum J is

$$f = 1 - \frac{4M}{r_- + r_+ + 2M + i \frac{J(r_- - r_+)}{\sqrt{M^4 - J^2}}} \quad (4.12)$$

where r_{\pm} are positive quantities defined by

$$r_{\pm}^2 = r^2 \left[\sin^2 \theta + \left(\cos \theta \pm \frac{\sqrt{M^4 - J^2}}{Mr} \right)^2 \right]$$

and the coordinates are the “spherical version” of the Weyl coordinates, with $\rho = r \sin \theta$

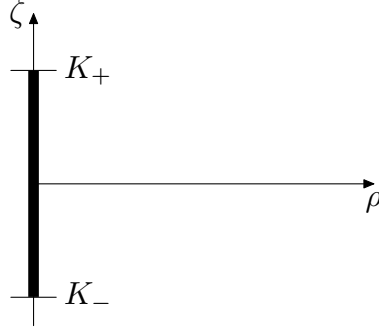


Figure 4.1: In Weyl coordinates, the horizon of the Kerr BH is a segment on the rotation axis, with the poles at $\rho = 0$, $\zeta = K_{\pm} = \pm\sqrt{M^2 - (J/M)^2}$. For the extreme Kerr BH ($J = M^2$), the horizon shrinks into a point at the origin.

and $\zeta = r \cos \theta$. The horizon is located on a segment of the rotation axis between the points $(r = \sqrt{M^2 - (J/M)^2}, \theta = 0)$ and $(r = \sqrt{M^2 - (J/M)^2}, \theta = \pi/2)$, as illustrated in Fig. 4.1.

The potential can be converted into a function of M and Ω using the relation in Eq.(2.25). We can then transform the parameters and coordinates into dimensionless quantities using powers of either 2Ω or M as explained above. The normalized potential can be easily computed as a power series of $\varepsilon \equiv 1 - 2\Omega M$, and we can take advantage of this to produce the series for the whole space (not just the axis). The series, normalized with 2Ω , reads

$$\begin{aligned}
 f(\varepsilon; \tilde{r}, \theta) = & \frac{\tilde{r} - 1 - i \cos \theta}{\tilde{r} + 1 - i \cos \theta} + \frac{2\tilde{r}}{(\tilde{r} + 1 - i \cos \theta)^2} \varepsilon \\
 & + \frac{\tilde{r}^3(2 - i \cos \theta) + \tilde{r}^2(1 + i \cos \theta) + \sin^2 \theta(\tilde{r} + i \cos \theta + \cos^2 \theta)}{\tilde{r}^2(\tilde{r} + 1 - i \cos \theta)^3} \varepsilon^2 \\
 & - \frac{2 \sin^2 \theta[(\tilde{r} + i \cos \theta)^2 + 2 \cos^2 \theta(\tilde{r} + 1)] + i \cos \theta[(\tilde{r}^2 + 4\tilde{r} + 2i \cos \theta)\tilde{r}^2 + \sin^4 \theta]}{\tilde{r}^2(\tilde{r} + 1 - i \cos \theta)^4} \varepsilon^3 \\
 & + \mathcal{O}(\varepsilon^4),
 \end{aligned} \tag{4.13}$$

and with the other normalization,

$$f(\varepsilon; \hat{r}, \theta) = \frac{\hat{r} - 1 - i \cos \theta}{\hat{r} + 1 - i \cos \theta} + \frac{\hat{r} \sin^2 \theta + (\hat{r}^2 + \sin^2 \theta) i \cos \theta}{\hat{r}^2(\hat{r} + 1 - i \cos \theta)^2} (\varepsilon^2 + \varepsilon^3) + \mathcal{O}(\varepsilon^4). \tag{4.14}$$

The first impression we get from those series is how concise Eq.(4.14) is in comparison to (4.13). In the ‘‘tilde’’ expansion, the second term (ε^1) seems to play a particular

function: it introduces the sole correction that the series needs to read the exact mass of the black hole at spatial infinity. If we expand Eq.(4.13) at $\tilde{r} \rightarrow \infty$, we find:

$$f = 1 - \frac{2(1 - \varepsilon)}{\tilde{r}} + \mathcal{O}\left(\frac{1}{\tilde{r}^2}\right) = 1 - \frac{2M}{r} + \mathcal{O}\left(\frac{1}{r^2}\right)$$

Compared with Eq.(4.11) on the axis, we can also say that no further orders of ε are expected to contribute in r^{-1} for the black hole.

A second observation concerns the horizon. For the extreme Kerr BH, the horizon is degenerated to a single point at $r = 0$. A parametric transition from the extreme Kerr to the Schwarzschild BH is illustrated in Weyl coordinates by a point-like horizon becoming a small line on the rotation axis and then growing until its length becomes $2M$ in the static case (see Fig. 4.1). If we set $\theta = 0$, so we stay on the “positive part” of the rotation axis, the north pole of the horizon should be met at the point where $e^{2U} \equiv \Re f = 0$. In Eq.(4.13), if we consider only the two first terms, we always find $\Re f = 0$ at $\tilde{r} = r = 0$, which suggests that we do not move away from the extreme Kerr geometry until we consider terms in ε^n with $n > 1$, as is obviously the case for Eq.(4.14).

4.3. Ernst Potential of the Uniformly Rotating Disk of Dust

The Ernst equation simplifies significantly the form of Einstein’s field equations. But this formalism is restricted to vacuum, and thus, it is insufficient for solving a global problem where matter fills a part of the spacetime. On the other hand, solving the full stationary and axisymmetric Einstein field equations with a source is still an arduous task today, and almost all fully relativistic solutions with matter have been obtained through numerical methods. Well, not all... If it is possible to model an astrophysical body where the pressure p vanishes everywhere (also in the body), this would set to zero the r.h.s. of each equation in (2.13), except (2.13a). Even more, the fact that the r.h.s. of Eq.(2.13c) becomes zero allows us to adopt the Weyl coordinates ($W = \rho$) for the whole spacetime, including inside the body. It is then possible to describe the interior of the body in the same coordinate system as is needed for the use of the Ernst equation in empty space. Such a model could be realized if we imagine a uniformly rotating fluid ball which flattens until it becomes an infinitely thin pressureless fluid disk, more commonly called the rigidly rotating disk of dust.

The relativistic uniformly rotating disk of dust was already well studied numerically

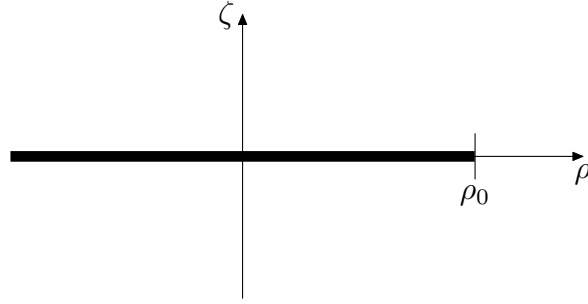


Figure 4.2: The thick line is the infinitesimally thin disk of dust. The disk has a radius ρ_0 and rotates around the axis ζ .

in [BW69, BW71], more than two decades before a complete exact analytical solution of the metric was given in [NM93, NM94, NM95]. A uniformly rotating disk seems to be unrealistic as an astrophysical object, especially because it is very unstable to fragmentation [BW71]. Nevertheless, this simple model can provide precious information regarding the general physical properties of a wider class of highly relativistic and rapidly rotating objects. The use of the disk model becomes even more interesting for us, since apart from rings, it is the only known uniformly rotating body that has a sequence of solutions reaching the extreme Kerr BH limit. And we know the exact solution analytically!

4.3.1. Ernst Potential of the Disk

The thin disk of dust is represented in Fig. 4.2. It rotates at a constant angular velocity Ω and the dust is distributed everywhere within $0 \leq \rho \leq \rho_0$ around the rotation axis at $\zeta = 0$. The parameter ρ_0 is the radius of the disk and the co-rotating metric potential V has a constant value, denoted V_0 , everywhere on the surface of the disk. On the other hand, the energy and baryonic surface mass densities are not constant within the disk: they must vary in a unique way such that each particle of dust can follow a geodesic of constant ρ and Ω by the sole effect of gravitation. The physical parameters that we just mentioned can be combined into a “relativistic parameter” called:

$$\mu = 2\Omega^2 \rho_0^2 e^{-2V_0} . \quad (4.15)$$

The disk has a sequence of solutions that can be tuned to a specific solution by fixing two parameters. But by using normalized and dimensionless coordinates, the disk can be characterized by a unique parameter. Thus, from the Ernst potential (we will write

it soon), we can extract dimensionless combinations of physical parameters as functions of only μ . If we consider also the gravitational mass M and the imaginary part of the Ernst potential at the centre of the disk b_0 , we have the following relations

$$e^{2v_0} = \frac{h' \operatorname{cn}(\hat{I}, h')^2}{h}, \quad b_0 = -\frac{\operatorname{sn}(\hat{I}, h') \operatorname{dn}(\hat{I}, h')}{h}, \quad (4.16a)$$

$$\Omega_0 \equiv \Omega \rho_0 = \frac{1}{2} \sqrt{1 - \frac{h'^2}{h^2}} \operatorname{cn}(\hat{I}, h'), \quad (4.16b)$$

$$\widetilde{M} \equiv 2\Omega M = -b_0 - \Omega_0 c_1, \quad (4.16c)$$

where $\operatorname{am}(u, k)$, $\operatorname{sn}(u, k)$, $\operatorname{cn}(u, k)$ and $\operatorname{dn}(u, k)$ are the Jacobian elliptic functions, and h , h' , \hat{I} and c_1 are the following functions of μ :⁴

$$h = \sqrt{\frac{1}{2} \left(1 + \frac{1}{\sqrt{\mu^{-2} + 1}} \right)}, \quad h' = \sqrt{\frac{1}{2} \left(1 - \frac{1}{\sqrt{\mu^{-2} + 1}} \right)}, \quad (4.16d)$$

$$\hat{I} = \frac{\sqrt{1 + \mu^2}}{\pi} \int_0^\mu \frac{g(x)}{\sqrt{\mu - x}} dx, \quad g(x) = \frac{\ln(\sqrt{1 + x^2} + x)}{\sqrt{1 + x^2}}, \quad (4.16e)$$

$$c_1 = \frac{1}{\sqrt{\mu}} \left\{ 2\sqrt{1 + \mu^2} E(\operatorname{am}(\hat{I}, h'), h') - (\mu + \sqrt{1 + \mu^2}) I_0 + I_1 \right\}, \quad (4.16f)$$

$$\text{and } I_n = \frac{1}{\pi} \int_0^\mu \frac{g(x) x^n}{\sqrt{\mu - x}} dx. \quad (4.16g)$$

We will make extensive use of elliptic functions from now, so we refer you to the definitions and conventions that we use in Appendix A. To make our equations easier to read, we will not specify the argument and modulus of the Jacobian elliptic functions when they mean ⁵:

$$am \equiv \operatorname{am}(\hat{I}, h'), \quad sn \equiv \operatorname{sn}(\hat{I}, h'), \quad cn \equiv \operatorname{cn}(\hat{I}, h'), \quad dn \equiv \operatorname{dn}(\hat{I}, h'). \quad (4.16h)$$

The Ernst potential for a uniformly rotating disk of dust is given in [NM95] for the whole spacetime. The form given there uses integrals that need to follow particular paths on a Riemann surface, but it is possible to rewrite it in the form of Rosenhain's

⁴We need to introduce here a function called \hat{I} with a “hat”, but this “hat” (written a little bit smaller), is not related to our normalization notation (written with a bigger “hat”). We prefer to write it like this to stay consistent with the notation used in other works in Jena, and hope it will not lead to confusion.

⁵Notice italic vs roman fonts to distinguish

theta function where it is not necessary to consider the Riemann surface anymore. We could decide to face up to this full form of the potential and compute the derivatives that interest us, but although the disk of dust is considered a simple model, its associated Ernst potential is lengthy and complicated. Since the multipole moments of stationary and axisymmetric configurations can be entirely obtained from the axis potential, and thus all information of the gravitation in the vacuum domain can be derived from the axis potential, it is sufficient to restrict ourselves to the rotation axis, where the potential becomes simpler. The representation of the potential that we will use is considerably different from the one given in [NM95], but the transformations are provided in detail in [MAK⁺08] (as well as other interesting information concerning the disk solution).

To make the Ernst potential of the disk a function of one physical parameter, in our case μ , we begin by introducing the normalized and dimensionless coordinates $x := \rho/\rho_0$ and $y := \zeta/\rho_0$. The potential on the axis is obtained by evaluating it in the limit $x \rightarrow 0$; it then becomes a function of two variables: $f(\mu; x = 0, y) \rightarrow f(\mu; y)$. By restricting ourselves to the positive part of the axis ($y > 0$), the Ernst potential can be written as follows:

$$f(\mu; y) = \frac{1 - iNQ_-}{N + iQ_+}, \quad (4.17a)$$

with the following functions defined as real functions of μ and y :

$$Q_{\pm} = \frac{1 - 2\Omega_0^2(y^2 + 1 + \sqrt{(y^2 + 1)^2 + \mu^{-2}})}{-b_0 \mp 2\Omega_0 y}, \quad (4.17b)$$

$$N = \exp\left\{R - 2\hat{I}(S + V + Z + U) + T\right\}, \quad (4.17c)$$

$$R = \frac{y\sqrt{\mu}}{\pi\sqrt{(y^2 + 1)^2 + \mu^{-2}}} \int_0^{\mu} \frac{x(y^2 + 1) + \mu^{-1}}{\mu(y^2 + 1) - x} \cdot \frac{g(x)}{\sqrt{\mu - x}} dx, \quad (4.17d)$$

$$S = \frac{h'(y^2 - \tau^2)}{2\sqrt{(y^2 + 1)^2 + \mu^{-2}}}, \quad (4.17e)$$

$$V = \text{sign}(y - \tau) \frac{h\sqrt{P(1 - hP)(P - h)}}{1 - hP - h'}, \quad (4.17f)$$

$$Z = X - \frac{E(h')}{K(h')} Y, \quad (4.17g)$$

$$U = \frac{\pi}{4K(h)} \left(\frac{2Y}{K(h')} - 1 \right), \quad (4.17h)$$

$$T = \ln \vartheta_2 \left(W_+, -\pi \frac{K(h')}{K(h)} \right) - \ln \vartheta_2 \left(W_-, -\pi \frac{K(h')}{K(h)} \right), \quad (4.17i)$$

$$W_{\pm} = \frac{\pi}{2K(h)} \left[\hat{I} \pm \left(Y - \frac{K(h')}{2} \right) \right], \quad (4.17j)$$

$$X = \text{sign}(y - \tau) E(v, h'), \quad (4.17k)$$

$$Y = \text{sign}(y - \tau) F(v, h'), \quad (4.17l)$$

$$v = \arcsin \left[\frac{\sqrt{1 - hP}}{h'} \right], \quad (4.17m)$$

$$P = \frac{\sqrt{(y^2 + 1)^2 + \mu^{-2}} + 2h\tau y}{(y + \tau)^2} \quad (4.17n)$$

and all the other functions (also real) depend on μ only, namely the Eqs(4.16) and

$$\tau = \sqrt[4]{\mu^{-2} + 1}.$$

The function Z is a Jacobian Zeta function like the general form given in Eq.(A.9), and ϑ_2 is the Jacobian theta function given in Eqs(A.10).

The disk solution is physically relevant between the Newtonian limit given by $\mu \rightarrow 0$ and the ultra-relativistic limit, the black hole limit, given by the smallest positive value of μ for which $\text{cn}(\hat{I}, h') = 0$. This ‘‘upper limit’’, called μ_0 , is:

$$0 \leq \mu \leq \mu_0 = 4.6296618434743420427\dots$$

Because we are interested in the behaviour of the disk near the black hole limit, where $2\Omega M \rightarrow 1$, we will later need the two normalized coordinates of Eq.(4.1). This can be achieved by substituting $y = y(\mu)$ in the Ernst potential with the help of $2\Omega M = \widetilde{M}(\mu)$ and $\Omega\rho_0 = \Omega_0(\mu)$:

$$y(\mu) = \frac{\zeta}{\rho_0} = \frac{2\Omega M}{2\Omega\rho_0} \frac{\zeta}{M} = \frac{\widetilde{M}(\mu)}{2\Omega_0(\mu)} \widehat{\zeta}, \quad (4.18a)$$

$$y(\mu) = \frac{\zeta}{\rho_0} = \frac{2\Omega\zeta}{2\Omega\rho_0} = \frac{\widetilde{\zeta}}{2\Omega_0(\mu)}. \quad (4.18b)$$

It has the consequence that $\widehat{\zeta} := \zeta/M$ makes the mass M independent of μ and $\widetilde{\zeta} := 2\Omega\zeta$ makes the angular velocity Ω independent of μ .

4.3.2. Ernst Potential of the Disk in the Black Hole Limit

The black hole limit is reached for $\mu \rightarrow \mu_0$. But simply calculating $f(\mu_0, y)$ will not give us the expected black hole potential of Eq.(2.31) on the axis, because the normalized

coordinate y becomes the axis coordinate of the inner world (see section 2.3.2). So the limit $\mu \rightarrow \mu_0$ must be achieved with a second condition that guarantees that we end up with the axis of the outside world. This is achieved by using the non-normalized coordinate ζ instead of y , which permits the radius of the disk to shrink to zero, or by evaluating the functions in the limit $y \rightarrow \infty$ along with $\mu \rightarrow \mu_0$.

Because of Eq.(4.16b), it is also equivalent to saying that the limit is reached for $\Omega_0 \rightarrow 0$ or $\rho_0 \rightarrow 0$ (Ω cannot be zero). If we evaluate all the functions in the black hole limit, we find

$$\begin{aligned} am &= \frac{\pi}{2}, \quad sn = 1, \quad cn = 0, \quad dn = h(\mu_0), \quad \hat{I} = K(h'(\mu_0)), \\ \rho_0 &= 0, \quad \Omega_0 = 0, \quad b_0 = -1, \quad 2\Omega M \equiv \widetilde{M} = 1, \\ P &= 1, \quad X = \frac{E(h'(\mu_0)) + 1 - h'(\mu_0)}{2}, \quad Y = \frac{K(h'(\mu_0))}{2}, \\ R &= 0, \quad S = \frac{h'(\mu_0)}{2}, \quad V = \frac{h(\mu_0) - h'(\mu_0) - 1}{2}, \quad Z = \frac{1 - h(\mu_0)}{2}, \\ S + V + Z &= 0, \quad U = 0, \quad T = 0 \end{aligned}$$

which give all together $N = 1$, and with the help of $2\Omega_0 y = 2\Omega\zeta$ and $2\Omega M = 1$:

$$Q_{\pm} = 1 \pm 2\Omega\zeta \quad \text{or equivalently} \quad Q_{\pm} = 1 \pm \frac{\zeta}{M}. \quad (4.19)$$

Finally, the Ernst potential of the disk from Eq.(4.17a) becomes identical to the potential of the extreme Kerr BH on the axis:

$$f(\mu_0; \widehat{\zeta}) = \frac{\widehat{\zeta} - 1 - i}{\widehat{\zeta} + 1 - i} \quad \text{or} \quad f(\mu_0; \widetilde{\zeta}) = \frac{\widetilde{\zeta} - 1 - i}{\widetilde{\zeta} + 1 - i}. \quad (4.20)$$

This is again the Ernst potential of the extreme Kerr solution on the axis, and the solution can be uniquely extended to the whole spacetime by performing a Bäcklund transformation, which gives Eq.(2.31).

4.3.3. Derivatives of the Ernst Potential in the Black Hole Limit

The next step would be to verify if the conjecture that we observed for rings is also true for the disk. In this sense, we want to verify if Eq.(4.10) holds. It can be verified by computing the derivative of the Ernst potential in the normalized parameter set $f(\mu; \widehat{\zeta})$, or equivalently, by using the non-normalized parameter set $f(M, \mu; \zeta)$ and keeping the

mass M constant for the derivatives. So we would expect, considering M constant,

$$f'(M, \mu; \zeta) \equiv \frac{df}{d\widetilde{M}} = \frac{df}{d\mu} / \frac{d\widetilde{M}}{d\mu} \quad (4.21)$$

to vanish in the black hole limit. From the chain rule, the last equation can be decomposed into

$$\frac{df}{d\mu} = \frac{-1}{N + iQ_+} \left[(f + iQ_-) \frac{dN}{d\mu} + if \frac{dQ_+}{d\mu} + iN \frac{dQ_-}{d\mu} \right], \quad (4.22a)$$

$$\frac{d\widetilde{M}}{d\mu} = -\frac{db_0}{d\mu} - c_1 \frac{d\Omega_0}{d\mu} - \Omega_0 \frac{dc_1}{d\mu} \quad (4.22b)$$

where we expect in the limit that either the first derivative vanishes or the second one blows up to infinity.

With the help of derivatives of elliptic functions in appendix A and also with Eqs(B.3), let us first compute the derivatives for Eq.(4.22b):

$$\begin{aligned} \frac{db_0}{d\mu} &= 2h'cn \left\{ 2h'^2 sn \, cn \, dn + [1 - 2dn^2] \left[E(am, h') - h^2 \hat{I} + \sqrt{1 + \mu^2} \frac{d\hat{I}}{d\mu} \right] \right\}, \\ \frac{d\Omega_0}{d\mu} &= \frac{h'^2 cn}{2} \sqrt{1 - \frac{h'^2}{h^2} \left[\frac{1}{\mu} + \frac{sn^2}{\sqrt{1 + \mu^2}} \right]} - \frac{h' sn \, dn}{\sqrt[4]{\mu^{-2} + 1}} \left[\sqrt{1 + \mu^2} \frac{d\hat{I}}{d\mu} + E(am, h') - h^2 \hat{I} \right], \\ \frac{dc_1}{d\mu} &= \frac{-I_1}{2\mu^{3/2}} + \frac{\sqrt[4]{\mu^{-2} + 1}}{2} \left[\frac{\hat{I} - 2E(am, h')}{\mu(1 + \mu^2)} + 4 \frac{dE(am, h')}{d\mu} - 2 \frac{d\hat{I}}{d\mu} \right] \end{aligned}$$

and

$$\begin{aligned} \frac{dE(am, h')}{d\mu} &= \frac{1}{\sqrt{1 + \mu^2}} \left\{ \frac{\hat{I} sn^2}{1 + \mu^2} + h'^2 \left(E(am, h') cn^2 - sn \, cn \, dn \right) \right\} + dn^2 \frac{d\hat{I}}{d\mu}, \\ \frac{d\hat{I}}{d\mu} &= \frac{\sqrt[4]{1 + \mu^2}}{2\pi} \left\{ \frac{2g(\mu)}{\sqrt{\mu}} + \int_0^\mu \frac{g(\mu) - g(x)}{(\mu - x)^{3/2}} dx + \frac{\mu}{1 + \mu^2} \int_0^\mu \frac{g(x)}{\sqrt{\mu - x}} dx \right\}. \end{aligned}$$

For the derivative of \hat{I} , we used the following substitution to have a regular function, which avoids the presence of a zero in the denominator:

$$\lim_{x \rightarrow \mu} \frac{g(x)}{\sqrt{\mu - x}} - \int_0^\mu \frac{g(x)}{2(\mu - x)^{3/2}} dx \equiv \frac{g(\mu)}{\sqrt{\mu}} + \int_0^\mu \frac{g(\mu) - g(x)}{2(\mu - x)^{3/2}} dx. \quad (4.25)$$

We can now evaluate Eq.(4.22b) in the limit $\mu \rightarrow \mu_0$:

$$\begin{aligned} \frac{d\hat{I}}{d\mu} &= 0.2404694628\dots, \\ E(am, h') &= E(h') = 1.566360837\dots, \quad \frac{dE(am, h')}{d\mu} = 0.2414654076\dots, \\ \frac{db_0}{d\mu} &= 0, \quad \frac{d\Omega_0}{d\mu} = \frac{1}{2\tau} \left[\frac{h^2 K(h') - E(h')}{\sqrt{1 + \mu^2}} - \frac{d\hat{I}}{d\mu} \right] = -0.1197970406\dots, \\ \frac{dc_1}{d\mu} &= 0.1263305681\dots \end{aligned}$$

And we can see now that the derivative of \widetilde{M} does not become zero and stays finite:

$$\frac{d\widetilde{M}}{d\mu}(\mu_0) = -c_1(\mu_0) \frac{d\Omega_0}{d\mu}(\mu_0) = 0.1256363714\dots \quad (4.26)$$

Since (4.22b) stays finite, then we expect Eq.(4.22a) to vanish in the limit.

Most terms in (4.22a) are already known by taking the results in section (4.3.2), so only the three derivatives of N , Q_+ and Q_- need extra computations. We first use Eqs(4.18) to express the Eqs(4.17a) as functions of M , μ and ζ , then we split Q_{\pm} into numerator and denominator parts to perform the derivative:

$$Q_{\pm} = \frac{2M^2 - \widetilde{M}^2(\zeta^2 + \rho_0^2 + \sqrt{(\zeta^2 + \rho_0^2)^2 + \mu^{-2}\rho_0^4})}{2M(\mp \widetilde{M}\zeta - Mb_0)} = \frac{Q_{\text{NUM}}}{Q_{\text{DEN}_{\pm}}},$$

where \widetilde{M} , ρ_0 and b_0 are functions of μ . The derivative gives:

$$\begin{aligned} \frac{dQ_{\pm}}{d\mu} &= \frac{1}{Q_{\text{DEN}_{\pm}}} \left[\frac{dQ_{\text{NUM}}}{d\mu} - Q_{\pm} \frac{dQ_{\text{DEN}_{\pm}}}{d\mu} \right], \quad (4.27) \\ \frac{dQ_{\text{NUM}}}{d\mu} &= -2\widetilde{M} \left[\zeta^2 + \rho_0^2 + \sqrt{(\zeta^2 + \rho_0^2)^2 + \mu^{-2}\rho_0^4} \right] \frac{d\widetilde{M}}{d\mu} \\ &\quad - 2\widetilde{M}^2 \rho_0 \left[1 + \frac{\zeta^2 + (1 + \mu^{-2})\rho_0^2}{\sqrt{(\zeta^2 + \rho_0^2)^2 + \mu^{-2}\rho_0^4}} \right] \frac{d\rho_0}{d\mu} + \frac{\widetilde{M}^2 \rho_0^4}{\mu^3 \sqrt{(\zeta^2 + \rho_0^2)^2 + \mu^{-2}\rho_0^4}}, \\ \frac{dQ_{\text{DEN}_{\pm}}}{d\mu} &= 2M(\mp \zeta \frac{d\widetilde{M}}{d\mu} - M \frac{db_0}{d\mu}), \end{aligned}$$

with the derivatives of \widetilde{M} and b_0 already calculated and

$$\frac{d\rho_0}{d\mu} = \frac{2M}{\widetilde{M}} \left[\frac{d\Omega_0}{d\mu} - \frac{\Omega_0}{\widetilde{M}} \frac{d\widetilde{M}}{d\mu} \right]. \quad (4.28)$$

In the limit $\mu \rightarrow \mu_0$ (involving $\rho_0 \rightarrow 0$), Eqs (4.28) and (4.27) become:

$$\frac{d\rho_0}{d\mu}(\mu_0) = 2M \frac{d\Omega_0}{d\mu}(\mu_0) \approx -0.2395940813 M, \quad (4.29)$$

$$\frac{dQ_{\pm}}{d\mu}(\mu_0) = \pm \frac{d\widetilde{M}}{d\mu}(\mu_0) \frac{\zeta}{\widetilde{M}} = \mp c_1(\mu_0) \frac{d\Omega_0}{d\mu}(\mu_0) \frac{\zeta}{\widetilde{M}} \approx \pm 0.1256 \frac{\zeta}{\widetilde{M}}. \quad (4.30)$$

The last derivatives that remain are those needed for N :

$$\frac{dN}{d\mu} = N \left\{ \frac{dR}{d\mu} - 2\hat{I} \left[\frac{dS}{d\mu} + \frac{dV}{d\mu} + \frac{dZ}{d\mu} + \frac{dU}{d\mu} \right] - 2 \frac{d\hat{I}}{d\mu} [S + V + Z + U] + \frac{dT}{d\mu} \right\}. \quad (4.31)$$

The derivative of R is finite for any value of $0 < \mu \leq \mu_0$, but this becomes evident only if we use a similar substitution like in Eq.(4.25) to keep all terms regular. The result yields

$$\begin{aligned} \frac{dR}{d\mu} = & \left\{ \frac{\zeta^4 - \rho_0^4 \tau^4}{\rho_0} \frac{d\rho_0}{d\mu} + \frac{(\zeta^2 + \rho_0^2)^2 - \mu^{-2} \rho_0^4}{2\mu} \right\} \frac{R}{(\zeta^2 + \rho_0^2)^2 + \mu^{-2} \rho_0^4} \\ & + \frac{\rho_0}{\pi \sqrt{(\zeta^2 + \rho_0^2)^2 + \mu^{-2} \rho_0^4}} \left\{ (\zeta^2 + \rho_0^2 \tau^4) \frac{g(\mu)}{\zeta} + \zeta \sqrt{\mu} \int_0^{\mu} \frac{G(x, \mu, \zeta) dx}{\sqrt{\mu - x}} \right\}, \end{aligned}$$

with the integrand function

$$\begin{aligned} G(x, \mu, \zeta) = & \frac{g(\mu)}{2(\mu - x)} \left(1 + \frac{\rho_0^2 \tau^4}{\zeta^2} \right) + \frac{g(x)}{\mu(\zeta^2 + \rho_0^2) - x\rho_0^2} \left[2(x + \mu^{-1})\rho_0 \frac{d\rho_0}{d\mu} - \frac{\rho_0^2}{\mu^2} \right. \\ & \left. - \frac{x(\zeta^2 + \rho_0^2) + \mu^{-1} \rho_0^2}{2(\mu - x)} - \frac{x(\zeta^2 + \rho_0^2) + \mu^{-1} \rho_0^2}{\mu(\zeta^2 + \rho_0^2) - x\rho_0^2} \left(\zeta^2 + \rho_0^2 - 2(\mu - x)\rho_0 \frac{d\rho_0}{d\mu} \right) \right]. \end{aligned}$$

The derivatives for S , V , U and Z give

$$\begin{aligned} \frac{dS}{d\mu} = & \frac{S \rho_0}{(\zeta^2 + \rho_0^2)^2 + \mu^{-2} \rho_0^4} \left[\frac{\rho_0^3}{\mu^3} - 2(\zeta^2 + \tau^4 \rho_0^2) \frac{d\rho_0}{d\mu} \right] \\ & - \frac{1}{\sqrt{(\zeta^2 + \rho_0^2)^2 + \mu^{-2} \rho_0^4}} \left[\frac{h(\zeta^2 - \tau^2 \rho_0^2)}{4(1 + \mu^2)} + h' \tau^2 \rho_0 \left(\frac{d\rho_0}{d\mu} - \frac{\rho_0}{2\mu(1 + \mu^2)} \right) \right], \\ \frac{dV}{d\mu} = & V \left\{ h'^3 h \left[2 - \frac{hP}{1 - hP} - \frac{h}{P - h} + \frac{2h(h'P - h)}{h'(1 - hP - h')} \right] \right\} \end{aligned}$$

$$\begin{aligned}
& + \frac{1}{2} \frac{dP}{d\mu} \left[\frac{1}{P} - \frac{h}{1-hP} + \frac{1}{P-h} + \frac{2h}{1-hP-h'} \right] \Big\} , \\
\frac{dZ}{d\mu} &= \frac{dX}{d\mu} - \frac{E(h')}{K(h')} \frac{dY}{d\mu} - \frac{Y}{\sqrt{1+\mu^2}} \left[h^2 + \frac{E(h')}{K(h')} \left(\frac{E(h')}{K(h')} - 2h^2 \right) \right] , \\
\frac{dU}{d\mu} &= \frac{\pi}{4K(h)} \left\{ \frac{1}{\sqrt{1+\mu^2}} \left[\frac{E(h)}{K(h)} - h^2 - \frac{2Y}{K(h')} \left(\frac{E(h)}{K(h)} - \frac{E(h')}{K(h')} + \frac{\mu}{\sqrt{1+\mu^2}} \right) \right] \right. \\
& \left. + \frac{2}{K(h')} \frac{dY}{d\mu} \right\} ,
\end{aligned}$$

where the derivatives of X , Y and P are

$$\begin{aligned}
\frac{dY}{d\mu} &= \text{sign}(\zeta - \tau\rho_0) \frac{dF(v, h')}{d\mu} , \quad \frac{dX}{d\mu} = \text{sign}(\zeta - \tau\rho_0) \frac{dE(v, h')}{d\mu} , \\
\frac{dF(v, h')}{d\mu} &= \frac{1}{\sqrt{hP}} \frac{dv}{d\mu} + \frac{1}{\sqrt{1+\mu^2}} \left[h^2 F(v, h') - E(v, h') + \sqrt{(1-hP)(1-h/P)} \right] , \\
\frac{dE(v, h')}{d\mu} &= \sqrt{hP} \frac{dv}{d\mu} + \frac{h^2}{\sqrt{1+\mu^2}} \left[F(v, h') - E(v, h') \right] , \\
\frac{dv}{d\mu} &= \frac{1}{\sqrt{h(P-h)}} \left[\frac{-h}{2\sqrt{1-hP}} \left(\frac{dP}{d\mu} + \frac{h^2 P}{\sqrt{1+\mu^2}} \right) + \frac{h^2 \sqrt{1-hP}}{\sqrt{1+\mu^2}} \right] , \\
\frac{dP}{d\mu} &= \frac{1}{(\zeta + \tau\rho_0)^2} \left\{ \frac{\rho_0}{\sqrt{(\zeta^2 + \rho_0^2)^2 + \mu^{-2} \rho_0^4}} \left[2(\zeta^2 + \tau^4 \rho_0^2) \frac{d\rho_0}{d\mu} - \frac{\rho_0^3}{\mu^3} \right] \right. \\
& \left. + h\tau\rho_0\zeta \left[\frac{1}{\sqrt{1+\mu^2}} - \frac{1}{\mu} \right] + 2h\tau\zeta \frac{d\rho_0}{d\mu} - 2P\tau(\zeta + \tau\rho_0) \left[\frac{-\rho_0}{2\mu(1+\mu^2)} + \frac{d\rho_0}{d\mu} \right] \right\} .
\end{aligned}$$

Finally, only the derivative of T remains, which is made of theta functions. Later in this work, we will need an elegant way to produce a series of the theta functions of T . So we spend some effort on writing the derivative of T in a form which involves functions that were already familiar or used above and where no theta functions are called anymore. If we consider in general a function $\vartheta_2(w, B)$ where w and B are functions of a variable x , one can obtain with the help of Eq.(A.12), Eq.(A.11) and Heuman's Lambda function (A.8) the following result:

$$\begin{aligned}
\frac{d}{dx} \ln \vartheta_2(w, B) &= \Lambda_0 \frac{dw}{dx} + \left\{ \frac{\Lambda_0^2}{4} + \frac{K^2(k)}{\pi^2} \left[\text{dn}^2(u, k') - 1 + \frac{E(k)}{K(k)} \right] \right\} \frac{dB}{dx} \quad (4.32) \\
\text{with } w &= \frac{\pi u}{2K(k)} , \quad B = -\pi \frac{K(k')}{K(k)} \quad \text{and} \quad \Lambda_0 \equiv \Lambda_0(\text{am}(u, k'), k) .
\end{aligned}$$

This can be used for the theta functions of T , so we get

$$\frac{dT}{d\mu} = \Lambda_{0+} \frac{dW_+}{d\mu} - \Lambda_{0-} \frac{dW_-}{d\mu} + \left\{ \frac{\Lambda_{0+}^2 - \Lambda_{0-}^2}{4} + \frac{K^2(h)}{\pi^2} [\text{dn}^2(u_+, h') - \text{dn}^2(u_-, h')] \right\} \frac{dB}{d\mu}, \quad (4.33a)$$

$$\frac{dW_{\pm}}{d\mu} = \frac{\pi}{2K(h)} \left\{ \frac{h'^2 K(h) - E(h)}{K(h)\sqrt{1+\mu^2}} u_{\pm} + \frac{d\hat{I}}{d\mu} \pm \frac{dY}{d\mu} \mp \frac{h^2 K(h') - E(h')}{2\sqrt{1+\mu^2}} \right\}, \quad (4.33b)$$

$$\frac{dB}{d\mu} = \frac{\pi}{K(h)\sqrt{1+\mu^2}} \left[E(h') - K(h') \left(1 - \frac{E(h)}{K(h)} \right) \right], \quad (4.33c)$$

with the use of the short forms $B \equiv -\pi K(h')/K(h)$, $\Lambda_{0\pm} \equiv \Lambda_0(\text{am}(u_{\pm}, h'), h)$ and $u_{\pm} \equiv \hat{I} \pm (Y - K(h')/2)$. The derivative of the Ernst potential with respect to the relativistic parameter μ for disks of constant mass is now fully known.

Only the derivatives in Eq.(4.31) remain to be evaluated in the black hole limit. First, we need the following derivatives in the limit $\mu \rightarrow \mu_0$:

$$\begin{aligned} \frac{dP}{d\mu} &= 4\tau(h-1) \frac{M}{\zeta} \frac{d\Omega_0}{d\mu}(\mu_0), \quad \frac{dv}{d\mu} = \sqrt{h} \left[2\tau \frac{M}{\zeta} \frac{d\Omega_0}{d\mu}(\mu_0) + \frac{h-1}{2\sqrt{1+\mu_0^2}} \right], \\ \frac{dY}{d\mu} &= + \frac{dF(v, h')}{d\mu} = 2\tau \frac{M}{\zeta} \frac{d\Omega_0}{d\mu}(\mu_0) + \frac{h^2 K(h') - E(h')}{2\sqrt{1+\mu_0^2}}, \\ \frac{dX}{d\mu} &= + \frac{dE(v, h')}{d\mu} = h \left[2\tau \frac{M}{\zeta} \frac{d\Omega_0}{d\mu}(\mu_0) + \frac{hK(h') - hE(h') - h'^2}{2\sqrt{1+\mu_0^2}} \right], \\ \frac{dW_{\pm}}{d\mu} &= \frac{\pi}{2K(h)} \left\{ \frac{K(h')}{\sqrt{1+\mu_0^2}} \left(h'^2 - \frac{E(h)}{K(h)} \right) + \frac{d\hat{I}}{d\mu} \pm 2\tau \frac{M}{\zeta} \frac{d\Omega_0}{d\mu}(\mu_0) \right\}, \\ \Lambda_{0\pm} &= \Lambda_0\left(\frac{\pi}{2}, h'(\mu_0)\right) = 1, \end{aligned}$$

where τ , h and h' are obviously evaluated at μ_0 . Then, the limit $\mu \rightarrow \mu_0$ for the derivatives of R , S , V , Z , U and T gives

$$\begin{aligned} \frac{dR}{d\mu} &= \frac{2I_1(\mu_0)}{\sqrt{\mu_0}} \frac{M}{\zeta} \frac{d\Omega_0}{d\mu}(\mu_0), \quad \frac{dS}{d\mu} = \frac{-h}{4(1+\mu_0^2)}, \\ \frac{dV}{d\mu} &= \frac{h'+h}{4(1+\mu_0^2)} + 2\tau h(h-1) \frac{M}{\zeta} \frac{d\Omega_0}{d\mu}(\mu_0), \\ \frac{dZ}{d\mu} &= \left(h - \frac{E(h')}{K(h')} \right) 2\tau \frac{M}{\zeta} \frac{d\Omega_0}{d\mu}(\mu_0) - \frac{h'}{4(1+\mu_0^2)}, \\ \frac{dU}{d\mu} &= \frac{\pi\tau}{K(h)K(h')} \frac{M}{\zeta} \frac{d\Omega_0}{d\mu}(\mu_0), \quad \frac{dT}{d\mu} = \frac{2\pi\tau}{K(h)} \frac{M}{\zeta} \frac{d\Omega_0}{d\mu}(\mu_0). \end{aligned}$$

The identities (B.2) are helpful to simplify the results. Now, we can combine these last results with the functions evaluated at μ_0 in section 4.3.2 to write down the black hole limit of Eq.(4.31), which becomes:

$$\frac{dN}{d\mu} = \frac{2M}{\zeta} \frac{d\Omega_0}{d\mu}(\mu_0) \left\{ \frac{I_1(\mu_0)}{\sqrt{\mu_0}} - 2\tau h^2 K(h') + 2\tau E(h') \right\} .$$

What is found between the brackets is just c_1 evaluated at μ_0 (see Eq.(4.16f)). So the limit can be simply written:

$$\frac{dN}{d\mu}(\mu_0) = \frac{2M}{\zeta} c_1(\mu_0) \frac{d\Omega_0}{d\mu}(\mu_0) . \quad (4.34)$$

We are now able to evaluate the derivative for the Ernst potential, in Eq.(4.22a). With $N(\mu_0) = 1$, Eqs (4.19), (4.20), (4.30) and (4.34), we find the expected result:

$$\frac{df}{d\mu}(\mu_0) = 0 .$$

This also means that (4.21) vanishes since the denominator given by (4.26) remains finite:

$$\frac{df}{d\widetilde{M}}(\widetilde{M} = 1) = 0 .$$

4.4. Taylor Series of the Disk

Beyond the single task of verifying if Eq.(4.10) holds for the disk, we can expand the Ernst potential of the disk using a Taylor series near the BH limit, written in an explicit form similar to Eqs(4.8) and (4.9). Since the functions of the disk are all written as function of μ and ζ , we choose to keep the relativistic parameter $(\mu - \mu_0)$ in the expansions instead of converting everything into the more universal parameter $\varepsilon = 1 - 2\Omega M$.

To realize an explicit form of the Taylor series, we make use of a “computer algebra system” (i.e. Maple and Mathematica) and we divide the work in two steps. First, we write down the series of all functions that depend on μ only. Then, we do the same for the remaining functions which depend on μ and ζ . To perform these calculations, the technical challenge was to program the series such that the time and memory space of the computation do not blow up. We present here some technical choices to compute efficiently and compare the series with the exact functions in the context of physics. For functions depending on ζ , the computation is done twice with using the two normaliza-

tions already introduced before: either with $\tilde{\zeta} = 2\Omega\zeta$ or $\hat{\zeta} = \zeta/M$. [KLM10]

4.4.1. Series of Functions of μ

The set of functions that depend on μ only are listed in Eqs(4.16). For each of these functions, the resulting derivatives of μ in the limit $\mu \rightarrow \mu_0$ give pure numbers (no other variables).

The direct computation of a series of \hat{I} with the form given previously is impracticable because zeros come out for some denominators, which was the reason for using the substitution (4.25) previously. To avoid this pathology, we rewrite the function with the substitution $x = \mu \sin^2 \phi$. This has also the effect of removing the dependence on μ in the interval of integration:

$$\hat{I}(\mu) = \frac{\sqrt[4]{1+\mu^2}}{\pi} \int_0^\mu \frac{g(x)}{\sqrt{\mu-x}} dx = \frac{2\sqrt[4]{\mu^2+\mu^4}}{\pi} \int_0^{\pi/2} g(\mu \sin^2 \phi) \sin \phi d\phi. \quad (4.35)$$

The derivatives of \hat{I} are then easy to calculate by using recursively the relation in Eq.(B.3d). The series starts with

$$\begin{aligned} \hat{I}(\mu) = & 1.5752 + 0.24046 (\mu - \mu_0) - 0.017245 (\mu - \mu_0)^2 \\ & + 0.0017270 (\mu - \mu_0)^3 + \mathcal{O}[(\mu - \mu_0)^4], \end{aligned} \quad (4.36)$$

where decimal numbers are truncated after 5 significant digits. Similarly, the derivatives of all other functions of μ that we need for the Ernst potential can be expressed recursively with the help of the relations given in Eqs(B.3), (A.5) and (A.7).

After this first task, we can already express in a Taylor series a few functions with physical meaning, such as the Ernst potential at the origin, given by $f(\rho = 0, \zeta = 0) \equiv f_0 = e^{2V_0} + ib_0$, as well as the dimensionless products $\Omega\rho_0$ and $2\Omega M$. These four functions and other functions within them need to be expanded with significant numerical precision since they are needed in the remaining series expansions.

Let us now introduce the following notation for the n -th order Taylor approximation \mathcal{A}_n of a function of μ near the extreme Kerr BH limit:

$$\mathcal{A}_n(\Omega\rho_0(\mu)) = \sum_{j=0}^n c_j (\mu - \mu_0)^j, \quad (4.37)$$

$$\text{with } \mathcal{A}_\infty(\Omega\rho_0(\mu)) = \Omega\rho_0(\mu),$$

j	e^{2V_0}	b_0	$\Omega\rho_0$	$2\Omega M$
0	0	-1	0	1
1	0	0	$-1.1979704 \times 10^{-1}$	1.2563637×10^{-1}
2	6.1997318×10^{-3}	2.8702661×10^{-2}	8.2373333×10^{-3}	$-2.2207483 \times 10^{-2}$
3	$-2.1917290 \times 10^{-3}$	$-3.9472326 \times 10^{-3}$	4.3533289×10^{-4}	1.1246071×10^{-3}
4	4.5766410×10^{-4}	3.5824068×10^{-4}	$-1.9230828 \times 10^{-4}$	1.7087311×10^{-5}
5	$-7.5851829 \times 10^{-5}$	$-2.0388433 \times 10^{-5}$	3.8239383×10^{-5}	$-1.4784817 \times 10^{-5}$
6	1.1139165×10^{-5}	$-9.6924305 \times 10^{-7}$	$-6.5882003 \times 10^{-6}$	3.0205335×10^{-6}
7	$-1.5243204 \times 10^{-6}$	6.0947891×10^{-7}	1.0947125×10^{-6}	$-5.0848591 \times 10^{-7}$
8	1.9941471×10^{-7}	$-1.4423676 \times 10^{-7}$	$-1.8180382 \times 10^{-7}$	8.0708022×10^{-8}
9	$-2.5296376 \times 10^{-8}$	2.7737508×10^{-8}	3.0627438×10^{-8}	$-1.2616141 \times 10^{-8}$
10	3.1381072×10^{-9}	$-4.9011518 \times 10^{-9}$	$-5.2656087 \times 10^{-9}$	1.9805535×10^{-9}

Table 4.1: First coefficients c_j of the expansions defined in Eq.(4.37) for the functions e^{2V_0} , b_0 , $\Omega\rho_0$ and $2\Omega M$. The single digit numbers are exact values, while the eight digits numbers are truncated.

where $\Omega\rho_0(\mu)$ is used here only as an example. For the short list of functions that we introduced, we show their first expansion coefficients c_j in Table 4.1. The same functions are also plotted in Fig. 4.3 with their respective Taylor approximations of order $n = 5$ and $n = 10$. This last figure allows us to assess a first opinion on the quality of the Taylor series. Approximations with $n = 5$ and $n = 10$ are indistinguishable from the exact function on the plot for $\mu > 2$, while polynomials of higher orders ($n = 10$ vs $n = 5$ on the plot) improve the approximation near the Newtonian limit ($\mu \rightarrow 0$) reasonably well. In Fig. 4.4, one can see that the Taylor series seem to converge to their respective exact functions from the extreme Kerr BH limit ($\mu = \mu_0$) all the way down to the Newtonian limit ($\mu = 0$). The convergence is readily seen in the figure with e^{2V_0} , while for the three other functions, one must take into account the logarithmic scale to appreciate it. Since the function e^{2V_0} is related to the redshift of photons emitted from the surface, as defined in Eq.(2.8), we can calculate how wrong the redshift becomes from the approximations. In the Newtonian limit, where the Taylor approximations have the greatest deviations, the redshifts of these photons become $Z_0 = 0.17691$, 9.0567×10^{-3} , 4.2302×10^{-4} for $n = 5, 10, 15$ respectively, while obviously no redshift is expected from exact Newtonian solutions.

4.4.2. Series of Functions of $(\mu, \tilde{\zeta})$

The following step to obtain a series of the Ernst potential of the disk is to expand the remaining terms which depend on both μ and $\tilde{\zeta}$. At this point, we introduce the

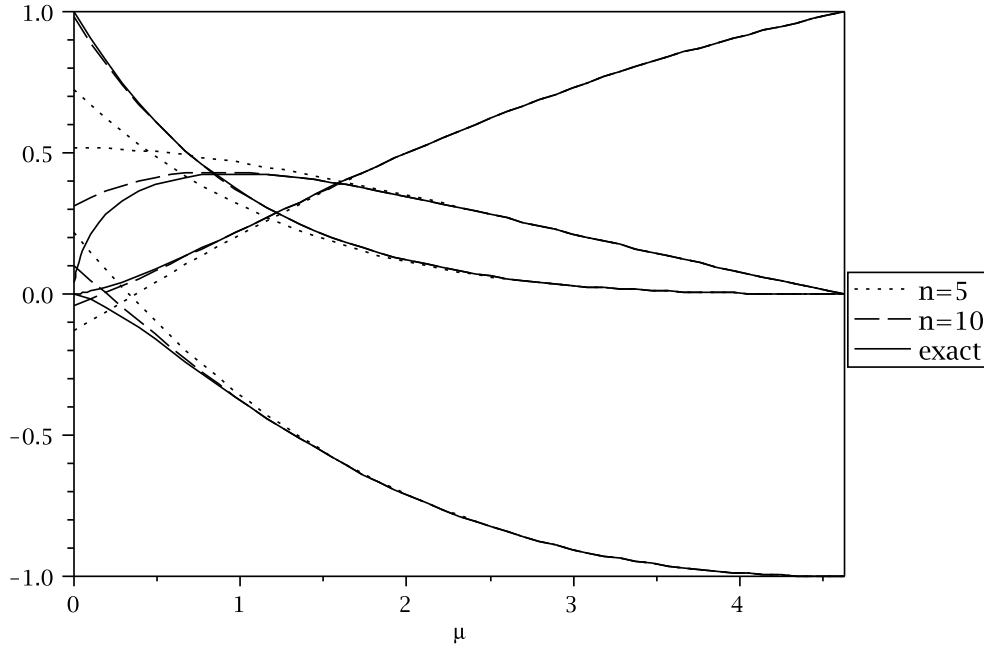


Figure 4.3: Four exact functions of μ compared to their Taylor approximations with orders $n = 5$ and 10 . On the right side of the graphic, the functions are from the top to the bottom: $2\Omega M$, $\Omega\rho_0$, e^{2V_0} and b_0 .

normalized coordinate $\tilde{\zeta} \equiv 2\Omega\zeta$ in every function given in Eqs (4.17). By computing series near $\mu = \mu_0$ for $R(\mu, \tilde{\zeta})$, $S(\mu, \tilde{\zeta})$, $V(\mu, \tilde{\zeta})$, $Z(\mu, \tilde{\zeta})$, $U(\mu, \tilde{\zeta})$ and $T(\mu, \tilde{\zeta})$, we can then determine the series of $N(\mu, \tilde{\zeta})$ which can be combined with the series of $Q_{\pm}(\mu, \tilde{\zeta})$ to obtain the Ernst potential of the disk on the axis.

For the function $R(\mu, \tilde{\zeta})$, it is necessary to rearrange the integral with the substitution $x = \mu \sin^2 \phi$, similarly to Eq.(4.35), in order to calculate numerically:

$$R(\mu, \tilde{\zeta}) = \frac{\sqrt{2}\Omega_0\tilde{\zeta}}{\pi\sqrt{(\tilde{\zeta}^2 + 4\Omega_0^2)^2\mu^2 + 2\Omega_0^4}} \int_0^{\pi/2} \frac{(\tilde{\zeta}^2 + 4\Omega_0^2)\mu^2 \sin^2 \phi + 4\Omega_0^2}{\tilde{\zeta}^2 + 4\Omega_0^2 \cos^2 \phi} \cdot g(\mu \sin^2 \phi) \sin \phi \, dx$$

where Ω_0 is a function of μ already expanded before. Once the integrand is expanded in a series of $(\mu - \mu_0)$, the integral becomes easier to perform on each individual term of the expansion. This series contains polynomials of $1/\tilde{\zeta}$ with odd exponents and starts with

$$R(\mu, \tilde{\zeta}) = -\frac{0.24697}{\tilde{\zeta}}(\mu - \mu_0) - \frac{0.015102}{\tilde{\zeta}}(\mu - \mu_0)^2$$

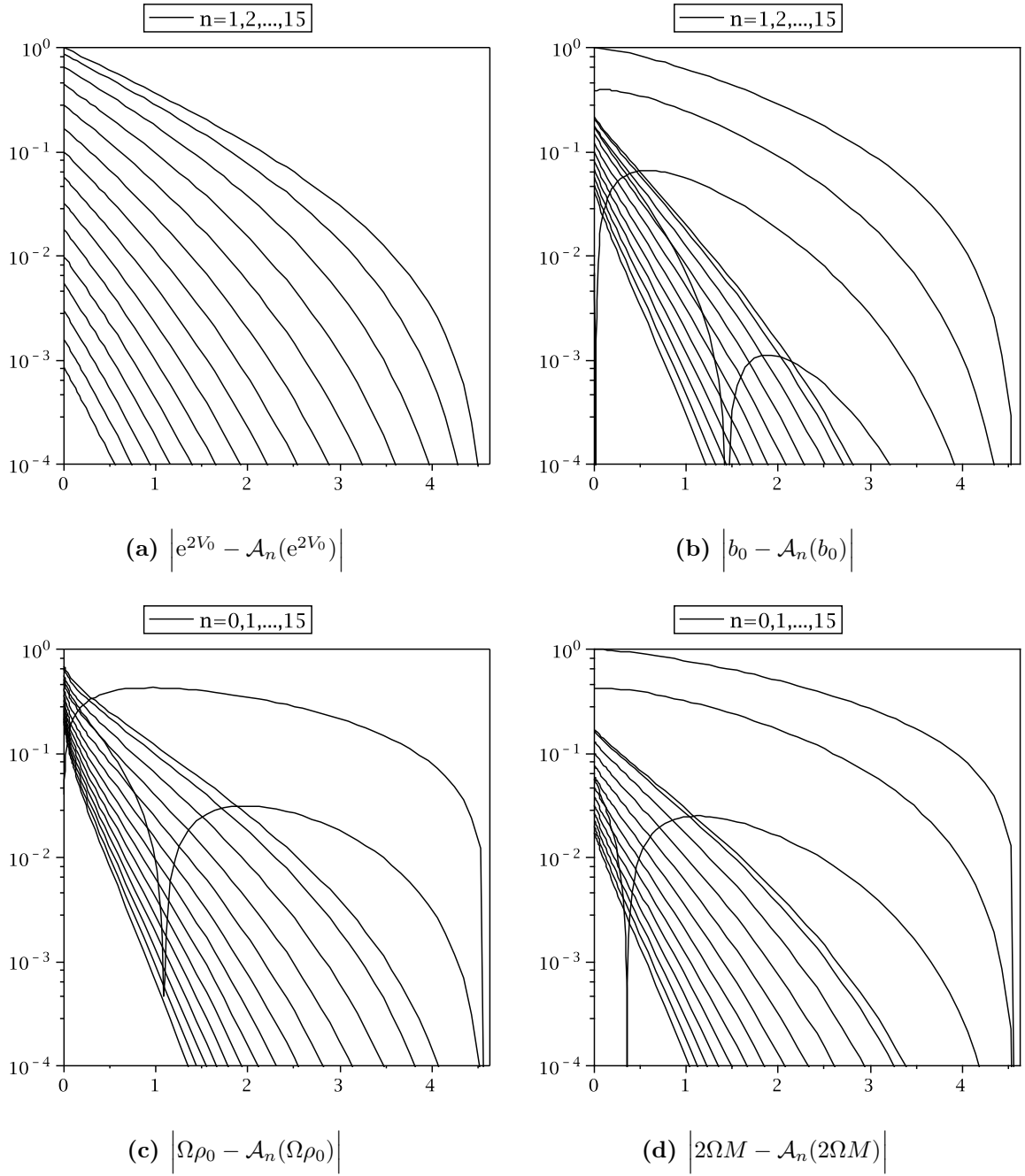


Figure 4.4: These figures show the deviation of n -th order Taylor approximation \mathcal{A}_n to their respective exact functions. The Taylor series are truncated into polynomials of order $n = 1$ to 15 for the functions e^{2V_0} and b_0 , and from $n = 0$ to 15 for $\Omega\rho_0$ and $2\Omega M$. The lines are ordered from the smallest n to the largest when one follows the abscissa from right to left. The parameter μ is shown on the abscissae and the ordinates show on a logarithmic scale the absolute value of the deviations. The plunges to zero in the middle for a few curves only mean that the corresponding polynomials \mathcal{A}_n intersect the exact function at that point.

$$+ \left(\frac{0.0063269}{\tilde{\zeta}} + \frac{0.0021138}{\tilde{\zeta}^3} \right) (\mu - \mu_0)^3 + \mathcal{O}[(\mu - \mu_0)^4] \quad (4.38)$$

where numbers are again truncated after five significant digits. The next functions to expand, $S(\mu, \tilde{\zeta})$ and $P(\mu, \tilde{\zeta})$, do not require anything other than a direct computation of the series from the computer. The series of S reads

$$S(\mu, \tilde{\zeta}) = 0.053082 - 0.011080 (\mu - \mu_0) + \left(0.0022735 - \frac{0.0061646}{\tilde{\zeta}^2} \right) (\mu - \mu_0)^2 \\ + \left(-4.5822 \times 10^{-4} + \frac{0.0021646}{\tilde{\zeta}^2} \right) (\mu - \mu_0)^3 + \mathcal{O}[(\mu - \mu_0)^4]. \quad (4.39)$$

At this point, if someone were to look at plots of the series R , S and P in comparison to their exact functions, one would realize that the series diverge in a specific region of the axis $\tilde{\zeta}$. Indeed, none of the series which has the coordinate $\tilde{\zeta}$ in it converges on the entire domain, except obviously in the extreme Kerr BH limit. To get a better picture of the domain of convergence of our last series, let us have a closer look at the factor $\sqrt{(y^2 + 1)^2 + \mu^{-2}}$ which is present in each of the three functions. It is known that a Taylor series (binomial series) of a function $(1 + x)^k$ at $x = 0$ converges only for $|x| \leq 1$. Let write now our square root, with our coordinate $\tilde{\zeta} = 2\Omega_0 y$, in a form which looks like the binomial $(1 + x)^k$:

$$\frac{\sqrt{(y^2 + 1)^2 + \mu^{-2}}}{y^2 + 1} = \left[1 + \frac{16\Omega_0^4}{\mu^2 \tilde{\zeta}^4} \left[1 + \frac{4\Omega_0^2}{\tilde{\zeta}^2} \right]^{-2} \right]^{1/2}. \quad (4.40)$$

We obtain a function made of a binomial ($k = -2$) included in a second larger one ($k = 1/2$), here enclosed in square brackets. Series near the extreme Kerr BH are series near the value $\mu = \mu_0$, where $\Omega_0(\mu_0) = 0$. If we identify Ω_0 as our relativistic parameter and make μ a function of it, $\mu(\Omega_0)$, we can now interpret Taylor series near the black hole limit as series near the value $\Omega_0 = 0$.⁶ Our two binomials can now be solved for the convergence condition of binomial series. The series of our square root function converges only for

$$\tilde{\zeta} \geq 2\Omega_0 \quad \text{and} \quad \tilde{\zeta} \geq 2\Omega_0 \Re \left(\sqrt{\frac{1}{\mu} - 1} \right). \quad (4.41)$$

The first condition is important for $\mu \geq 1/2$ while the second is relevant for $\mu \leq 1/2$. Since the square root function from Eq.(4.40) is called in all remaining functions needed

⁶In the Newtonian limit $\Omega_0 = 0$ also holds, so it is a bad relativistic parameter, but this can be ignored for the purpose of finding a domain of convergence.

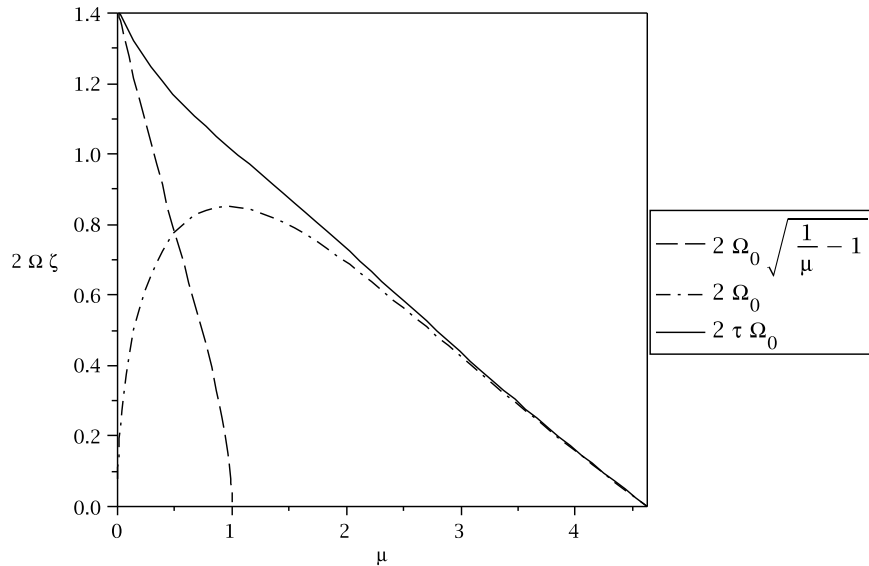


Figure 4.5: Sign change boundary from $\text{sign}(\tilde{\zeta} - 2\tau\Omega_0)$ in comparison to the limit of convergence from Eq.(4.41). Functions which depend on $\sqrt{(y^2 + 1)^2 + \mu^{-2}}$ are expected to diverge below either $2\Omega_0$ or $2\Omega_0\sqrt{\mu^{-1} - 1}$, which makes series with negative $\text{sign}(\tilde{\zeta} - 2\tau\Omega_0)$ almost irrelevant.

for the Ernst potential, its domain of convergence is expected to constrain the convergence of all series that remain to be calculated, including the final series of the Ernst potential. Note that condition $\tilde{\zeta} \geq 2\Omega_0$ is equivalent to saying $\zeta \geq \rho_0$, which suggests that the segment of the axis where the divergence occurs is equal to the radius of the disk. As the disk shrinks to the origin ($\rho_0 \rightarrow 0$) as we approach the BH limit, so does the region in which the functions diverge.

The function $V(\mu, \tilde{\zeta})$ is not difficult to expand by calling $P(\mu, \tilde{\zeta})$ where needed. But which sign should we choose from the factor “ $\text{sign}(y - \tau)$ ”? As we know from Eq.(4.41), series are expected to diverge in a region near the disk, so we might prefer to use the sign which is valid far from the disk: the “plus sign”. Moreover, it happens that the sign boundary, $\tilde{\zeta} = 2\tau\Omega_0$ in our normalized coordinates, follows closely the limits of convergence given above, as one can see in Fig. 4.5. The result is that $\tilde{\zeta} = 2\tau\Omega_0$ approximates very well the limit of convergence from above, and indeed, series like $V(\mu, \tilde{\zeta})$ diverge close to the sign change boundary, which makes the domain with “negative sign” almost irrelevant for our series. Although we choose the “plus sign”, the series of V is anchored

($\mu = \mu_0$) on a negative value:

$$\begin{aligned}
V(\mu, \tilde{\zeta}) = & -0.055908 + \left(0.012264 + \frac{0.0013618}{\tilde{\zeta}}\right) (\mu - \mu_0) \\
& + \left(-0.0026412 - \frac{6.6713 \times 10^{-4}}{\tilde{\zeta}} + \frac{0.0064947}{\tilde{\zeta}^2}\right) (\mu - \mu_0)^2 \\
& + \left(5.5869 \times 10^{-4} - \frac{2.1410 \times 10^{-4}}{\tilde{\zeta}} - \frac{0.0023506}{\tilde{\zeta}^2} - \frac{2.3723 \times 10^{-4}}{\tilde{\zeta}^3}\right) (\mu - \mu_0)^3 \\
& + \mathcal{O}[(\mu - \mu_0)^4] .
\end{aligned} \tag{4.42}$$

The remaining functions $Z(\mu, \tilde{\zeta})$, $U(\mu, \tilde{\zeta})$ and $T(\mu, \tilde{\zeta})$ depend all on the elliptic integrals given by $X(\mu, \tilde{\zeta})$ and $Y(\mu, \tilde{\zeta})$. Since we restrict ourselves from now on to the “plus sign” domain, the latter functions become simply $X = E(v, h')$ and $Y = F(v, h')$. The derivatives needed for the series are all defined in Appendix A, but one must be careful to compute a routine which generates series out of elliptic functions in a reasonable amount of computation time and memory. Instead of using recursively Eqs(A.7) for each derivative of the Jacobian elliptic functions, a better strategy is to produce instead series of these functions by expanding the right hand sides of

$$\begin{aligned}
v = \text{am}(Y, h') &= \arcsin \left[\frac{\sqrt{1 - hP}}{h'} \right] , \\
\sin(v) = \text{sn}(Y, h') &= \frac{\sqrt{1 - hP}}{h'} , \\
\cos(v) = \text{cn}(Y, h') &= \frac{\sqrt{h(P - h)}}{h'} , \\
\sqrt{1 - h'^2 \sin^2(v)} = \text{dn}(Y, h') &= \sqrt{hP} .
\end{aligned}$$

Then, the Taylor series of $F(v, h')$ and $E(v, h')$ can be computed as series containing derivatives of the Jacobian elliptic functions. Each time that the derivatives of Jacobian elliptic functions need to be evaluated, the answer can be easily picked up in the four series obtained from above. By properly combining the series of $F(v, h')$, $E(v, h')$, $K(h)$, $K(h')$ and $E(h')$, we obtain:

$$\begin{aligned}
Z(\mu, \tilde{\zeta}) = & 0.0028257 + \left(-0.0011830 + \frac{1.9350 \times 10^{-6}}{\tilde{\zeta}}\right) (\mu - \mu_0) \\
& + \left(3.6763 \times 10^{-4} - \frac{1.7627 \times 10^{-6}}{\tilde{\zeta}} - \frac{3.3002 \times 10^{-4}}{\tilde{\zeta}^2}\right) (\mu - \mu_0)^2
\end{aligned}$$

$$\begin{aligned}
& + \left(-1.0047 \times 10^{-4} + \frac{9.5848 \times 10^{-7}}{\tilde{\zeta}} + \frac{1.8595 \times 10^{-4}}{\tilde{\zeta}^2} + \frac{3.3835 \times 10^{-7}}{\tilde{\zeta}^3} \right) (\mu - \mu_0)^3 \\
& + \mathcal{O}[(\mu - \mu_0)^4], \tag{4.43}
\end{aligned}$$

$$\begin{aligned}
U(\mu, \tilde{\zeta}) = & - \frac{0.066452}{\tilde{\zeta}} (\mu - \mu_0) + \frac{0.0085785}{\tilde{\zeta}} (\mu - \mu_0)^2 \\
& + \left(-\frac{7.1026 \times 10^{-4}}{\tilde{\zeta}} + \frac{0.0012715}{\tilde{\zeta}^3} \right) (\mu - \mu_0)^3 + \mathcal{O}[(\mu - \mu_0)^4]. \tag{4.44}
\end{aligned}$$

To achieve the Taylor series of $T(\mu, \tilde{\zeta})$ with a minimum of effort, we produced first a series from its derivative given by Eqs(4.33). Thanks to Eq.(4.32), this form of the derivative avoids theta functions, and moreover, all functions that make up this derivative were already expanded for the previous series. So we only need to insert the series from the former functions into Eqs(4.33), rearrange the terms into a proper series, then integrate it to recover T in the form of a series. This gives

$$\begin{aligned}
T(\mu, \tilde{\zeta}) & = \int \left[\text{series of } \frac{dT}{d\mu} \right] d\mu = \int \left[\sum_{n=1}^{\infty} T^{(n)}(\mu_0, \tilde{\zeta}) \frac{(\mu - \mu_0)^{n-1}}{(n-1)!} \right] d\mu \\
& = T(\mu_0, \tilde{\zeta}) + \sum_{n=1}^{\infty} T^{(n)}(\mu_0, \tilde{\zeta}) \frac{(\mu - \mu_0)^n}{n!} \\
& = 0 - \frac{0.20935}{\tilde{\zeta}} (\mu - \mu_0) - \frac{0.0042719}{\tilde{\zeta}} (\mu - \mu_0)^2 \\
& \quad + \left(\frac{0.0038072}{\tilde{\zeta}} + \frac{0.0040061}{\tilde{\zeta}^3} \right) (\mu - \mu_0)^3 + \mathcal{O}[(\mu - \mu_0)^4], \tag{4.45}
\end{aligned}$$

where the zero is to emphasize that a constant of integration, which is $T(\mu_0, \tilde{\zeta}) = 0$, was indeed added.

At this stage, the remaining computations are straight forward. The series of $N(\mu, \tilde{\zeta})$ is obtained by combining together the series from Eqs (4.36), (4.38), (4.39), (4.42), (4.43), (4.44) and (4.45):

$$\begin{aligned}
N(\mu, \tilde{\zeta}) = & 1 - \frac{0.25127}{\tilde{\zeta}} (\mu - \mu_0) + \left(-\frac{0.012990}{\tilde{\zeta}} + \frac{0.031568}{\tilde{\zeta}^2} \right) (\mu - \mu_0)^2 \\
& + \left(\frac{0.0056452}{\tilde{\zeta}} + \frac{0.0032641}{\tilde{\zeta}^2} + \frac{2.1819 \times 10^{-4}}{\tilde{\zeta}^3} \right) (\mu - \mu_0)^3 + \mathcal{O}[(\mu - \mu_0)^4]. \tag{4.46}
\end{aligned}$$

And the expansions of $\Omega_0(\mu)$ and $b_0(\mu)$ are needed for $Q_{\pm}(\mu, \tilde{\zeta})$, which gives:

$$\begin{aligned} Q_{\pm}(\mu, \tilde{\zeta}) = & 1 \pm \tilde{\zeta} - 0.028702 (\mu - \mu_0)^2 + 0.0039472 (\mu - \mu_0)^3 \\ & + \left(-3.5824 \times 10^{-4} - \frac{3.8436 \times 10^{-5} (1 \pm \tilde{\zeta})}{\tilde{\zeta}^2} \right) (\mu - \mu_0)^4 \\ & + \mathcal{O}[(\mu - \mu_0)^5]. \end{aligned} \quad (4.47)$$

4.4.3. Series of the Ernst Potential of the Disk

Both real series (4.46) and (4.47) can now be combined into the complex Ernst potential. This potential, given by Eq.(4.17a), can be expanded around $\mu \rightarrow \mu_0$, and it takes the following form:

$$\begin{aligned} f(\mu; \tilde{\zeta}) = & \frac{\tilde{\zeta} - 1 - i}{\tilde{\zeta} + 1 - i} - \frac{0.25127 \tilde{\zeta}}{(\tilde{\zeta} + 1 - i)^2} (\mu - \mu_0) \\ & + \left[\frac{0.063137 i}{(\tilde{\zeta} + 1 - i)^3} - \frac{0.012845(1 + i)}{(\tilde{\zeta} + 1 - i)^2} + \frac{0.044414}{\tilde{\zeta} + 1 - i} \right] (\mu - \mu_0)^2 \\ & + \left[\frac{0.015864}{(\tilde{\zeta} + 1 - i)^4} + \frac{-0.0065282 + 0.0064556 i}{(\tilde{\zeta} + 1 - i)^3} - \frac{0.0034840 - 0.022452 i}{(\tilde{\zeta} + 1 - i)^2} \right. \\ & \left. + \frac{-0.0066618 + 0.0033960 i}{\tilde{\zeta} + 1 - i} - 0.0022492 \right] \frac{(\mu - \mu_0)^3}{\tilde{\zeta}} + \mathcal{O}[(\mu - \mu_0)^4]. \end{aligned} \quad (4.48)$$

We only wrote down the beginning of our results and with only five significant digits, since the space needed for further orders inflates rapidly. But the method that we used to compute the Ernst potential allows us to generate the series beyond ten orders with more than ten significant digits in a reasonable amount of time; e.g. a personal computer with a 2.2 GHz CPU takes around 2 minutes to compute all series up to ten orders and ten significant digits.

In Fig. 4.6, the series of the Ernst potential is shown as Taylor polynomials for $n = 3, 6$ and 9 at different positions on the axis, and it is compared to the exact potential. One can see that for large distances from the disk (in Fig. 4.6, $\tilde{\zeta} = 10$ or 2), the series seems to converge for any value of μ . Closer to the disk ($\tilde{\zeta} = 0.5$ in Fig. 4.6), the series does not converge any more for values of μ too much smaller than μ_0 . This divergence is expected, as was discussed in Section 4.4.2. One can also see that for very relativistic disks ($\mu > 2$), the series with orders like $n = 3$ or 6 give excellent approximations as long as the series is evaluated for sufficiently large $\tilde{\zeta}$.

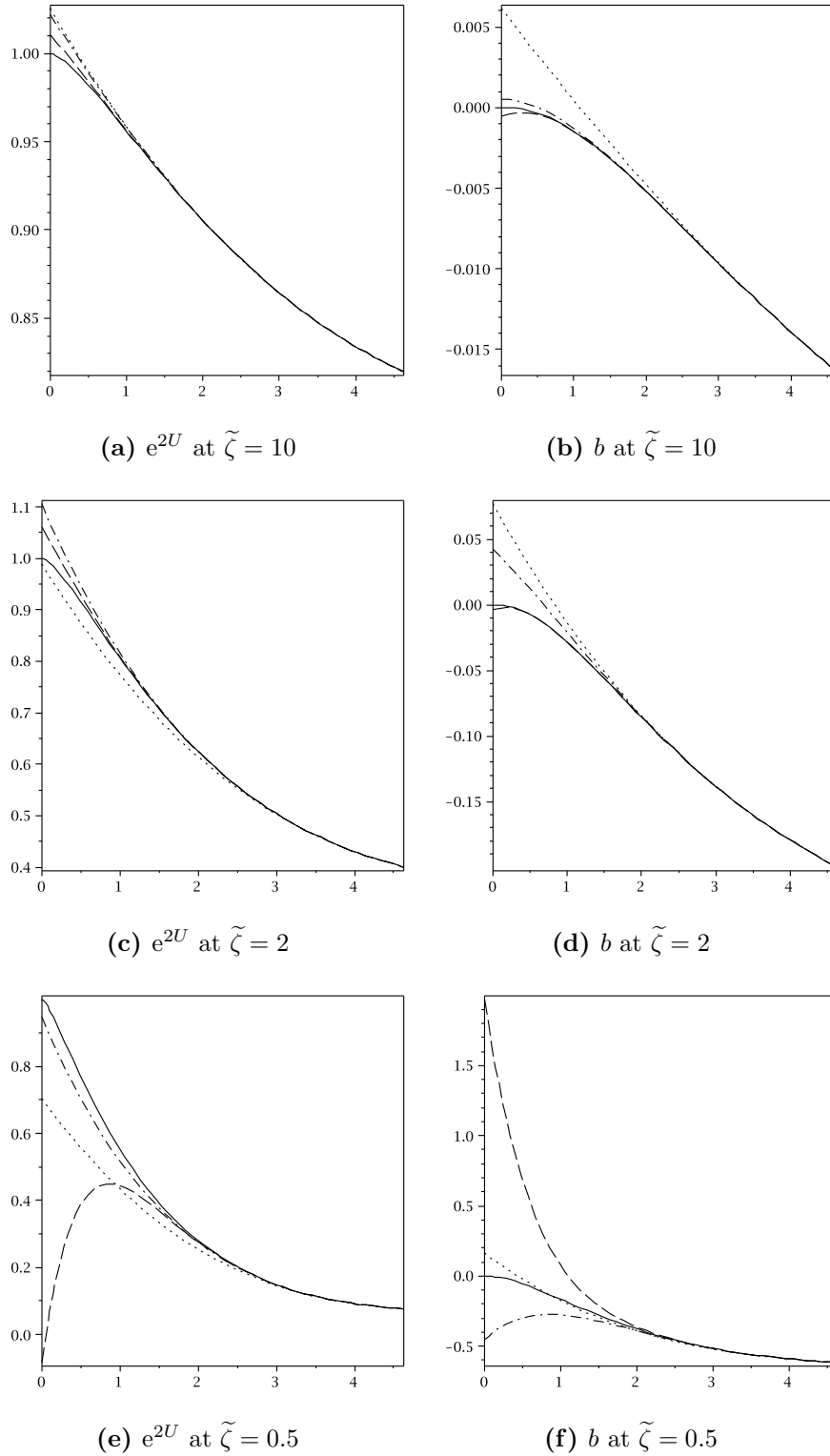


Figure 4.6: Real and imaginary parts of the Ernst potential and their respective Taylor approximation as function of μ for $\tilde{\zeta} = 10, 2$ and 0.5 . The solid lines are from the exact Ernst potential, while the dotted, dash-dotted and dashed lines are Taylor polynomials with orders $n = 3, 6, 9$ respectively.

Analogous Taylor series can be computed using the other normalized and dimensionless coordinate, $\widehat{\zeta} \equiv \zeta/M$, which we already introduced earlier in this work. The method to find these series is the same as before, so we do not need to present each step again. The final result starts with:

$$f(\mu; \widehat{\zeta}) = \frac{\widehat{\zeta} - 1 - i}{\widehat{\zeta} + 1 - i} - \frac{0.025836 i}{(\widehat{\zeta} + 1 - i)^2} (\mu - \mu_0)^2 \quad (4.49)$$

$$+ \frac{-0.0062737 + 0.0032261 i \widehat{\zeta}}{\widehat{\zeta} (\widehat{\zeta} + 1 - i)^2} (\mu - \mu_0)^3 + \mathcal{O}[(\mu - \mu_0)^4].$$

The latter normalization ($\widehat{\zeta}$) shows again series that are systematically more concise than the former normalization; this was also true for the black hole series in section 4.2. We can already see that the beginning of Eq.(4.49) agrees with what we conjectured in Eq.(4.9) since the first order correction vanishes, although the two series do not use the same expansion term for the next orders (ε vs $(\mu - \mu_0)$). Similarly, the two first terms of Eq.(4.48) should agree with what we conjectured in Eq.(4.8). This can be seen if ε from this second series is expanded in a power series of the disk parameter $(\mu - \mu_0)$:

$$\varepsilon = 1 - \widetilde{M}(\mu) = -\frac{d\widetilde{M}}{d\mu}(\mu_0)(\mu - \mu_0) + \mathcal{O}[(\mu - \mu_0)^2].$$

By picking the numerical value from Eq.(4.26), we find then that both series agree since the second term of the black hole becomes:

$$\frac{2\widetilde{\zeta}}{(\widetilde{\zeta} + 1 - i)^2} \varepsilon = -\frac{2\widetilde{\zeta}}{(\widetilde{\zeta} + 1 - i)^2} \frac{d\widetilde{M}}{d\mu}(\mu_0)(\mu - \mu_0) + \mathcal{O}[(\mu - \mu_0)^2]$$

$$= -\frac{0.2512727428 \widetilde{\zeta}}{(\widetilde{\zeta} + 1 - i)^2} (\mu - \mu_0) + \mathcal{O}[(\mu - \mu_0)^2].$$

It means that the coefficient 0.25127... does not represent a quantity which distinguishes the disk from a black hole with the same mass M and angular velocity Ω : it is a mere effect of the choice of the expansion parameter (within the class of uniformly rotating, stationary and axisymmetric bodies).

On the other hand, the coefficients of further expansion terms vary depending on what kind of body the source is. In this manner, they allow us to identify whether we have a black hole or some uniformly rotating fluid. Comparing Eqs(4.14) and (4.49), we find that both the black hole and the disk of dust have potentials with the following structure

on the axis:

$$f(\varepsilon; \widehat{\zeta}) = \frac{\widehat{\zeta} - 1 - i}{\widehat{\zeta} + 1 - i} + \frac{C_2 i}{(\widehat{\zeta} + 1 - i)^2} \varepsilon^2 + \mathcal{O}(\varepsilon^3) \quad (4.50)$$

where C_2 is a coefficient which is different for both bodies. If we take the series for $2\Omega M$ in Table 4.1, we find:

$$\begin{aligned} \varepsilon &= 1 - 2\Omega M = -1.2563637 \times 10^{-1}(\mu - \mu_0) + \mathcal{O}[(\mu - \mu_0)^2] , \\ (\mu - \mu_0)^2 &= 63.353298 \varepsilon^2 + \mathcal{O}(\varepsilon^3) . \end{aligned}$$

The last result can be used to substitute $(\mu - \mu_0)^2$ by ε^2 in Eq.(4.49), which thus provides the series with the same relativistic parameter ε used for the black hole. We finally find out that the characteristic coefficient C_2 is, for the two bodies:

$$\begin{aligned} C_2 &= +1 && \text{for the Kerr black hole,} \\ C_2 &= -1.636816606\dots && \text{for the disk of dust.} \end{aligned}$$

It would be interesting to know if other bodies such as rings have also the same form as given in Eq.(4.50).

In Fig. 4.7, we compare Eq.(4.50) up to ε^2 with the respective exact functions for the disk and the black hole, using the coordinate $\widehat{\zeta}$. The different behaviours can be seen near the source ($\widehat{\zeta} < 3$) for the Ernst potentials and their approximations; in the far field, the correction terms wane and the Ernst potentials are essentially identical to a extreme Kerr BH of the same mass (see Eq.(4.11)). For the black hole, the series up to ε^2 follows the exact potential closely. The approximation for e^{2U} even crosses zero into negative values near the centre, suggesting that the source might have a horizon⁷. For the disk, both curves of e^{2U} stay positive everywhere.

If we compare the series of the Ernst potential at the centre of the disk⁸, $f_0 = e^{2V_0} + ib_0$, with our two series (4.48) and (4.49) at the origin of the normalized axis, $\widetilde{\zeta} = \widehat{\zeta} = 0$, the result might look surprising as they are not the same:

$$\begin{aligned} f_0(\mu) &= -i + (0.0061997 + 0.028702 i) (\mu - \mu_0)^2 + \mathcal{O}[(\mu - \mu_0)^3] , \\ f(\mu; \widetilde{\zeta} = 0) &= -i + 0.012918 (\mu - \mu_0)^2 + \left(\text{higher orders diverge to } \infty \text{ as } \widetilde{\zeta} \rightarrow 0 \right) , \\ f(\mu; \widehat{\zeta} = 0) &= -i + 0.012918 (\mu - \mu_0)^2 + \left(\text{higher orders diverge to } \infty \text{ as } \widehat{\zeta} \rightarrow 0 \right) . \end{aligned}$$

⁷on the axis, the horizon is situated where $e^{2U} = 0$.

⁸The Ernst potential is identical on the axis ζ with either non-rotating or co-rotating coordinate.

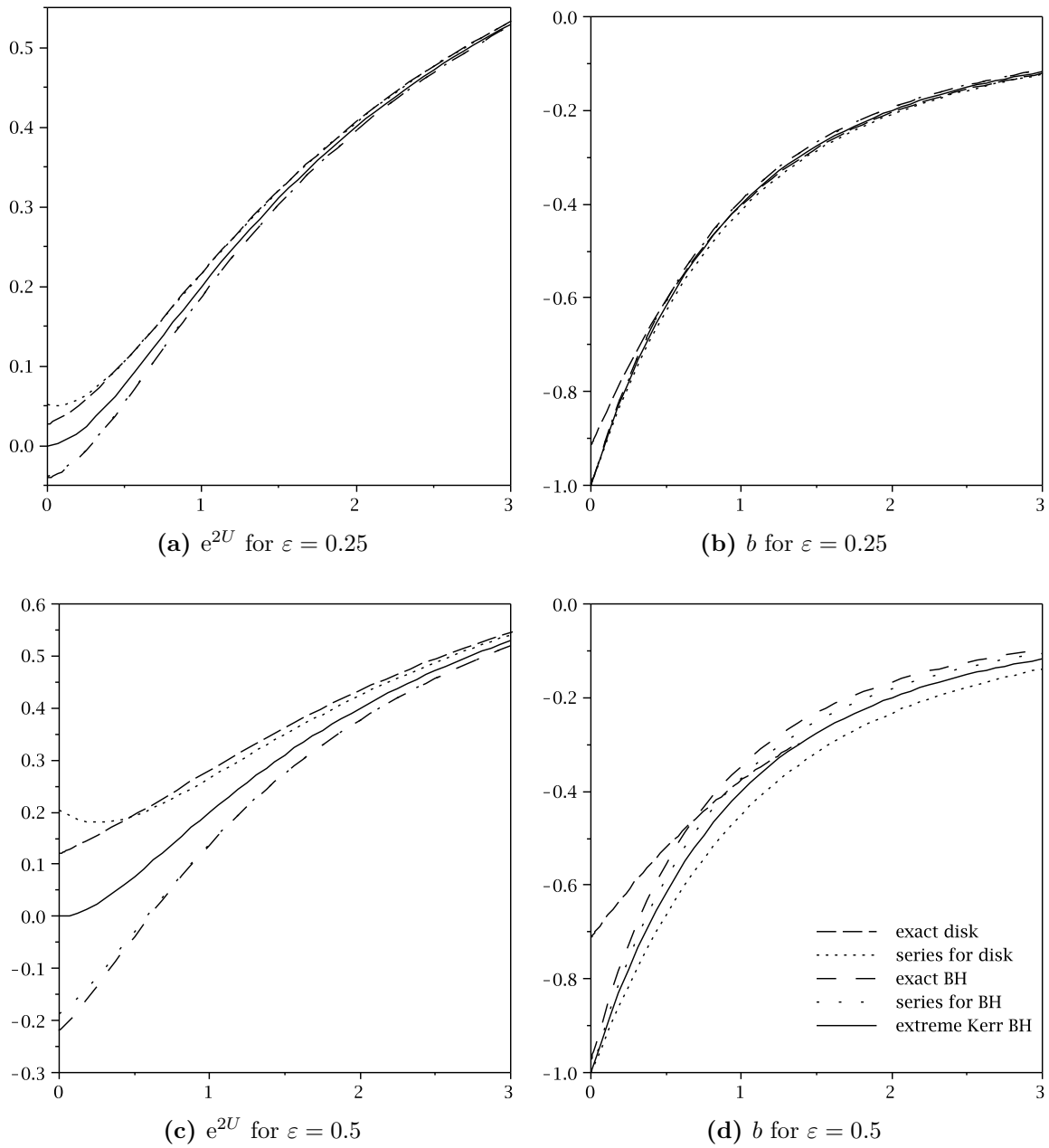


Figure 4.7: Real and imaginary parts of Ernst potentials of disks and black holes compared to their series up to order ε^2 , plotted along the axis $\hat{\zeta}$ for different values of the parameter $\varepsilon \equiv 1 - 2\Omega M$. The curves are the followings: exact disk (— — —), series of disk (⋯⋯⋯), exact black hole (- · - ·), series of black hole (· · · ·). The extreme Kerr BH (solid line) is shown as reference, independently of ε .

This difference can be explained by the normalization of the coordinate system and the unique property of the extreme Kerr BH geometry. As explained in section 2.3.2, the disk of dust, in its extreme Kerr BH limit, is contained in an “inner world” which is separated from an “outer world” by an infinitely long “throat geometry”. The normalized coordinate that we chose for the series, $\tilde{\zeta} \equiv 2\Omega\zeta$ and $\hat{\zeta} \equiv \zeta/M$, are such that the disk shrinks to the origin as we approach the BH limit: it describes then an asymptotically flat spacetime with a degenerate black hole horizon at the origin. If we had chosen a different normalization such as $y = \zeta/\rho_0$, the coordinate system would have ended up describing the inner world: a disk of dust with finite radius surrounded by the throat geometry in the far field.

5. Conclusion

We began our work by investigating in chapter 3 the relativistic solutions of fluid bodies made of strange quark matter. Through sequences of highly accurate numerical solutions, it was possible to identify extremal solutions (maximal mass, angular momentum, etc.) and to define the limits of these fluids in equilibrium with great precision.

Whereas it is known analytically that the EOS describing strange matter tends to that of a homogeneous body in the Newtonian limit, we saw here that sequences of configurations with these two EOS are similarly bounded by a mass-shedding limit, an infinite central pressure, the extreme Kerr black hole limit, etc. All continuously connected solutions are said to form a “class”. Strange matter bodies can be divided up into the same classes as for homogeneous fluids: a “Schwarzschild class” containing only spheroids, and a “ring class” where continuous transitions between spheroidal and toroidal bodies exist, etc. But strange stars also have characteristics which distinguish them from homogeneous bodies. We have shown in Figs 3.2, 3.3 and 3.4, that a domain of the Schwarzschild class is unstable. Indeed, along sequences of constant angular momentum, maximal masses are found at intermediate configurations. The accuracy of our solutions allowed us to find that the configurations in the class with maximal mass or maximal angular momentum are not exactly at the mass-shedding limit, contrary to what was believed.

It was also shown numerically that a parametric transition exists from strange matter rings to the extreme Kerr BH. It is expected that $E \leq 1$ always holds on the surface of a fluid body. Indeed, this inequality was used to prove that for rotating fluids the extreme Kerr black hole necessarily results if $e^{2V_0} \rightarrow 0$ [Mei06]. We have verified that this inequality is correct for a large class of rings. Figs 3.7 and 3.8 suggest that the transition to the black hole is rather slow as $e^{2V_0} \rightarrow 0$. This can be made more precise through the comparison with the Kerr solution, which leads us to conjecture that for every stationary rotating body permitting a transition to a black hole, the multipole moments y_n tend to one according to the formula

$$\frac{dy_n}{dy_0}(y_0 = 1) = n + 1 . \quad (5.1)$$

The plots of the multipole moments provide evidence suggesting that any given moment y_n , $n > 0$, of such bodies is always greater than that of the Kerr solution with the same y_0 . It then follows that the Kerr metric could never represent the exterior of these configurations.

In chapter 4, we discussed again the multipoles and the result from Eq.(5.1) by using two types of normalization. There it was found that the conjecture for $n = 1$ in Eq.(5.1) is a consequence of the first “law of thermodynamics” for uniformly rotating fluids. If the Ernst potential of a uniformly rotating fluid can be expanded by the relativistic parameter $2\Omega M$ near the extreme Kerr BH limit, we showed that Taylor series on the positive part of the axis would read

$$f = \frac{\zeta/M - 1 - i}{\zeta/M + 1 - i} + \emptyset + \mathcal{O}[(1 - 2\Omega M)^2] ,$$

where the first term is from the extreme Kerr BH solution and the vanishing first correction term is equivalent to the previous conjecture. Using the Ernst potential on the axis of the uniformly rotating disk of dust, we first proved that the conjecture indeed holds for this body by computing the derivative of the potential. Then, we developed a computer routine which can generate the Taylor series of the Ernst potential for the disk up to arbitrary order. Although it might only be useful for few expansion terms near the black hole limit, the series indeed seems to converge for the entire sequence of disk configurations and everywhere on the axis, except for a tiny segment near the disk.

As our knowledge of astrophysical collapse scenarios improves, it will be interesting to see how strong the connections can be to the quasi-stationary collapse considered here. Although the conjecture from Eq.(5.1) holds for the disk and our sequences of rings, it is proved for uniformly rotating fluids only for $n = 1$. It would also be interesting to provide an explanation of this conjecture for the further multipoles. And again, as the series for the black hole and the disk both begin with the same structure given in Eq.(4.50), one can ask if this form also holds for other bodies near the extreme Kerr BH limit, such as rings.

Bibliography

- [AFK⁺04] M. Ansorg, T. Fischer, A. Kleinwächter, R. Meinel, D. Petroff, and K. Schöbel. Equilibrium configurations of homogeneous fluids in general relativity. *Mon. Not. R. Astron. Soc.*, 355:682, 2004.
- [AFO86] C. Alcock, E. Farhi, and A. Olinto. Strange stars. *Astrophys. J.*, 310:261–272, 1986.
- [AK04] A. Ashtekar and B. Krishnan. Isolated and dynamical horizons and their applications, 2004. Online Publication: Referenced on December 12, 2005, <http://www.livingreviews.org/lrr-2004-10>.
- [AKM03a] M. Ansorg, A. Kleinwächter, and R. Meinel. Highly accurate calculation of rotating neutron stars: Detailed description of the numerical methods. *Astron. Astrophys.*, 405:711, 2003.
- [AKM03b] M. Ansorg, A. Kleinwächter, and R. Meinel. Relativistic Dyson rings and their black hole limit. *Astrophys. J. Lett.*, 582:L87, 2003.
- [BH99] J. Bardeen and G. T. Horowitz. Extreme Kerr throat geometry: A vacuum analog of $\text{AdS}_2 \times \text{S}^2$. *Phys. Rev. D*, 60:104030, 1999.
- [BHM⁺05] L. Baiotti, I. Hawke, P. J. Montero, F. Löffler, L. Rezzolla, N. Stergioulas, J. A. Font, and E. Seidel. Three-dimensional relativistic simulations of rotating neutron-star collapse to a Kerr black hole. *Phys. Rev. D*, 71:024035, 2005.
- [BL67] R. H. Boyer and R. W. Lindquist. Maximal analytic extension of the kerr metric. *J. Math. Phys.*, 8:265, 1967.
- [BPT72] J. M. Bardeen, W. H. Press, and S. A. Teukolsky. Rotating black holes: Locally nonrotating frames, energy extraction, and scalar synchrotron radiation. *Astrophys. J.*, 178:347, 1972.

- [Buc59] H. A. Buchdahl. General relativistic fluid spheres. *Phys. Rev.*, 116(4):1027–1034, Nov 1959.
- [BW69] J. M. Bardeen and R. V. Wagoner. Uniformly rotating disks in general relativity. *Astrophys. J.*, 158:L65, 1969.
- [BW71] J. M. Bardeen and R. V. Wagoner. Relativistic disks. I. uniform rotation. *Astrophys. J.*, 167:359, 1971.
- [Cha31] S. Chandrasekhar. The Maximum Mass of Ideal White Dwarfs. *Astrophys. J.*, 74:81–82, July 1931.
- [CJJ⁺74] A. Chodos, R. L. Jaffe, K. Johnson, C. B. Thorn, and V. F. Weisskopf. New extended model of hadrons. *Phys. Rev. D*, 9(12):3471–3495, Jun 1974.
- [CJJT74] A. Chodos, R. L. Jaffe, K. Johnson, and C. B. Thorn. Baryon structure in the bag theory. *Phys. Rev. D*, 10(8):2599–2604, Oct 1974.
- [Ern68] F. J. Ernst. New formulation of the axially symmetric gravitational field problem. *Phys. Rev.*, 167:1175, 1968.
- [FHA05] T. Fischer, S. Horatschek, and M. Ansorg. Uniformly rotating rings in general relativity. *Mon. Not. R. Astron. Soc.*, 364:943, 2005.
- [FHP89] G. Fodor, C. Hoenselaers, and Z. Perjés. Multipole moments of axisymmetric systems in relativity. *J. Math. Phys.*, 30(10):2252, 1989.
- [FJ84] E. Farhi and R. L. Jaffe. Strange matter. *Phys. Rev. D*, 30(11):2379–2390, Dec 1984.
- [FK09] R. Filter and A Kleinwächter. On the multipole moments of a rigidly rotating fluid body. *Ann. Phys. (Berlin)*, 18:102, 2009.
- [Fon03] J. A. Font. Numerical hydrodynamics in general relativity, 2003. Online Publication: Referenced on December 12, 2005, <http://www.livingreviews.org/lrr-2003-4>.
- [Ger70] R. Geroch. Multipole moments. II. curved space. *J. Math. Phys.*, 11(8):2580, 1970.
- [GHL⁺99] E. Gourgoulhon, P. Haensel, R. Livine, E. Paluch, S. Bonazzola, and J. A. Marck. Fast rotation of strange stars. *Astron. Astrophys.*, 349:851, 1999.

- [GR94] I. S. Gradshteyn and I. M. Ryzhik. *Table of Integrals, Series and Products*. Academic Press Inc, 5th revised edition, 1994.
- [Han73] R. O. Hansen. Multipole moments of stationary space-times. *J. Math. Phys.*, 15(1):46, 1973.
- [HS67] J. B. Hartle and D. H. Sharp. Variational principle for the equilibrium of a relativistic, rotating star. *Astrophys. J.*, 147:317, 1967.
- [Ker63] R. P. Kerr. Gravitational field of a spinning mass as an example of algebraically special metrics. *Phys. Rev. Lett.*, 11:237, 1963.
- [KLM10] A. Kleinwächter, H. Labranche, and R. Meinel. On the black hole limit of rotating disks and rings. (*in preparation*), 2010.
- [KMN95] A. Kleinwächter, R. Meinel, and G. Neugebauer. The multipole moments of the rigidly rotating disk of dust in general relativity. *Phys. Lett. A*, 200:82, 1995.
- [KN68] D. Kramer and G. Neugebauer. Zu axialsymmetrischen stationären Lösungen der Einsteinschen Feldgleichungen für das Vakuum. *Communications in Mathematical Physics*, 10:132–139, June 1968.
- [Kor95] P. Kordas. Reflection-symmetric, asymptotically flat solutions of the vacuum axisymmetric Einstein equations. *Class. Quantum Grav.*, 12:2037, 1995.
- [KT66] W. Kundt and M. Trümper. Orthogonal decomposition of axi-symmetric stationary spacetimes. *Zeitschrift für Physik*, 192:419–422, August 1966.
- [KWWG95] Ch. Kettner, F. Weber, M. K. Weigel, and N. K. Glendenning. Structure and stability of strange and charm stars at finite temperatures. *Phys. Rev. D*, 51(4):1440–1457, Feb 1995.
- [Lin92] L. Lindblom. On the symmetries of equilibrium stellar models. *Philos. Trans. R. Soc. London, Ser. A*, 340:353, 1992.
- [LPA07] H. Labranche, D. Petroff, and M. Ansorg. The parametric transition of strange matter rings to a black hole. *Gen. Rel. and Grav.*, 39:129–143, 2007.

- [MAK⁺08] R. Meinel, M. Ansorg, A. Kleinwächter, G. Neugebauer, and D. Petroff. *Relativistic Figures of Equilibrium*. Cambridge University Press, Cambridge, 2008.
- [Mei02] R. Meinel. Black holes: A physical route to the Kerr metric. *Ann. Phys. (Leipzig)*, 11:509–521, August 2002.
- [Mei04] R. Meinel. Quasistationary collapse to the extreme Kerr black hole. *Ann. Phys. (Leipzig)*, 13:600–603, October 2004.
- [Mei06] R. Meinel. On the black hole limit of rotating fluid bodies in equilibrium. *Class. Quantum Grav.*, 23:1359, 2006.
- [MK95] R. Meinel and A. Kleinwächter. Dragging effects near a rigidly rotating disk of dust. In J. B. Barbour and H. Pfister, editors, *Mach's Principle: From Newton's Bucket to Quantum Gravity*, page 339, Boston, 1995. Birkhäuser.
- [MN95] R. Meinel and G. Neugebauer. Asymptotically flat solutions to the Ernst equation with reflectional symmetry. *Class. Quantum Grav.*, 12:2045, 1995.
- [NM93] G. Neugebauer and R. Meinel. The Einsteinian gravitational field of a rigidly rotating disk of dust. *Astrophys. J.*, 414:L97, 1993.
- [NM94] G. Neugebauer and R. Meinel. General relativistic gravitational field of a rigidly rotating disk of dust: Axis potential, disk metric, and surface mass density. *Phys. Rev. Lett.*, 73:2166, 1994.
- [NM95] G. Neugebauer and R. Meinel. General relativistic gravitational field of a rigidly rotating disk of dust: Solution in terms of ultraelliptic functions. *Phys. Rev. Lett.*, 75:3046–3047, October 1995.
- [SA03] K. Schöbel and M. Ansorg. Maximal mass of uniformly rotating homogeneous stars in einsteinian gravity. *Astron. Astrophys.*, 405:405, 2003.
- [Web05] F. Weber. Strange quark matter and compact stars. *Prog. Part. Nucl. Phys.*, 54:193–288, 2005.

A. Elliptic Integrals and Functions

This appendix provides our definitions of the different functions related to elliptic integrals and some useful relations or identities. Most definitions, conventions or notations are inspired from [GR94].

Elliptic integral of the first and second kind respectively:

$$F(\phi, k) := \int_0^\phi \frac{d\theta}{\sqrt{1 - k^2 \sin^2 \theta}} = \int_0^{\sin \phi} \frac{dx}{\sqrt{(1 - x^2)(1 - k^2 x^2)}} \quad (\text{A.1})$$

$$E(\phi, k) := \int_0^\phi \sqrt{1 - k^2 \sin^2 \theta} d\theta = \int_0^{\sin \phi} \sqrt{\frac{1 - k^2 x^2}{1 - x^2}} dx \quad (\text{A.2})$$

The number k is called the modulus of these integrals, and $k' := \sqrt{1 - k^2}$ is called the complementary modulus.

Complete elliptic integrals:

$$K(k) := F\left(\frac{\pi}{2}, k\right), \quad E(k) := E\left(\frac{\pi}{2}, k\right). \quad (\text{A.3})$$

Functional relations between elliptic integrals:

$$E(k)K(k') + K(k)E(k') - K(k)K(k') = \frac{\pi}{2} \quad (\text{A.4})$$

$$\frac{\partial F(\phi, k)}{\partial \phi} = \frac{1}{\sqrt{1 - k^2 \sin^2 \phi}}, \quad (\text{A.5a})$$

$$\frac{\partial F(\phi, k)}{\partial k} = \frac{1}{k'^2} \left(\frac{E(\phi, k) - k'^2 F(\phi, k)}{k} - \frac{k \sin \phi \cos \phi}{\sqrt{1 - k^2 \sin^2 \phi}} \right), \quad (\text{A.5b})$$

$$\frac{\partial E(\phi, k)}{\partial \phi} = \sqrt{1 - k^2 \sin^2 \phi}, \quad (\text{A.5c})$$

$$\frac{\partial E(\phi, k)}{\partial k} = \frac{E(\phi, k) - F(\phi, k)}{k}. \quad (\text{A.5d})$$

Jacobian elliptic functions:

$$u := F(\phi, k)$$

$$\operatorname{am} u \equiv \operatorname{am}(u, k) := \phi, \quad (\text{A.6a})$$

$$\operatorname{sn} u \equiv \operatorname{sn}(u, k) := \sin \phi, \quad (\text{A.6b})$$

$$\operatorname{cn} u \equiv \operatorname{cn}(u, k) := \cos \phi, \quad (\text{A.6c})$$

$$\operatorname{dn} u \equiv \operatorname{dn}(u, k) := \sqrt{1 - k^2 \sin^2 \phi}. \quad (\text{A.6d})$$

Derivatives of the Jacobian elliptic functions:

$$\frac{\partial \operatorname{am} u}{\partial u} = \operatorname{dn} u, \quad (\text{A.7a})$$

$$\frac{\partial \operatorname{sn} u}{\partial u} = \operatorname{cn} u \operatorname{dn} u, \quad (\text{A.7b})$$

$$\frac{\partial \operatorname{cn} u}{\partial u} = -\operatorname{sn} u \operatorname{dn} u, \quad (\text{A.7c})$$

$$\frac{\partial \operatorname{dn} u}{\partial u} = -k^2 \operatorname{sn} u \operatorname{cn} u, \quad (\text{A.7d})$$

$$\frac{\partial \operatorname{am} u}{\partial k} = \frac{\operatorname{dn} u}{kk'^2} \left[-E(\operatorname{am} u, k) + k'^2 u + k^2 \frac{\operatorname{sn} u \operatorname{cn} u}{\operatorname{dn} u} \right], \quad (\text{A.7e})$$

$$\frac{\partial \operatorname{sn} u}{\partial k} = \frac{\operatorname{dn} u \operatorname{cn} u}{kk'^2} \left[-E(\operatorname{am} u, k) + k'^2 u + k^2 \frac{\operatorname{sn} u \operatorname{cn} u}{\operatorname{dn} u} \right], \quad (\text{A.7f})$$

$$\frac{\partial \operatorname{cn} u}{\partial k} = -\frac{\operatorname{dn} u \operatorname{sn} u}{kk'^2} \left[-E(\operatorname{am} u, k) + k'^2 u + k^2 \frac{\operatorname{sn} u \operatorname{cn} u}{\operatorname{dn} u} \right], \quad (\text{A.7g})$$

$$\frac{\partial \operatorname{dn} u}{\partial k} = -\frac{k \operatorname{sn} u \operatorname{cn} u}{k'^2} \left[-E(\operatorname{am} u, k) + k'^2 u + \frac{\operatorname{sn} u \operatorname{dn} u}{\operatorname{cn} u} \right]. \quad (\text{A.7h})$$

Heuman's Lambda function:

$$\Lambda_0(\phi, k) := \frac{2}{\pi} [E(k)F(\phi, k') + K(k)E(\phi, k') - K(k)F(\phi, k')] \quad (\text{A.8})$$

Jacobian Zeta function:

$$Z(u, k) := E(\operatorname{am} u, k) - \frac{E(k)}{K(k)} u \quad (\text{A.9})$$

Jacobian theta functions:

$$\vartheta_1(w, B) = \sum_{n=-\infty}^{\infty} (-1)^n \exp \left\{ \left[\frac{1}{2}(2n+1) \right]^2 B + (2n+1)w \right\} , \quad (\text{A.10a})$$

$$\vartheta_2(w, B) = \sum_{n=-\infty}^{\infty} \exp \left\{ \left[\frac{1}{2}(2n+1) \right]^2 B + (2n+1)w \right\} , \quad (\text{A.10b})$$

$$\vartheta_3(w, B) = \sum_{n=-\infty}^{\infty} \exp \{ n^2 B + 2nw \} , \quad (\text{A.10c})$$

$$\vartheta_4(w, B) = \sum_{n=-\infty}^{\infty} (-1)^n \exp \{ n^2 B + 2nw \} . \quad (\text{A.10d})$$

One particular partial derivative with ϑ_2 :

$$\frac{\partial}{\partial w} \ln (\vartheta_2(w, B)) = \Lambda_0(am(u, k'), k) \quad (\text{A.11})$$

with $w = \frac{\pi u}{2K(k)}$ and $B = -\pi \frac{K(k')}{K(k)}$

One general property with partial derivatives of ϑ_2 :

$$\frac{\partial}{\partial B} \vartheta_2(w, B) = \frac{1}{4} \frac{\partial^2}{\partial w^2} \vartheta_2(w, B) \quad (\text{A.12})$$

B. Some Useful Functions for the Disk of Dust

B.1. List of Functions in the Ernst Potential of the Disk

Functions which depend only on the relativistic parameter μ :

$$\begin{aligned}\tau &= \sqrt[4]{1 + \frac{1}{\mu^2}}, \\ h &= \sqrt{\frac{1}{2} \left(1 + \frac{1}{\sqrt{\mu^{-2} + 1}} \right)}, \\ h' &= \sqrt{\frac{1}{2} \left(1 - \frac{1}{\sqrt{\mu^{-2} + 1}} \right)}, \\ g(x) &= \frac{\ln(\sqrt{1+x^2} + x)}{\sqrt{1+x^2}} = \frac{\operatorname{arcsinh} x}{\sqrt{1+x^2}} \quad \left(= \frac{1}{2} \frac{d}{dx} [\operatorname{arcsinh} x]^2 \right), \\ I_n &= \frac{1}{\pi} \int_0^\mu \frac{g(x) x^n}{\sqrt{\mu-x}} dx, \\ \hat{I} &= \sqrt[4]{1 + \mu^2} I_0 = \frac{\sqrt[4]{1 + \mu^2}}{\pi} \int_0^\mu \frac{\ln(\sqrt{1+x^2} + x)}{\sqrt{1+x^2} \sqrt{\mu-x}} dx,\end{aligned}$$

$$am \equiv \operatorname{am}(\hat{I}, h'), \quad sn \equiv \operatorname{sn}(\hat{I}, h'), \quad cn \equiv \operatorname{cn}(\hat{I}, h'), \quad dn \equiv \operatorname{dn}(\hat{I}, h'),$$

$$\begin{aligned}c_1 &= \frac{1}{\sqrt{\mu}} \left\{ 2\sqrt[4]{1 + \mu^2} E(am, h') - (\mu + \sqrt{1 + \mu^2}) I_0 + I_1 \right\}, \\ e^{2v_0} &= \frac{h' cn^2}{h}, \quad b_0 = -\frac{sn \, dn}{h}, \\ \Omega_0 \equiv \Omega \rho_0 &= \frac{1}{2} \sqrt{1 - \frac{h'^2}{h^2}} cn, \\ \widetilde{M} \equiv 2\Omega M &= -b_0 - \Omega_0 c_1,\end{aligned}$$

The functions “am”, “sn”, “cn” and “dn” call the Jacobian elliptic functions which are defined in Appendix A.

Functions which depend only on μ and the axis coordinate ζ :

$$\begin{aligned}
y &= \frac{\zeta}{\rho_0} = \frac{\tilde{\zeta}}{2\Omega_0} = \frac{\tilde{M}}{2\Omega_0} \hat{\zeta}, \\
R &= \frac{y\sqrt{\mu}}{\pi\sqrt{(y^2+1)^2+\mu^{-2}}} \int_0^\mu \frac{x(y^2+1)+\mu^{-1}}{\mu(y^2+1)-x} \cdot \frac{g(x)}{\sqrt{\mu-x}} dx, \\
S &= \frac{h'(y^2-\tau^2)}{2\sqrt{(y^2+1)^2+\mu^{-2}}}, \\
P &= \frac{\sqrt{(y^2+1)^2+\mu^{-2}}+2h\tau y}{(y+\tau)^2}, \\
V &= \text{sign}(y-\tau) \frac{h\sqrt{P(1-hP)(P-h)}}{1-hP-h'}, \\
v &= \arcsin \left[\frac{\sqrt{1-hP}}{h'} \right], \\
X &= \text{sign}(y-\tau) E(v, h'), \\
Y &= \text{sign}(y-\tau) F(v, h'), \\
Z &= X - \frac{E(h')}{K(h')} Y, \\
U &= \frac{\pi}{4K(h)} \left(\frac{2Y}{K(h')} - 1 \right), \\
W_\pm &= \frac{\pi}{2K(h)} \left[\hat{I} \pm \left(Y - \frac{K(h')}{2} \right) \right], \\
T &= \ln \vartheta_2 \left(W_+, -\pi \frac{K(h')}{K(h)} \right) - \ln \vartheta_2 \left(W_-, -\pi \frac{K(h')}{K(h)} \right), \\
N &= \exp \left\{ R - 2\hat{I}(S+V+Z+U) + T \right\}, \\
Q_\pm &= \frac{1 - 2\Omega_0^2(y^2+1 + \sqrt{(y^2+1)^2+\mu^{-2}})}{-b_0 \mp 2\Omega_0 y}.
\end{aligned}$$

Again, K , E , F and ϑ_2 call elliptic functions which are defined in Appendix A. Finally, the complex Ernst potential on the axis of the rigidly rotating disk reads:

$$f(\mu; y) = \frac{1 - iNQ_-}{N + iQ_+}.$$

B.2. Some Other Useful Relations

The following identities can be useful:

$$h^2 + h'^2 = 1, \quad 2h h' = \frac{1}{\sqrt{1 + \mu^2}} \quad (\text{B.1})$$

$$(1 - h - h')(h - h' - 1) = 2h(1 - h), \quad \frac{h - h' - 1}{1 - h - h'} = \frac{h}{1 - h'} \quad (\text{B.2})$$

Some derivatives can take a recursive form:

$$\frac{d\tau}{d\mu} = \frac{-\tau}{2\mu(1 + \mu^2)}, \quad (\text{B.3a})$$

$$\frac{dh}{d\mu} = 2h^2 h'^3, \quad (\text{B.3b})$$

$$\frac{dh'}{d\mu} = -2h'^2 h^3, \quad (\text{B.3c})$$

$$\frac{dg(x)}{dx} = \frac{1 - xg(x)}{1 + x^2}. \quad (\text{B.3d})$$

Danksagung

Mein besonderer Dank gilt Prof. Reinhard Meinel für die Möglichkeit der Promotion in der Allgemeinen Relativitätstheorie am TPI in Jena und für seine fachliche Betreuung meiner Doktorarbeit. Besonders seine präzisen Erklärungen zu vielen meiner Fragen über die Gravitationstheorie waren sehr hilfreich.

Weiterhin danke ich Dr. David Petroff, Dr. Andreas Kleinwächter und Dr. Marcus Ansorg für die wissenschaftliche Unterstützung, die massgeblich zum Gelingen meiner Arbeit beitrug, Insbesondere danke ich Dr. David Petroff für seine Hilfe bei der Berechnung von Konfigurationen aus “strange quark matter” und für das Korrekturlesen der Arbeit, sowie Dr. Andreas Kleinwächter für seine Unterstützung bei der Untersuchung des Ernst-Potentials der Staubscheibe, welche Voraussetzung für die Berechnung der Taylor-Reihe war.

Dank gilt auch meinen weiteren Kollegen Stefan Horatschek, Christian Teichmüller, Michael Brüggemann, Guillaume Faye sowie den Diplomanden des TPI für die vielen interessanten Diskussionen und die angenehme Arbeitsatmosphäre.

Weiterhin danke ich meinen Eltern für ihre liebevolle Ermunterung, sowie meinen Freunden Marc Bergevin, Sylvie Brunet, David Côté und Vincent Bouchard, mit denen ich meine Studienzeit in Montréal und mein Interesse an der Physik geteilt habe.

Ehrenwörtliche Erklärung

Ich erkläre hiermit ehrenwörtlich, dass ich die vorliegende Arbeit selbstständig, ohne unzulässige Hilfe Dritter und ohne Benutzung anderer als der angegebenen Hilfsmittel und Literatur angefertigt habe. Die aus anderen Quellen direkt oder indirekt übernommenen Daten und Konzepte sind unter Angabe der Quelle gekennzeichnet.

Niemand hat von mir unmittelbar oder mittelbar geldwerte Leistungen für Arbeiten erhalten, die im Zusammenhang mit dem Inhalt der vorgelegten Dissertation stehen. Insbesondere habe ich hierfür nicht die entgeltliche Hilfe von Vermittlungs- bzw. Beratungsdiensten (Promotionsberater oder andere Personen) in Anspruch genommen.

Die Arbeit wurde bisher weder im In- noch im Ausland in gleicher oder ähnlicher Form einer anderen Prüfungsbehörde vorgelegt.

Die geltende Promotionsordnung der Physikalisch-Astronomischen Fakultät ist mir bekannt.

Ich versichere ehrenwörtlich, dass ich nach bestem Wissen die reine Wahrheit gesagt und nichts verschwiegen habe.

Jena, den 13. Januar 2010

Hendrick Labranche

Lebenslauf

Angaben zur Person

Name: Labranche, Hendrick
geboren am 2. Juli 1979 in Québec, Québec (QC), Kanada
Staatsangehörigkeit: kanadisch
Anschrift: Dornburger Str. 15, 07743 Jena

Schulbildung

1985-1988 École primaire Du Buisson, Sillery, QC
1988-1991 École primaire Saint-Michel, Sillery, QC
1991-1996 Petit Séminaire de Québec, QC
Abschluss: Diplôme d'études secondaires
1996-1998 Petit Séminaire de Québec, QC
Abschluss: Diplôme d'études collégiales & International Baccalaureate Diploma

Ausbildung an der Universität

1998-2001 Université de Montréal, QC
Abschluss: B.Sc. en physique
2001-2003 University of Guelph, Ontario, Kanada
Abschluss: M.Sc. in Physics
2004-2010 Friedrich-Schiller-Universität Jena
Abschluss: Dr. rer. nat. in Physik (eventuell
nach Abgabe der Dissertation in der ThULB)